Chapter 19

On Error Estimators and Bayesian Approaches in Computational Model Validation

Chapter details

Chapter DOI:

https://doi.org/10.4322/978-65-86503-88-3.c19

Chapter suggested citation / reference style:

Jorge, Ariosto B., et al. (2022). “On Error Estimators and Bayesian Approaches in Computational Model Validation”. *In* Jorge, Ariosto B., et al. (Eds.) *Uncertainty Modeling: Fundamental Concepts and Models*, Vol. III, UnB, Brasilia, DF, Brazil, pp. 640–743. Book series in Discrete Models, Inverse Methods, & Uncertainty Modeling in Structural Integrity.

P.S.: DOI may be included at the end of citation, for completeness.

Book details

Book: Uncertainty Modeling: Fundamental Concepts and Models

Edited by: Jorge, Ariosto B., Anflor, Carla T. M., Gomes, Guilherme F., & Carneiro, Sergio H. S.

Volume III of Book Series in:

Discrete Models, Inverse Methods, & Uncertainty Modeling in Structural Integrity

Published by: UnB City: Brasilia, DF, Brazil Year: 2022

DOI: https://doi.org/10.4322/978-65-86503-88-3

On Error Estimators and Bayesian Approaches in Computational Model Validation

Ariosto B. Jorge[1a*], Sergio H. S. Carneiro[1b], Jhon N. V. Goulart[1c], Marcus V. G. Morais[1d], Guilherme F. Gomes[2], Carla T. M. Anflor[1e], Jalusa M. S. Ferrari[1f], and José L. C. R. Vila[1g]

[1]Post-Graduate Program - Integrity of Engineering Materials, University of Brasilia, Brazil. E-mail: a) ariosto.b.jorge@gmail.com; b) shscarneiro@unb.br; c) jvaz@unb.br; d) mvmorais@unb.br; e) anflor@unb.br; f) jalusaferrari@gmail.com; g) jl.vila@hotmail.com
[2]Mechanical Engineering Institute, Federal University of Itajubá, Brazil. E-mail: guilhermefergom@unifei.edu.br

*Corresponding author

Abstract

This chapter presents an overview of computational models and formulations, a description of some error estimators in Boundary Element Methods (BEM) and in Finite Element Methods (FEM), and some perspectives of the use of these error estimators in Bayesian approaches for Model Validation.

Keywords: Error Estimators, Finite Element Methods, Boundary Element Methods, Bayesian Approaches, Model Validation.

1 Introduction

Modeling and simulation is an important field in engineering and has been the object of relevant research and publications. To illustrate, a non-exhaustive list and overview of related research work in modeling, simulation, applications, etc. in this area may include, among others, (Chong et al., 2004) (Oberkampf & Trucano, 2002) (Oberkampf et al., 2004) (Oberkampf & Trucano, 2006) (Oberkampf & Trucano, 2008) (Oberkampf, 2009)(R. G. Hills & Trucano, 1999) (R. G. U. Y. Hills & Trucano, 2002) (Easterling, 1998) (Sokolowski & Banks, 2010) (Kerns et al., 1992) (Oberkampf & Barone, 2006) (Roy & Oberkampf, 2010) (Oberkampf & Roy, 2010) (Swiler et al., 2017) (Inman et al., 2005).

This chapter presents an overview of computational models and formulations, a description of some error estimators in Boundary Element Methods (BEM) and in Finite Element Methods (FEM), and some perspectives of the use of these error estimators in Bayesian approaches for Model Validation.

Section 2 presents an overview of modeling of physical systems.

Section 3 discusses some error estimators in computational / numerical methods, with focus in error estimators for Finite Element Methods (FEM) and for Boundary Element Methods (BEM).

Section 4 discusses some aspects on model validation under uncertainty, with focus on a consistent error estimation strategy for model validation and on combining error estimators and Bayesian hypothesis testing in a model validation procedure.

Section 5 discusses some perspectives for the use of Validation Techniques in FEM Condensation Models, and also some perspectives for aeronautical structures applications, such as modeling of structural damage detection/localization problems and modeling of damage detection/identification problems in structural fasteners / joints.

Section 6 presents some concluding remarks.

2 Modeling of Physical Systems: Overview

This overview of the different mathematical models of physical systems and numerical formulations used in engineering problems follows (Basu, 2002) (Basu et al., 2003), (Basu, 2007), (Basu & Jorge, 2009). Current state of affairs and future of modeling and simulation in engineering design is discussed. Various modeling schemes and all the associated aspects like multiscale modeling, risk and reliability, multi-disciplinary modeling and optimization, and the role of digital computers are also discussed.

2.1 Introduction

Engineers and scientists routinely use mathematical models for physical systems to simulate the real behavior. Such a model embodies the mathematical interpretation of a phenomenon based on well-defined physical laws of nature and is based on some conceptual description of the physical problem. Such models are normally ordinary or partial differential equations with spatial (in one-, two-, or three-dimensions) and/or temporal dependence. For instance, the mathematical model of a bar under distributed axial traction is based on Hooke's law and the concept of equilibrium of forces acting on the body. For instance in the case of the bar shown in Fig. 1, the one-dimensional mathematical model can be shown to be

$$-\frac{d}{dx}\left(AE\frac{du}{dx}\right)+Ac\frac{\partial u}{\partial t}+A\rho\frac{\partial^2 u}{\partial t^2}=b \tag{1}$$

Here: A = cross-sectional area of the bar, which may be function of x
E = Young's modulus of bar material
(Hooke's Law: $\sigma = E\varepsilon$, where σ = stress, and ε = strain)
ρ = mass density per unit volume
c = viscous damping coefficient per unit volume
u = displacement of a point in the bar in the positive x-direction
b = time and space dependent distributed axial force in the bar

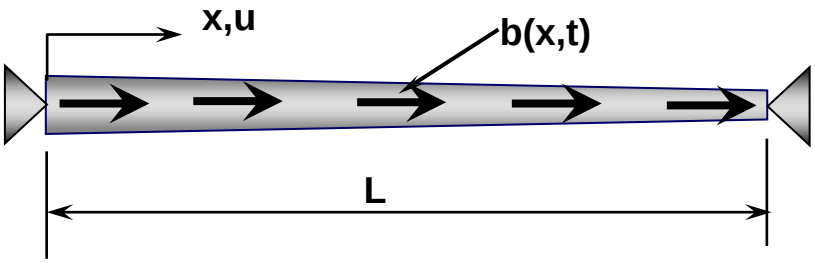

Figure 1: axial bar problem - adapted from (Basu & Jorge, 2009)

By applying the principle of conservation of energy and Fourier law, namely, $Q_i = -k_i \frac{\partial T}{\partial x_i}$, the mathematical model for a two-dimensional heat transfer problem, shown in Fig. 2, is:

$$\frac{\partial}{\partial x_i}\left(k_i \frac{\partial T}{\partial x_i}\right) - \rho c \frac{\partial T}{\partial t} = f \qquad in\ \Omega,\ \mathrm{i} = 1,2 \tag{2}$$

With the boundary conditions;

$$T = T_g \text{ on } \Gamma_g$$

$$k_i \frac{\partial T}{\partial x_i} n_i = q_n \text{ on } \Gamma_n$$

$$k_i \frac{\partial T}{\partial x_i} n_i = \beta(T_\infty - T) \text{ on } \Gamma_\beta$$

$$k_i \frac{\partial T}{\partial x} n_i = \alpha q_r - \kappa \varepsilon T^4 \text{ on } \Gamma_r$$

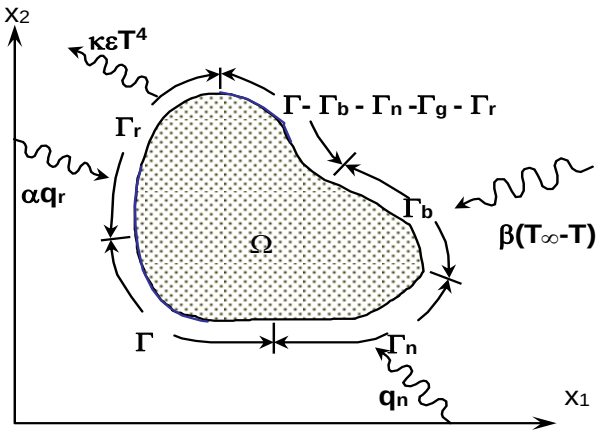

Figure 2: Two-dimensional heat transfer - adapted from (Basu & Jorge, 2009)

In Eq. (2):

T_g = the specified temperature on Γ_g

q_n = specified flow of heat per unit area on Γ_n

β = coefficient of convective heat transfer at Γ_β

T_∞ = ambient temperature of surrounding medium

α = coefficient of surface absorpivity at Γ_r

κ = Steffan - Boltzman constant

ε = coefficient of surface emissivity

q_r = radiant heat flow per unit area

k_x, k_y = coefficients of conductivity in x - and y - directions

f = heat input (or generation) per unit volume

It is only in the simplest (or, trivial) cases a closed form analytical solution of such mathematical models is possible. In most real life situations, a theoretical solution of such models becomes overly complex, well-nigh impossible. Complexities may be introduced by geometry, material characteristics, external influences, and other physical attributes. This calls for the use of discrete numerical methods, which essentially discretize the problem domain into small enough sub-regions on which the mathematical model is exercised using local attributes in space and time.

Additional complexities affecting the model and the solution are the presence of multiphysics effects – namely, the interaction of electromagnetic, thermal and mechanical effects. At the present time, there is an increased emphasis to depart from traditionally deterministic treatment of problems and use stochastic approach instead, accounting for the random nature of the problem parameters. The above possibilities are summarized in the block chart shown in Fig. 3.

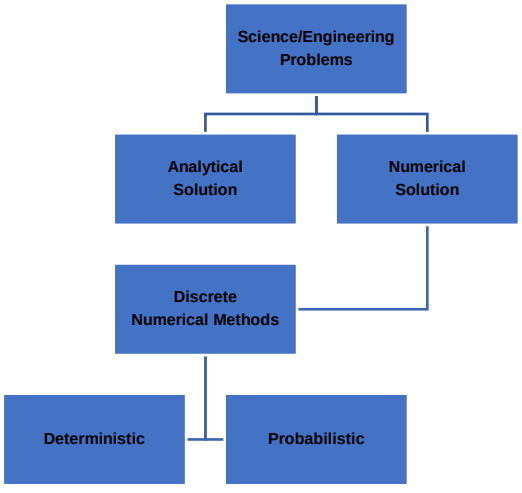

Figure 3: Solution of science and engineering problems - adapted from (Basu & Jorge, 2009)

To successfully compete in this global economy, it is necessary to create safe and reliable products which are economic too, by using optimization methods in the design process.

Safety evaluation requires consideration of performance under service conditions as well as at limit states, when the behavior becomes highly nonlinear.

2.1.1 Continuum vs. Multi-scale Modeling

Traditionally, a mathematical model for modeling and simulation treats the problem domain as a continuum (or, uses a macro model) both under service conditions and at limit states. As the limit state is approached incrementally, the degradation in the continuum is reflected approximately in the problem parameters in the average sense by the smearing process. In reality, with the progress of the degradation process the response traverses through meso-, micro-, and nano-scale resolutions, as seen in Fig. 4.

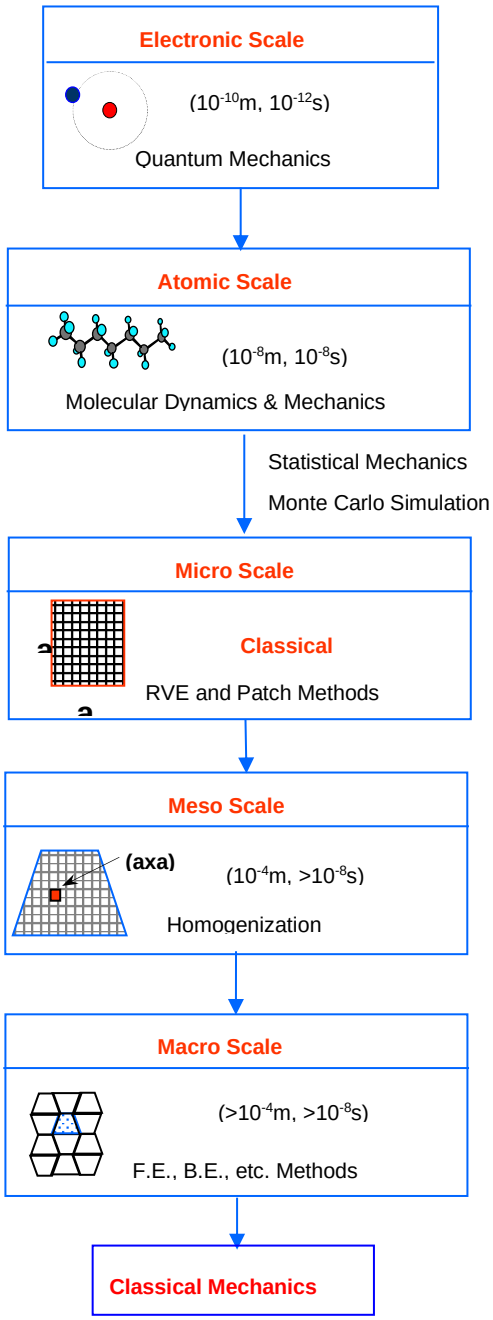

Figure 4: Multi-scale Modeling - adapted from (Basu & Jorge, 2009)

In other words, the material behavior is actually controlled by processes on wide range of length and time scales. At least in the critical (say, damaged) regions, this calls for multiscale modeling of the problem to capture the effect of highly localized behavior on problem parameters for used in the macro scale. Micro-scale modeling requires accounting for the local behavior of the material in the presence of damage and then coming up with homogenized problem parameters for use in the continuum model. For instance, to accurately simulate the deterioration process in complex materials, multiscale modeling is very important. Also, in the case of problem of contaminant transport in groundwater, it is necessary to use multiscale modeling to capture the effect of highly inhomogeneous nature of the substrata.

The need for using very high resolution (or, nano-scale) will be determined by the nature of the problem. Typical examples of such need are in the case of weathering resistance of cement mortar reinforced with carbon nanotubes, corrosion resistance of nano-crystalline coating on alloys, or material behavior near the interface of two bonded dissimilar materials. In nano-scale modeling, continuum physics is no more applicable and one needs to resort to molecular dynamics calculations considering the motion of atoms along with the application of Newtonian Mechanics to atomic systems. The results of molecular dynamics simulation can be used to find material properties at the continuum level by the application of statistical mechanics via Monte Carlo simulations. In most cases, however, damage characterization at the micro-scale leads to the desired level of accuracy in the predictions at the macro- or continuum scale.

Apart from multiple spatial scales, many problems in nature involve multiple temporal scales. For instance, if we examine the temperature variations experienced by a bridge structure, we can notice hourly variations, daily variations, seasonal variations, and annual variations. Another example is that of chemical reactions that may take seconds or hours. On the other hand, the vibrations of chemical bonds may occur at a time scale of femtoseconds (10-15s). In the case of most of such problems, the problems are considered at the scale of interest, ignoring the influence of other scales. It is evident from Fig. 4 that the smaller the physical scale smaller is the associated time scale.

2.1.2 Computational Tools

Far reaching changes in modeling and simulation techniques have been fueled by spectacular advances in digital computational technology, which has radically changed the way we do engineering. In developing new and more powerful techniques for modeling and simulation, the analysts and designers have always played the catch-up game with advances in digital technology. Meaningful molecular dynamics simulations would not have been possible without the power of today's massively parallel machines. Moore's law shows that computer speed (FLOPS) and memory increase approximately by a factor of 2 per 1.5 years. Consequently, the boundary between the power of personal computer and workstation and between network of workstations and powerful supercomputer has become blurred. As of June 2009, the No. 1 position as the fastest computer in the world with 129,600 processors belonged to IBM's Roadrunner System located at DOE's Los Alamos National Laboratory, California. It has reached the speed of 1.059 petaflops/s (quadrillions of floating point calculations per second) and continues to be the only system ever to break the petaflop/s. Linpack barrier. Many of these high powered systems consist of PC clusters. As PC is getting more powerful so are the new clusters. New PCs with Intel's Core i7 or AMD's Phenom II processor with speed

exceeding 3GHz are proving to be significantly more powerful than the high-powered workstations of just a few years before.

2.2 Discrete Numerical Methods

Discrete numerical methods are being almost exclusively used in the numerical solution of mathematical models of the continua expressed as initial and/or boundary value problems of differential calculus. The associated partial differential equations are formulated in space, either in the Lagrangian reference frame, or Eulerian reference frame.

In the first case, the selected reference points change with the continuum and hence more suited for solids; whereas, in the latter case, the selected reference points in the continua remain stationary and are more suited for fluids. The finite difference and Ritz type methods of the pre-computer era have largely been replaced in the computer era by finite element, boundary element, mesh-free, finite volume, and other evolving methods.

The first two of these methods were available to the general users in the seventies of the last century; whereas, the mesh-free methods became known during the early nineties. Finite volume method is specially used in fluid dynamics simulation or forms the basis of, what is termed as, hydro code. Wavelet and a host of other less known methods have appeared in the scene more recently.

As a matter of fact, all the new developments, in one way or other, involved modifying the first three mentioned methods. In all these methods the problem is reduced into one of finding numerical values at a discrete number of points covering the problem domain.

An essential difference between the boundary element method and other methods is that in this method the discrete points need to be selected at the boundary of the domain only; whereas, in the remaining methods the points are selected in the volume of the domain. For instance, in the case of three-dimensional problems, the boundary is a surface and hence the sub-regions selected on this bounding surface are two-dimensional. This fact introduces the possibility of higher computational efficiency in the boundary element method, especially, when the volume of the problem domain becomes significantly large compared to the area of the enclosing surface. In this method, an additional requirement is to append the fundamental solution of the problem, which is essentially the homogeneous solution of the differential equation due to a source term.

In the case of mesh-free method, the approximating function is not confined within a sub-region. For each integration point, it is defined over a predefined region of influence for that point. A more recent method, the wavelet method can be viewed as a method in which the approximating function is defined using multi-resolution technique based on the use of wavelets, similar to those used in signal processing.

In general, discrete numerical methods involve global discretization in space as well as time, coupled with the spatial approximation of the unknown function in terms of its values at discrete points within a sub-region, or in the neighborhood of a point of interest, and piecewise temporal approximation of the unknown function in terms of values at discrete instants of time in a temporal window.

As the spatial variation of the approximating function is represented by polynomial functions, difficulties associated with all the methods in modeling singular behavior is avoided in the boundary element method by introducing it through the fundamental

solution. In all other cases, the use of special functions near the singular point becomes necessary.

The ability to predict solution quality through a posteriori analysis and adaptive mesh refinement has assumed great importance in recent times and significant efforts are being put to advance in this area.

2.2.1 Finite Element Method (FEM)

After discretization of the problem domain into finite elements (Fig. 5) and appropriately defining the piecewise polynomial approximation over each finite element, a set of linear or nonlinear simultaneous equations is arrived at by applying the weighted residual method, if differential equations are used or, by applying the stationary condition to the functional for the problem, where applicable.

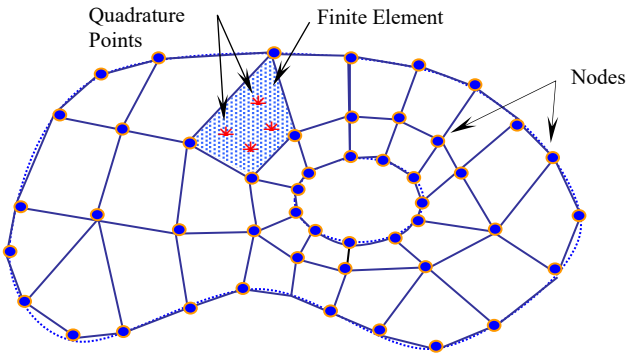

Figure 5: Multi-scale Modeling - adapted from (Basu & Jorge, 2009)

Sometimes, other approaches, like least squares method, are found to be more appropriate. The quality of the resulting approximate solution is controlled by the closeness of the finite element model to that represented by the mathematical model.

Solution can be improved by selective spatial refinement in the case of elliptic problems and local refinement in the case of hyperbolic problems, as the present may not affect the future.

In elements bordering a singular point, the polynomial basis can be appended by singular terms as shown below (Basu & Shah, 2000). In recent times, some investigators are terming it as x-FEM (Chessa & Belytschko, 2004). This is also conceptually similar to the, so-called, generalized finite element (Ivo Babuška et al., 2003) in which the choice of type of shape function is controlled by the nature of the problem to be solved.

Quality of the solution obtained can be assessed in a posteriori sense on the basis of the extent of violation of natural boundary conditions, and continuity requirements of functional derivatives at inter-element boundaries.

A number of schemes have been proposed to estimate the solution error in different norms, as discussed in subsequent sections.

Discrepancies between raw and improved estimates are accounted for through model refinement, with strategies such as *h*-, *p*-, *hp*-, etc, refinements.

2.2.2 Boundary Element Method (BEM)

In the case of boundary-element method (BEM), the governing partial differential equations are transformed to a set of integral equations which are numerically solved for the unknown boundary variables by discretizing the boundary of the element, as shown in Fig. 6.

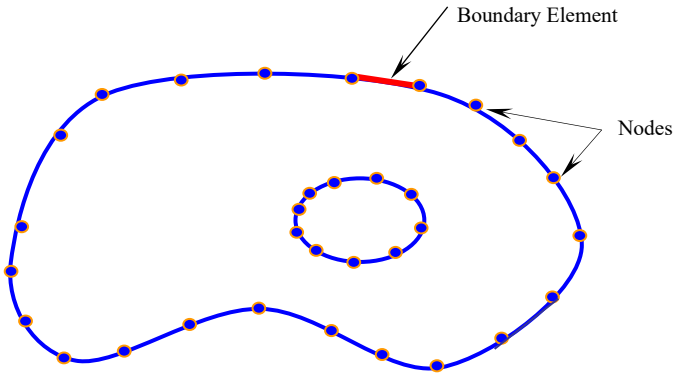

Figure 6: Boundary element method - adapted from (Basu & Jorge, 2009)

Apart from fewer unknown variables to be handled during the global solution, BEM handles singular problems, like those in linear fracture mechanics calculations, quite efficiently giving accurate point wise results close to the singular points; whereas, FEM gives damped global solution valid in the sense of energy norm.

Also, BEM is adept in handling problems of half-plane, or far-field problems. FEM is, however, better suited to handle complex domains and the presence of material nonlinearities.

In BEM, the system of equations are arrived at through the discretization of an integral identity, like Green's second identity in potential theory, or Somigliana's stress identity in elasticity theory, which is an exact representation of the original boundary-value problem. The system of equations in BEM arises from the discretization of integral identities, which are an exact representation of the original boundary-value problem.

A number of different BEM formulations have been proposed, for potential, elastostatics, fracture mechanics, acoustics, etc. problems, in 2D and in 3D. One can cite, for example, self-regular BEM formulation for potential problems (Jorge, Ribeiro, Cruse, et al., 2001), near-crack contour behaviour and extraction of log-singular stress terms of the self-regular traction boundary integral equation (Jorge, Cruse, & Fisher, 2003), variational self-regular traction-BEM formulation (Jorge, Cruse, Fisher, et al., 2003), variational self-regular flux-BEM formulation (Porto et al., 2005), non-singular BEM algorithms for potential problems (Ribeiro et al., 2009).

2.2.3 Mesh-Free Methods

In real-life large scale computations, generation, adaptation, and upgrading of finite element mesh is the costliest part of computational effort, especially, in situations involving crack propagation, penetration, large deformations causing significant mesh distortions, complex geometries, advanced materials, material degradation leading to discontinuities, etc.

In such situations, a group of methods called mesh-free methods may be the answer. In such methods, instead of associating the nodal points, to finite or boundary elements, the problem domain is covered by a network of nodal points, or, reference points of unknowns of the problem, with no fixed connectivity between them, as shown in Fig. 7.

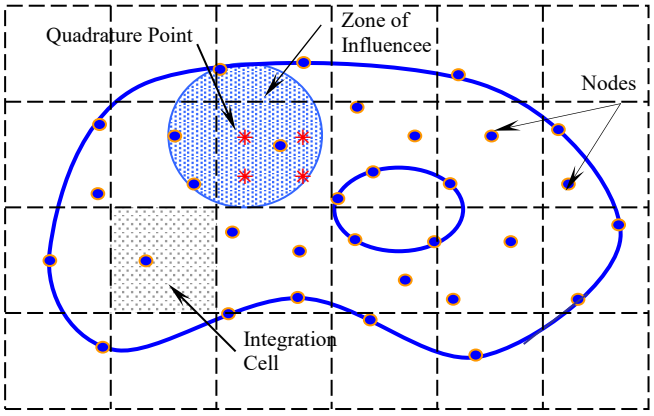

Figure 7: Element-Free Galerkin Method - adapted from (Basu & Jorge, 2009)

(Duarte, 1995) gives a comprehensive review of this method. The method can be applied either as a volume integral scheme, or as a boundary integral scheme. In both cases, the weak form of the governing differential equation can be satisfied at selected sampling or quadrature points based on weighted nodal values within a predefined sub-domain of influence assigned to the sampling point or, alternatively, the collocation method can be used.

The main idea of point collocation approach is to satisfy the governing differential equation at each of the nodal points covering the problem domain. At boundary points, as needed, the Dirichlet or Neumann boundary conditions are satisfied instead.

Depending upon the way the functional approximation is defined for the point of interest, a number of methods can be identified. According to the way this functional approximated is defined one may follow one of the three schemes – (a) Shepard's scheme (Shepard, 1968) which has a consistency of first order only, (b) Moving Least Squares Scheme (Lancaster & Salkauskas, 1981) which generalizes the Shepard's scheme, and (c) Partition of Unity p-version scheme (I. Babuška & Melenk, 1997), which generalizes Shepard's approach to higher consistency orders. A few of the methods based on these are:

(a) Diffuse Element Method (DEM) (Nayroles et al., 1992);
(b) Element-Free Galerkin Method (EFGM) (Belytschko et al., 1994);
(c) Natural Element Method (NEM) (Sukumar et al., 1998);
(d) Material Point Method (MPM) (Sulsky et al., 1995);
(e) hp-Clouds Method (HPCM) (Armando Duarte & Tinsley Oden, 1996);
(f) Finite Cloud Method (FCM) (Aluru & Li, 2001);
(g) Boundary Node Method (BNM) (Xie Mukherjee & Mukherjee, 1997);
(h) Boundary Cloud Method (BCM) (G. Li & Aluru, 2002), etc.

In the moving least squares method (MLS), the best interpolation in terms of nodal values is defined in a (moving) weighted least-squares sense. Diffuse element method uses the MLS approximation in the context of Galerkin method (Nayroles et al., 1992).

The EFG method is an extension of DEM (Belytschko et al., 1994). The primary differences between the two are that the EFG method (Fig. 7) includes certain extra terms in the derivatives of the approximating function that are not present in DEM. In addition, the EFG method uses Lagrange multipliers to enforce the essential boundary conditions.

In the Natural Element Method, natural neighbor interpolants are used to construct the trial and test functions. Such a multivariate data interpolation scheme is primarily used in data interpolation and modeling of geophysical phenomena (Sukumar et al., 1998).

In the Material Point Method (MPM) a solid continua is defined in terms of a collection of material points (Sulsky et al., 1995). Each material point is contained in a sub-domain assigned to it and carries information like mass, volume, velocity, strain, etc. of its sub-domain. Unlike the regular mesh-free method, MPM has a computational mesh of sub-domains associated with it. In this method, the material points do not interact with each other directly, rather the material point information is interpolated on to the mesh as the equation of motion is allowed to march in the time-domain. At any instant of time, the information on the new position of the mesh can be translated back onto the material points.

The hp-clouds method (Armando Duarte & Tinsley Oden, 1996) uses partition of unity scheme to construct radial basis functions of varying size of supports as circular patches (Fig. 8) or spherical volumes attached to each point and with polynomial reproducing properties of arbitrary order. The resulting basis functions are used in a Galerkin or collocation sense setting up a linear system of equations. The union of patches or volumes forms an open covering of the problem domain.

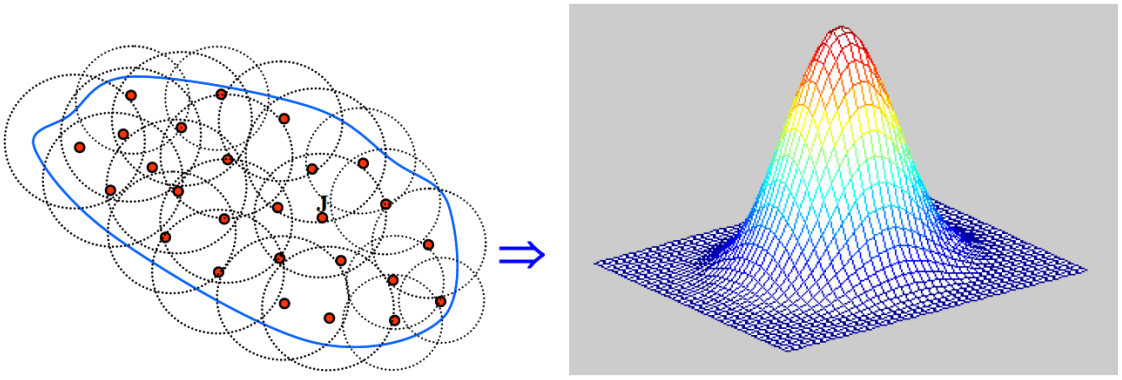

(a) Circular patches centered at the nodes (b) A typical patch

Figure 8: hp-clouds method - adapted from (Basu, 2007)

The finite cloud method (Aluru & Li, 2001) is a point collocation method based on reproducing kernel approximation with inherent multiresolution capability for error estimation and adaptivity. The basic idea of reproducing kernel approximation theory is to define the approximate function as the convolution of the original function with a kernel function, where the kernel function is sometimes called as the weighting function or the smoothing function.

The boundary node method (Xie Mukherjee & Mukherjee, 1997) is a boundary-only mesh-free method which combines MLSM interpolation scheme with the standard Boundary Integral Equations for a boundary value problem. Curvilinear boundary co-ordinates were originally proposed and used in this method for both two- and three-dimensional problems.

The boundary cloud method (BCM) was introduced by (G. Li & Aluru, 2002) as an improvement of BNM. Further improvements to BCM have also been proposed leading to the Extended Boundary Node Method (EBNM).

Variations of the mesh-free / meshless methods are in constant evolution, and can be used as tools for modeling and simulation of challenging problems of the continua, noting that they are suitable in multiscale modeling as well as in handling multiphysics problems.

2.2.4 Finite Volume Method

This method is an extension of the classical finite difference method. Here also the problem space is covered by a mesh of discrete number of points where the unknown function is supposed to be determined.

As a small volume is assumed to surround each such point in the mesh, it is termed as the finite volume method. The method is characterized by the conversion of divergence terms in the governing partial differential equation to surface integrals. The method is highly suited for unstructured meshes and is very popular for computational fluid dynamics computations.

2.2.5 Wavelet Method

An important aspect of discrete numerical solution of differential equations of the continua is the characterization of the variation of the unknown function over a sub-domain of the problem space. Like Fourier series expansion but without its restrictions, a wavelet is based on a series of scaled linear combination of a set of approximating functions (Burrus et al., 1998) (Dahmen, 1997) (Cohen et al., 1992) (Cohen & Masson, 1999).

Wavelets allow accurate representation of functions with rapid oscillations, or, possibly, with discontinuities, in localized regions. Although, initially wavelets found primary application in signal and image processing, its unique properties makes it a worthwhile candidate for the numerical solution of the partial differential equations of the continua having different kinds of irregularities (Basu & Shah, 1998) (Basu et al., 2003).

Wavelets based discrete numerical method for the solution of such equations may offer some unique advantages not available in other established discrete numerical methods, like those described above. In these methods, the presence of irregularities (or discontinuities) requires proper attention in spatial discretization, and, sometimes, requires the use of special approximating functions. But it is expected that the use of approximating functions based on wavelets will eliminate or reduce such restrictions.

In the finite element model, the element boundaries have to be located at the internal points of discontinuity. On the other hand, in the mesh-free method, the sub-domain boundaries cannot cross the same points. In the case of boundary element method applied to two-dimensional problems, similar consideration as in the case of finite element method is necessary. In view of positive experiences with wavelets in modeling localized

behavior related to signal and image processing, it is expected that traditional modeling restrictions in the case of problems of the continua can be relaxed. This is possible because this approach is so designed that it adapts itself to the local nature of the problem by retaining the finer wavelet components in the vicinity of an irregular point (say, near a singular point) whereas, the coarser components are retained in the smooth regions. The unknown function can be approximated by a series expansion and Galerkin method can be applied to the weighted residual of the equation. The equation expression for the unknown variable includes scaling functions, wavelet functions, coefficients, scaling parameters, translation. Of the many available scaling functions, two most commonly used ones in signal and image processing are the Haar functions, and the Hat functions. Hat wavelets are continuous and form orthonormal basis and can be obtained by integrating the Haar wavelets with proper scaling. Typical Hat scaling and wavelet functions are shown in Fig. 9.

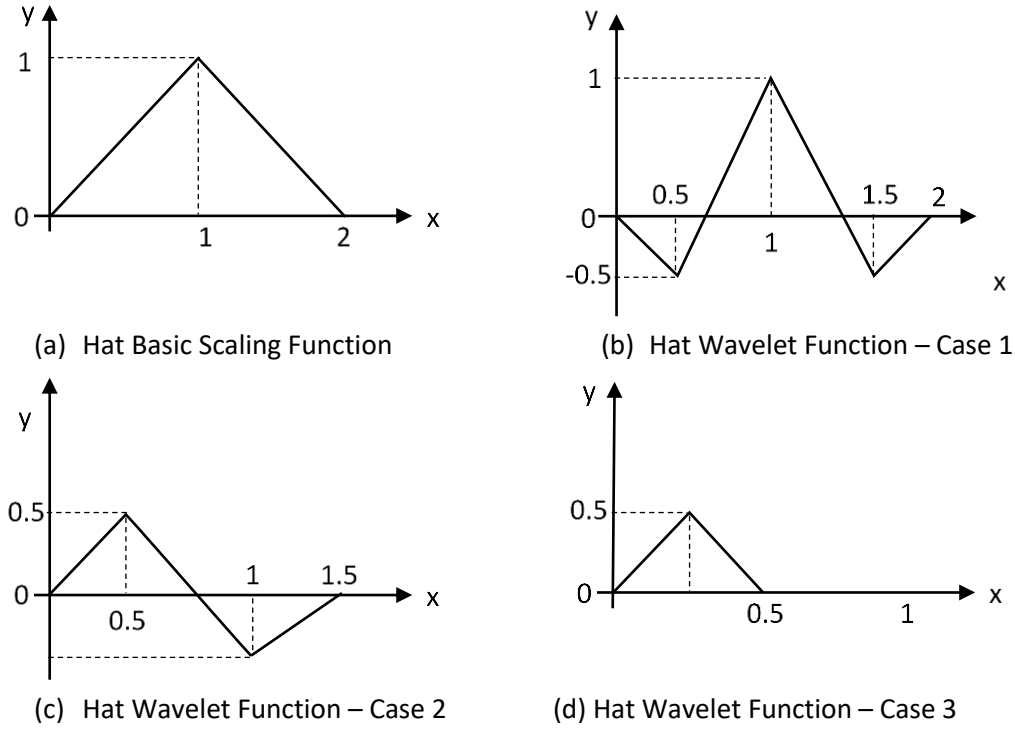

Figure 9: Typical Hat scaling and wavelet functions - adapted from (Basu et al., 2003)

A recent class of wavelets, known as multiwavelets (Aldroubi & Unser, 1993) (Aldroubi & Papadakis, 1998) are able to combine many of the properties of orthogonal wavelets, such as the famous Daubechies wavelets (Daubechies, 1988) (Daubechies, 1992) (Cohen et al., 1992) with the advantages of piecewise polynomial wavelets (such as the Hat wavelet). In particular, in (Donovan et al., 1996), families of orthogonal, smooth (continuous, and continuously differentiable), piecewise polynomial multi-wavelets are constructed.

2.2.6 Cellular Automata Inspired Modeling of Systems

In modeling and simulation of complex fluid systems as found in contaminant transport process in ground water, in slurry wall construction, in the use of fluid slurry during drilling for oil, industrial processes involving thermal variations, particular interactions, and colloidal mixtures, it is difficult to capture the mesoscopic features embedded in macroscopic phenomena of such fluids by using computational fluid dynamics (CFD).

In the CFD based continuum model, the macroscopic characteristics of fluids is based on Navier-Stokes type equations satisfying conservation of mass, energy, and momentum as well as continuity of flow and are discretized in space and time by finite element and finite difference methods.

In the other extreme, one may get most accurate simulation by using molecular dynamics requiring numerical solution of a set of ordinary differential equations in time for each molecule. While marching along time, the locations and velocities of each molecule are updated. The property values for a system of particles are arrived at by averaging in space and time the molecular positions and velocities and also by evaluating the moments and correlations.

However, one practical problem is that using even some of the most massively parallel computer only a few thousand molecules can be modeled at a time to get the results in reasonable time. So, in order to understand interactions between microscopic structure and macroscopic flows, it is necessary to use mesoscopic model, which is significantly less compute intensive than full blown molecular level modeling. At mesoscale an assemblage of fluid molecules termed as particle is used as discrete elements of the model.

Complex fluids exhibiting significant irregularity at molecular level appear homogeneous at the continuum level but exhibit an ordered structure at mesoscopic scale. In recent times it has been shown that such characterization can be effectively handled by using Lattice-Boltzman method (LBM) and Dissipative Particle method (DPM). The primary difference between LBM and DPM is that the latter includes thermal fluctuations but the former does not.

Lattice-Boltzman method (LBM) is essentially an extension of the concepts of cellular automata (Wolf-Gladrow, 2000). In 1940, Neuman and Ulam put forward the concepts of cellular automata. In this method the problem domain is represented by an array of cells. Each cell can be in one of the few possible states. At an instant of time, the state of each cell is determined by the prevailing state of the cells in its immediate neighborhood as well as its previous state. The process is repeated across all the cells in an array repeatedly in successive instants of time. In updating the state of the cells in the array, the same rule is applied to all. In other words, the model is homogeneous with respect to the rules. Updating of all the cells in the array leads to a new generation.

Cellular automata are best used to model situations where local interactions are predominant. This modeling technique has found applications in many areas of physical science, biology, engineering, mathematics, and social science. A popular example is lattice gas modeling (LGM). In this model (Frisch et al., 1986) (Chopard & Droz, 1998), the fluid ‘particles’ (a conglomerate of large number of molecules but is significantly smaller than the length scale of the simulation) are restricted to move on the links of the array of cells and the motion evolves in discrete time-steps.

LBM resulted from modifications made to LGM by removing the shortcomings. In LBM, instead of considering single particle occupation variables, particle distribution functions are used, linearization of the collision operator and the use of a single time relaxation approximation. As a result of these improvements, it was possible to eliminate statistical noise, and achieve enhanced computational efficiency. LBM, similar to LGA, however, is restricted to uniform lattice structures (Fig. 10), which severely limits its potential application to many practical problems, namely, flow through a porous media, where representations of complex pore geometry require a very fine uniform lattice, leading to computational inefficiency.

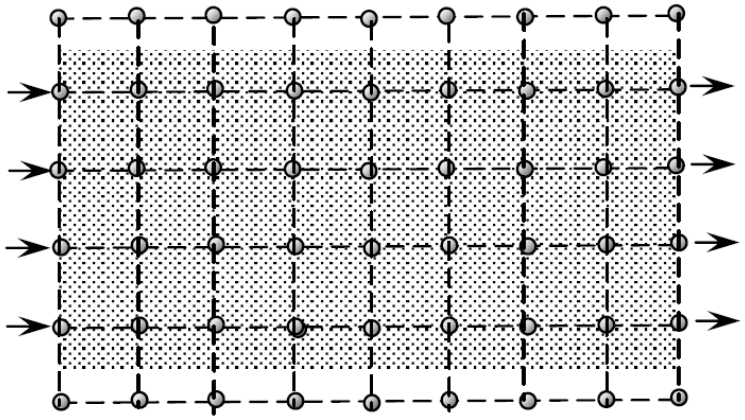

Figure 10: Uniform lattice structure for LBM - adapted from (Basu, 2007)

Least-squares finite element (LSFE) method (Y. Li et al., 2005), on the other hand, was recently shown to be a robust and efficient way to solve non-self-adjoint equations where convection operators are of first order (Jiang, 2000), always leading to symmetric, positive definite linear systems of equations without eliminating the need to use upwinding, staggered grids and operator splitting techniques (Ding & Tsang, 2001). Compared with Taylor-Galerkin-based FE methods, LSFE method possesses improved stability. Furthermore, for more complex systems, Taylor-Galerkin-based FE method may promote oscillations at discontinuities (Jiang, 2000) or at solid-liquid interfaces. Those oscillations may be suppressed by artificially adding dissipation terms like those in 'upwind' and 'artificial vioscosity' schemes, which, however, are dependent on the specific parameters of the problem. The model includes a statistical parameter (called as distribution function, from which the macroscopic properties of the fluid can be extracted), the particle velocity distribution (the nine possible velocity directions are shown in Fig. 11), the body force per unit mass, and a collision function. The collision operator is commonly approximated by the Bhatnagar-Gross-Krook (BGK) model (Bhatnagar et al., 1954).

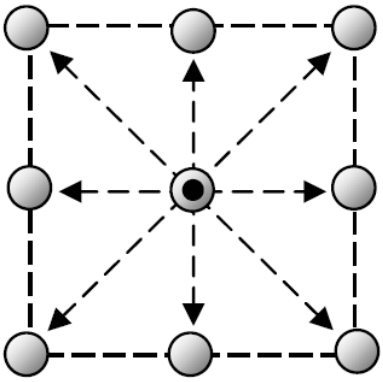

Figure 11: Nine possible directional velocities - adapted from (Basu, 2007)

An application for flow in a porous media is presented in (Y. Li et al., 2005), in which the porous media is considered as a statistical distribution of non-overlapping circular disks representing soil particles distributed in a rectangular two-dimensional uniform continuum representing the pore space through which a fluid flows. Simulation was conducted for randomly generated particle diameters, for both traditional LBM with uniform mesh and LSFE-LBM with unstructured mesh. Fig. 12 shows an irregular triangular mesh used for LSFE-LBM (Y. Li et al., 2005).

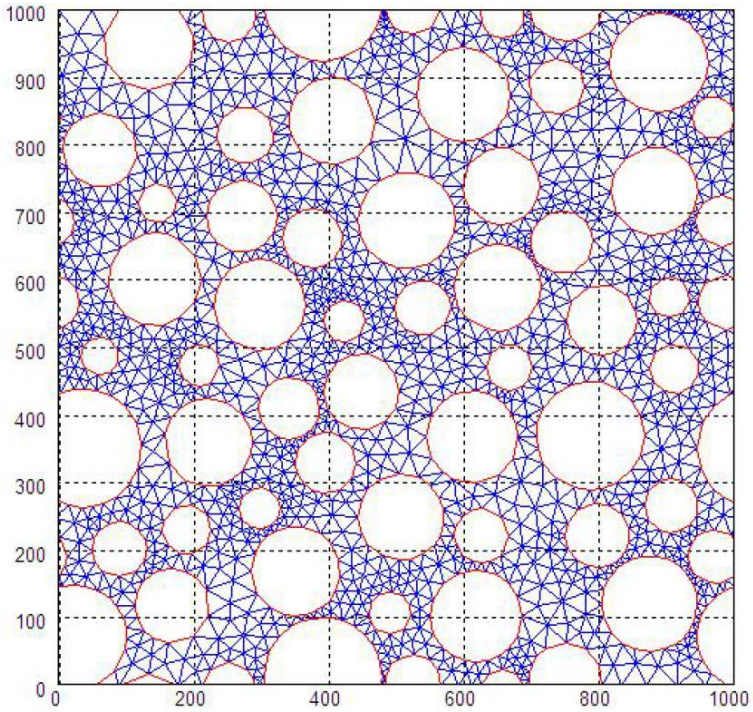

Figure 12: LSFE-LBM mesh used in permeability problem - adapted from (Basu, 2007)

2.2.7 Molecular Dynamics-Based Modeling

Modern materials, especially the complex composites, have hierarchical property in the sense that such materials have constituents which span across different length scales. The failure of such materials is controlled by the behavior at different length scales as well as the process of property transfer between different length-scales. Composite structures are

hierarchical in nature and are made up of substructures distributed across several length scales. The present day technology allows detection of single molecules.

The molecular scale (with nano scale as its subset) is the smallest scale at which modeling can be undertaken realistically. Nano-scale modeling has received further boost due to the recent advances in the synthesis of high-performance materials (like high performance concrete) using nanoscale material constituents. This development will eventually remove the knowledge gap on the interplay of molecular characteristics and continuum characteristics of engineering materials.

At nano scale, modeling can be undertaken by applying either the principles of molecular mechanics (Tomlinson, 1929) (Kontorova & Frenkel, 1938) or molecular dynamics. In molecular mechanics the molecule are treated as rigid balls connected by springs and depends strongly on concepts of bonding and involves energy minimization. Molecular dynamics involves deriving a set of equations of motion and solving these equations by discretization in time.

The equations of molecular (or atomic) motion are based on Newton's laws of motion, and the use of Lennard-Jones 6-12 Potential (Carey, 1999) (Liu et al., 2006). In other words, it shows how the molecules (or, atoms) in a system move with time in the nanosecond timescale (say, 10-15s).

If the coupled behavior of electrons and nucleus are considered, one needs to use complex quantum laws, such as Schrodinger equation. But as per Born-Oppenheimer approximation, the effect of electrons can be reasonably neglected. Thus, the movement of atoms involves the motion of nucleus only, and classical Newton's laws can be applied. As in many practical applications, it is necessary to consider the interaction of nanoscale behavior with the macro-scale behavior, multiscale modeling becomes necessary.

In Molecular Dynamics modeling, it is first necessary to determine the initial configuration of molecules (or atoms) through NMR spectroscopy, or X-ray crystallography. Initial molecular (or atomic) velocities are then assigned assuming random Gaussian distribution with zero mean and determine force F(xi) on individual molecule (or atom) (Fig. 13).

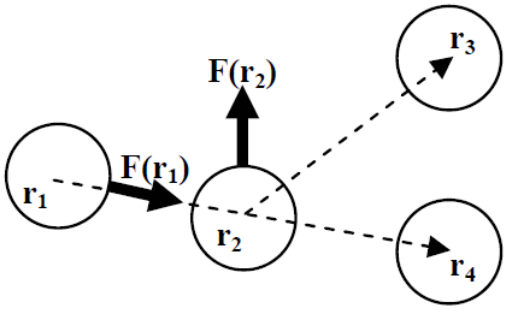

Figure 13: molecular velocities and forces - adapted from (Basu, 2007)

Newton's second law of motion is then applied to each molecule (or atom). The system is now advanced by a small time step during which the molecular forces are assumed to remain constant. The time steps may sometimes be of the order of femtosecond (1 fs =10-15sec). The molecular velocities and forces can now be calculated. In this manner the process can be repeated, as the simulation marches along time.

A typical plot of the Lennard-Jones potential V_{LJ} is shown in Fig. 14. Here the Lennard-Jones parameters σ and ε represent the collision diameter (the distance at which $V_{LJ} = 0$) and the distortion energy, respectively. These parameters are different for different interacting molecules. As for example, for water molecules, σ=0.316555 nm and ε=0.6501696 kJ/ml. The attraction results from induced dipole-dipole moment interaction between the particles.

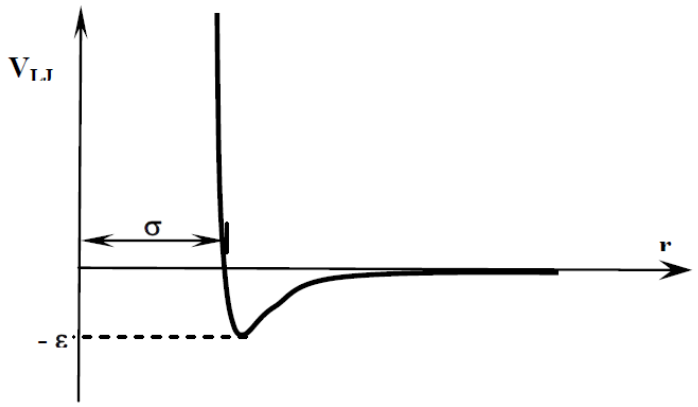

Figure 14: Lennard-Jones potential V_{LJ} - adapted from (Basu, 2007)

The steps involved in MD simulation are

1. Initialize values (Choose initial position and velocities of atoms)
2. Update molecular forces (Calculate forces from positions and potentials)
3. Set up equations of motion and solve for the selected time step, Δt (Calculate positions and velocities after time step Δt)
4. For t=t+Δt, compute physical quantities of interest (Calculate new forces)
5. Repeat step 2 onwards till maximum simulation time is reached (As the system evolves compute the average quantities of interest, like stresses, strains, pressure, volume, temperature, energy, etc.)
6. Compute the final results.

In problems of mechanics, the results of MD simulation can be used to compute stresses averaged over the N molecules using virial theorem (Tsai, 1979) (Zimmerman et al., 2004) and therefrom the mechanical properties.

2.2.8 Multiscale Modeling

A close examination of modern engineering materials will reveal different characteristics at different length scales. The objective of multiscale analysis is to qualify the load transfer between different length scales.

As for example, we can consider the case of laminated composites used in aircraft structures. In the macro-scale the property of the laminate as a whole is of interest. The next level is individual lamina, which in turn consists of high-strength fibers embedded in a lower strength matrix material. As long as the lamina is perfect, that is the fibers are straight, parallel, uniformly spaced, continuous (or unbroken), perfectly bonded with the matrix material, and are of uniform diameter and strength, the lamina properties are not difficult to define. The problem arises when one or more of these conditions are violated requiring further refinement of scale to account for the flaws which often cause geometrical singularities in the system.

Similar situation exists in the case of high performance concrete used in modern bridge structures because of the constituents used in such concrete. In the case of subsurface contaminant transport phenomenon, one needs to account for the effect of grossly inhomogeneous character and complex material structure of the substrata on the large scale flow characteristics through multiscale modeling. So, it is necessary to develop methods to define load transfer processes between length scales in deterministic sense and in statistical sense for systems with uncertainties. This will allow the definition of accurate macro-scale properties reflecting the behavior in finer scale, say, at the microstructure scale.

First, this will involve up scaling of the microscale characteristics to the macroscale through homogenization process. Very often engineering materials have a periodic microstructure which can be taken advantage of in the multiscaling process. The homogenization process enables the computation of average stresses and strains in the limit as the size of the periodic cell goes to zero. Next it will involve down scaling of the average response at the macroscale to the microscale to predict behavior at the micro scale so that damage initiation or propagation can be monitored.

Apart from multiple spatial scales, multiple temporal scales may also need to be considered. For instance, in the case of fatigue and fracture problems, multiple temporal scales coexist multiple spatial scales due to the wide difference between the period of a single load cycle acting on a structural component, which may be in the order of seconds, and the overall design life, which may span years. The multiple spatial scales exist in such problems, due to the presence of micro- size cracks or inclusions with respect to the large size of a structural component.

As the behavior of many modern engineering materials is controlled by processes subject to wide range of length and time scales, the objective of multiscale modeling is to capture relevant physics from all the scales by coupling the computations at different scales. This can be undertaken by adopting one of the following two schemes.

a) Hierarchic (or sequential) scheme: Undertake separate simulations at each selected scale passing on the results to the neighboring scale – this can happen from coarse to fine scale, or vice versa (Fig. 15). In this approach the computational simulations are undertaken at one scale and quantities that can be used to define parameters of the model applicable on a longer scale are extracted.
b) Undertake simultaneous coupled simulations with different scale resolutions in different regions of the problem domain (or discrete patches covering it), as needed. The patches are overlapped at the boundaries with each other applying the boundary values of one patch as the boundary condition of the other patch and vice-versa. This approach is considered to be more efficient.

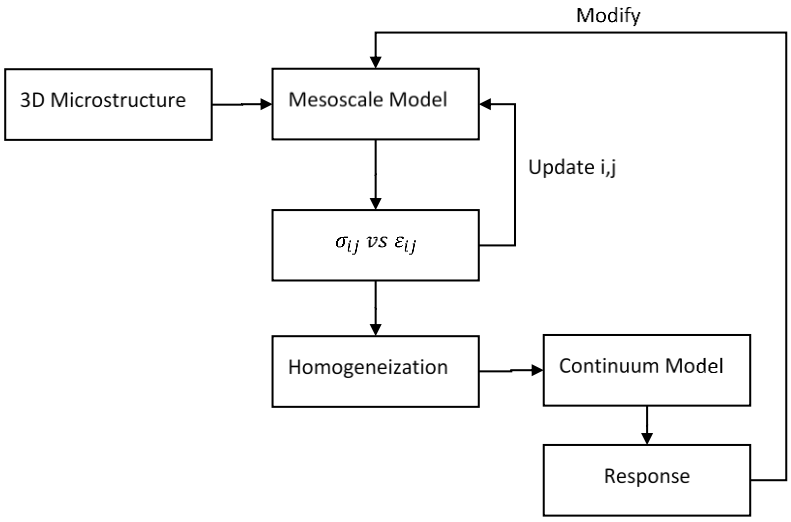

Figure 15: Hierarchic Scheme for Mechanics Problems - adapted from (Basu, 2007)

In analyzing heterogeneous medium, the mathematical homogenization theory (Bensoussan et al., 1979) (Sanchez-Palencia & Zaoui, 1985) has normally been used. The hierarchic scheme uses the assumption of microstructural periodicity and uniformity of macroscopic field within a unit cell domain, and the homogenization process decomposes the heterogeneous medium problem into the cell problem in the micro scale, and the continuum problem in the macro scale (Aboudi, 1991) (Aboudi, 1996). As shown in Fig. 18, the computational steps at an instant of time consist of

- Identification the representative volume element (RVE) and discretization into a regular grid of cells.
- Calculation of the cell problem
- Determination of the homogenized material properties
- Calculation of the continuum problem
- Evaluation of the results in the micro-scale
- Repetition of the above steps till convergence

In the case of composites, the constitutive properties of the matrix material, tye fibers, and fiber-matrix interface needs to be considered. For the interface, (Aboudi, 1991) used a bilinear model but more recently a model based on cohesion due to Needleman (Needleman, 1987) (Needleman, 1990b) (Needleman, 1990a) has become more popular. Accuracy of the above simulation scheme is largely dependent upon the validity of the assumptions of periodicity and uniformity. For instance, near steep stress gradient regions, the assumption of local uniform stress field in a unit cell is no more valid requiring the use of higher norms of local stress field. In general, these can be effectively addressed in the context of risk and reliability analysis.

2.2.9 Multiphysics Modeling

In engineering design it is necessary to allow for simultaneous influence of multiple physical and chemical phenomena, sometimes, requiring consideration of mutual interactions between them. The interactions may need to be considered at governing equations level, or at the constitutive laws level.

An example of the latter is diffusion process controlled by temperature. The solutions from an individual discipline may act as input for another discipline. This approach may be acceptable in the case of weakly coupled systems, but in the case tightly coupled systems this may not be acceptable. Typical examples of multidisciplinary coupling in modeling and simulation in science/engineering are given below (Basu, 2002).

- Structural-thermal: Thermal stress analysis of Highway Bridge structure allowing for coupling between stress analysis and heat transfer.
- Fluid-structure: Aeroelastic analysis of airplane structure allowing for interaction between airflow and structural response; or, action of waves on maritime structures or ships.
- Fluid-structure-thermal: Welded joint analysis beginning with weld metal deposition to cooling down to ambient temperature.
- Magneto-thermal: Induction heating analysis of, say, annealing process of electrically conducting material allowing for coupling between electromagnetic field and heat transfer.
- Acoustic-structure: Acoustic response of aeronautical structures and automotive structures.
- Magneto-structure: Structural response caused by transient magnetic field such as in the case of a speaker.
- Electro-structure: Piezoelectric sensor modeling allowing coupling between deformation and voltage distribution.
- Advection-diffusion-dispersion: Modeling of groundwater flow associated with pollution transport and remediation.
- MD-DD-CM: Multiphysics/multiscale modeling and simulation of radiation damage to nuclear reactor pressure vessel steel by using coupled molecular dynamics, damage dynamics, and continuum models.
- QM-MD-CM: Coupling of quantum mechanics, molecular dynamics and continuum modeling and simulation of carbon nano-tube devices.

The groundwater pollution transport problem mentioned above is a multiphysics, multiscale, and multiphase inhomogeneous porous media problem. The processes involved are advection, dispersion, adsorption, and decay requiring hierarchic modeling from pore-throat scale to the pore scale, to the core scale and beyond culminating at the field scale.

The problem involves three phases – fluid, solid, and vapor. During the remediation process, other physics components may be involved wrought by thermal enhancement, intrinsic bioremediation, electro-kinetics, etc. Number of, so called; grand challenge problems are also highly complex multiphysics/multiscale problems. For instance, the modeling of earth's crust primarily involves coupling between rock mechanics (elastic-plastic rheology), fluid flow (Darcy's law), thermal transport (Fourier's law), and chemical processes.

Another example is the weld cooling problem at a structural joint. This in fact is a coupled fluid-thermal-structural interaction problem. The fluid flow phenomenon during the weld deposition process is usually ignored, and the problem is traditionally treated as a two-stage process involving phase change in weld metal from liquid to solid. In the first stage, the heat transfer problem is solved to determine the temperature distribution. In the

second stage, thermal stress analysis is undertaken using the temperature distribution disclosed in the first as input.

If the governing equations are tightly coupled, the equations for all the disciplines are considered simultaneously, often, require allowing for nonlinearities. This approach may also be used in the case of loosely coupled system, if a large amount of data needs to be exchanged between different disciplines.

Other reasons for doing so in the case of loosely coupled and moderately coupled systems are:

a) difficulty in properly synchronizing the discipline modules;
b) proper mapping of transferred results from one module to another;
c) difficulties in monitoring of error and convergence characteristics of the results.

A big advantage favoring loose coupling is the existence of codes for individual disciplines. A major disadvantage of tightly coupled systems is that the code is very difficult to implement, especially, in the case of highly complex systems. Whereas, in the case of a moderately coupled system, the dominant disciplines is treated as primary, and the effect of other disciplines are added on after introducing some simplifications.

For instance, in the case of fluid-structure interaction simulation of a submarine, computational fluid dynamics (CFD) is the dominant feature and the simplified structural aspects of the problem will be added to CFD code. In the simplest model, the submarine can be treated as a rigid body and interaction with deformations is not accounted for.

2.2.10 Integrated Systems

The global economy of this millennium requires the development of superior products cheaply and quickly. Also, for instance, in the case of civil infrastructure, apart from safety and functionality, the emphasis is on life-cycle cost reflecting factors like projected life, risks, first cost, maintenance cost, replacement cost at the end of useful life, etc. In a nutshell, the driving force is the development of an optimal solution allowing for all the factors involved in the multi-disciplinary environment.

Another interesting example is that of a commercial aircraft design, which requires accurate prediction of its flight characteristics controlled by the interaction of disciplines like aerodynamics, structural dynamics, solid mechanics, acoustics, propulsion, thermodynamics, controls, and manufacturing processes, and the involvement of stakeholders like owners, pilots, flight attendants, maintenance people, passengers, environmental agencies, etc.

In designing Model 777, and its, decedent Model 787, commercial aircraft, Boeing fully exploited the interdisciplinary approach when 238 cross-functional design-build teams produced a paperless design that allowed engineers to design every component, electronically simulate the assembly process to eliminate errors in fitness and assembly process.

In the process, alternative designs could be evaluated as single integrated units before actual assemble and test flights. This eased the transition from the design stage to production for actual commercial introduction. Boeing has used similar concept design-build concept to the International Space Station with a mass of about one-half million

kilogram representing one of the largest and, perhaps, the most complex engineering project in history involving interdisciplinary effort of international scope.

It is obvious from above that in the global market place, in undertaking a new project, time-consuming trial-error approach require to be minimized. It is important that all aspects of realization of a new project (or product) – design, manufacture or construction, cost, reliability, and support process, be considered at the earliest stage.

To avoid unforeseen problems late in the design process, it is important to undertake design evaluations throughout the design process accounting for all possible interactions. It may be emphasized that the design process in many modern projects is prone to complex multidisciplinary interactions of a number of physical disciplines over several length and time scales. This no doubt is in sharp contrast to the conventional practice of using one discipline at a time.

As for example, in the case of a highly complex structure like high-speed airplane, the practice has been to simulate for each discipline, as stated earlier, individually and the effects of mutual interaction sorted out mostly through numerous expensive prototype tests over a considerable length of time. In opposition to this approach, modeling and simulation allowing for interaction amongst these disciplines will lead to significant savings in cost and development time can be achieved (Basu, 2002). For example, in the coupled dynamic stability analysis of an airplane, the interaction between aerodynamics, elastodynamics, and control theory are used (Crisfield, 2001). In addition, if piezoelectric controls are used, electromechanical coupling will also need to be considered.

2.2.11 Risk and Reliability

Engineering design is based on mathematical models, which are driven by all kinds of information based on experiments, observations, intuition, experience, assumptions, etc. which cannot by any stretch of imagination be considered as highly accurate. The response of the system being designed is predicted by exercising (or making simulation runs) on the mathematical model will have a degree of uncertainty due to inaccuracies in the information supplied.

Additional uncertainties are introduced during the execution of a project due to poor workmanship due to deficiencies in materials and methods used, errors, etc. Under these circumstances, it is not possible to predict the performance of a designed and built system in absolute terms or deterministically.

In order to account for the uncertainty of the parameters controlling the response of a system, it is necessary to undertake probabilistic simulation assuming that the sensitive parameters of the system are random in nature. In order for this to be possible, it is necessary to have enough information about the random nature (or distribution characteristics) of a parameter of interest. In the absence of adequate experimental data for a random variable, one of the available standard distributions based on qualitative judgment is used.

In reliability-based design, the objective is to proportion a structure so that the probability of failure, P_f, does not exceed certain threshold value. In structural engineering terms, the common formal procedures of reliability analysis are first order reliability methods (FORM), second order reliability methods (SORM), and Monte Carlo method (Ang & Tang, 1984) (Haldar & Mahadevan, 1999) (Shinozuka, 1983).

Of these, the last method is very compute intensive and essentially is a brute force method. In this method, once the probability function is defined, random sampling is followed by Monte Carlo simulation. After large enough number of such simulations, statistical analysis of the outputs of interest is undertaken to obtain quantities like expected value and standard deviation. This can be followed by the computation of reliability index β given by

$$\beta = \frac{\mu_R - \mu_Q}{\sqrt{\sigma_R^2 + \sigma_Q^2}} \tag{3}$$

Here, μ_R and μ_Q are expected values of resistance (R) and load effect (Q), and σ_R^2 and σ_Q^2 are variance of resistance and load effect. Graphically, reliability index signifies the shortest distance from the origin to the limit state function, $g(Z_R,Z_Q)$, where Z_R and Z_Q are the reduced variables defined as below. Larger the reliability index smaller is the probability of failure. For instance, if $\beta=2.33$, the probability of failure in 1 in 100.

$$Z_R = \frac{R - \mu_R}{\sigma_R} \quad \text{and} \quad Z_Q = \frac{Q - \mu_Q}{\sigma_Q} \tag{4}$$

Risk and reliability methods have lately matured lately. Component level reliability evaluations are being extended to systems level. Significant efforts are being made towards reliability-based optimization of systems, including multidisciplinary problems. Uncertainties introduced by the choice of mathematical model as well as the discrete numerical technique used in predicting the response are also being looked at.

In civil engineering design, purely deterministic design approach based on the use of safety factors have been replaced by load and resistance factor design (LRFD) which uses different uncertainty factors (load factors) with different external effects representing the demands on the system, and another set of uncertainty factors (resistance factors) applied to capacity measures (limit states) of the system.

These factors indirectly allow for the randomness of various design parameters without the need for undertaking formal risk and reliability (or probabilistic) analysis (Ellingwood & Galambos, 1982) (Thoft-Christensen & Baker, 1982). In railroad and automotive industries there is some interest to use probabilistic methods mainly for investigative purposes. In the aerospace industry also there is an ongoing effort to look at the possibility of adopting some of the risk and reliability methods in aerospace vehicle design, primarily, prompted by the US Department of Defense.

A number of reliability analysis, methods, formulations and applications have been proposed, for different types of problems. One can cite, for example, a study on formulations of the discretization of random fields in reliability structural analysis (Jorge, 2004), and a study of an application of reliability analysis for the design of a helicopter composite armor, with correlated design variables (Santos et al., 2016).

2.2.12 Optimization

Designing a system is an iterative process in which the design variables are adjusted to reach the levels which will lead to the best possible outcome. In other words, the final objective is to improve an existing design or replace an unacceptable design by one that meets the given requirements, that is, choosing the best possible design that satisfies all the special constraints.

This is called optimum design, which can be arrived at intuitively (that is, indirectly) or logically (that is, directly). The intuitive approach is based on past engineering experience and involves random selection and evaluation. On the other hand, the formal design optimization follows a logical approach to arrive at the optimal design.

The formalities include defining the behavioral constraints, the side constraints, and the objective function which is minimized or maximized. The objective may be weight minimization, cost minimization, quality maximization, or maximization of value, which is combination of cost and value. Other objectives can also be used, like minimizing vibrations in a vehicle (Wang et al., 2003) (Wang et al., 2004). The final objective is to achieve competitive advantage in today's global economy.

Mathematical programming algorithms include linear programming, nonlinear programming, geometric programming, dynamic programming, etc. (Rao, 2019) (Arora, 2012). Lately, genetic algorithms and neural networks have been used quite efficiently for certain types of optimization problems.

Genetic algorithms are evolutionary algorithms inspired by evolutionary biology and use techniques like mutation, selection, inheritance, and crossover in the abstract representation of candidate optimal solutions that evolve towards better solutions. Genetic algorithms are implemented as a computer simulation in which a population of abstract representations (called chromosomes or the genotype or the genome) of candidate solutions (called individuals, creatures, or phenotypes) to an optimization problem evolves toward better solutions.

A neural network consists of a network of simple processing elements with complex global characteristics, determined by the connections between the processing elements and element parameters. The genetic algorithm technique has been found to be extremely effective for small to medium sized constrained optimization problems.

However, in the case of more computational resource intensive complex problems, a combination of neural networks and genetic algorithm tend to improve the situation. In linear programming both objective function and the constraints are linear functions of design variables.

In civil engineering design, the objective function and/or the constraints are mostly nonlinear functions of design variables. In most cases, linear programming cannot be used, except when the nonlinear programming problem can be transformed into an equivalent linear programming problem.

A large number of software have been developed based on these algorithms and also encoded in many commercial modeling and simulation software. Also, software like GENESIS by VR&D was especially developed with the primary objective of design optimization. In addition, software for optimal design search, such as DOT by VR&D (Ghosh & Vanderplaats, 1997), which can be integrated with regular modeling and simulation software, are also available. In view of the fact that much of the design variables are random in nature, there is a surge towards reliability-based optimum design. The objective is to arrive at the optimum values of the design variables with a certain specified level of reliability. Software undertaking such optimization should also be able to undertake design sensitivity analysis to identify the critical design variables.

Another twist to optimization process appears when the objective functions and constraints represent a number of disciplines which may be coupled in some manner. In

this case, instead of a single objective function, multiple objective functions may need to be satisfied. Getting an optimal solution for such multidisciplinary problem is a more challenging proposition, especially when randomness of design variables is also considered. Another area of current interest allied to optimization process is the inverse problem in which for a given system response it is necessary to arrive at the design variables which will enable it.

There is significant increase in research effort research in the field of structural optimization in recent decades. The increasing interest in this field has been strongly boosted by the advent of reliable discrete numerical modeling tools, advances in design sensitivity analysis, and methods of mathematical programming, along with the exponentially increasing speed and capacity of digital computers.

2.3 Some Remarks in Modeling and Simulation Tools

This probably is the most challenging time for those using modeling and simulation tools as part of the engineering design process to effectively respond to the strong technological competition, which demands reduced design time and cost of products with greater functionality and higher quality, coupled with present day emphasis on energy savings, material recycling, and sensitivity to environment.

With ever-increasing power of digital computers coupled with continuous improvement of mathematical models and the significant advancement of numerical simulation techniques, the future for more accurate prediction of system behavior leading to optimal design of efficient systems meeting the global challenge seems to be bright. This section may be considered simply as an attempt to scratch the surface of this vast and expanding field.

3 On Error Estimators in Computational / Numerical Methods

The various discretized integral representations of Boundary Value Problems (BVP), including, for example, Finite Element Methods (FEM) and Boundary Element Methods (BEM) will produce results with some error with respect to the exact solution.

Some possible sources of error are inherent to almost all formulations, when these formulations are applied to a non-trivial problem. Several sources of error may be present in the numerical model of a problem. Some sources of error may play an important role in specific formulations, or may be inherent to a certain formulation. What source of error is the most important in a particular problem may depend on the representation being adopted. The same applies to the sensitivity of the response error due to a specific source.

The first source of error may be in the modeling of the problem. The importance of an error source in a certain representation depends on the problem being modeled. For example, corners may have different influences in the problem, depending if it is a potential problem or an elastostatics one, because corners will lead to discontinuous derivatives, and these discontinuous derivatives satisfy different relationships in each problem.

The potential problem is modeled by a scalar formulation derived from Laplace's equation. Normal and tangential derivatives will be discontinuous at these corners. The gradient of the potential is a continuous function in the interior domain. This gradient can

be written into components in two or three orthogonal directions, depending if it is a 2-D or 3-D problem. When taking the limit to the boundary, if the boundary is smooth, this gradient can be written in tangential and normal components, with the tangential and normal directions considered at the point in the boundary to where the limit was taken. The smoothness of the boundary guarantees that these directions are unique at some point in the boundary, so the decomposition of the unique gradient of the potential is also done in unique components. Now, if there is a corner, although the gradient could be considered as continuous in the limit process from an interior point to the boundary, its decomposition would be in different tangential and normal directions for the different elements sharing that point of the boundary. This circumstance leads to a different decomposition of the same gradient vector. Therefore, a relationship exists between tangent and normal components of the gradient vector in the two elements sharing the corner, by means of a simple rotation in the local coordinate system.

In elastostatics, normal and tangential derivatives of the displacement are the tractions, and they will also be discontinuous at the corners. A different relationship exists between theses derivatives in the two boundary elements sharing the corner. Hooke's law can be written for a small domain element having the two adjacent boundary elements as parts of its own boundary. As the stress in the interior of this domain element is continuous, a relationship appears between the tractions in the two boundary elements sharing the corner, to satisfy equilibrium in the domain element.

The second source is the round-off error. The round-off error may be different for different integral representations of the same problem. The parameter that controls this error is the condition number of the matrices obtained for a certain formulation. The condition number is the ratio between the greatest and the lowest eigenvalue of the obtained matrix of the system of equations. If the magnitude of this number is written as a power of 10, say, 10m, then m is the number of digits that shall be discarded in the numerical solution, because these digits are not significant, and contain only the error. A comparison between the condition number of the matrices as obtained from two different BEM formulations may show, for instance, the formulation where more round-off error is introduced.

The third source is errors in the evaluation of parameters that may be necessary in some formulations, like the tangential derivatives of the potential or the displacement. Tangential derivatives are obtained, in general, as a post-processed result, by taking local derivatives of the displacements in the tangential direction. For a 2-D element, the derivative in the tangential direction is the derivative with respect to the intrinsic coordinate ξ. Then the gradient is obtained combining the normal and the tangential derivatives. For isoparametric elements, the tangential derivative is, then, one degree less than the normal derivative. For example, if the element is quadratic, the displacement and the normal derivative are written in terms of quadratic shape functions, while the tangential derivative, which is the derivative of the displacement in the ξ direction, has linear shape functions. The gradient is, then, obtained in a somewhat "unbalanced" manner. The error introduced by the approximation in the tangential derivative is likely to be more significant in the regions of the boundary in which the tangential derivative is changing very fast, as its representation with shape functions that are one degree less is poorer than the representation of the normal derivative.

The fourth source is the discretization error. Usually this discretization error can be global or local. When a local error estimator is used, then an adaptive procedure to mesh refinement can be adopted.

Other sources are errors due to approximations of the boundary shape and errors due to simplifications or approximations on the intrinsic necessary hypothesis of a specific representation. For example, not all representations allow for discontinuities or non-smoothness in the boundary. So, if corners are present, an error may be introduced in some representations.

Besides the above-mentioned deterministic errors, the inherent randomness of the problem may be itself a source of additional stochastic error terms, which might appear due to uncertainties in the various parameters and variables of the problem, such as the material properties, the geometry, the boundary conditions, the loading, etc. These uncertainties may be treated through modeling these parameters and/or variables as:

- random variables (mean and standard deviation are constant over time and over position);
- random fields (mean and standard deviation are constant over time, but variable over position)
- stochastic processes (mean and standard deviation varying over time, but constant over position)
- a mixture of the above cases.

3.1 Error Estimators in Finite Element Methods (FEM)

3.1.1 Introduction

This section presents a summary of the discussion as presented in (Huebner et al., 2008). If the exact 2-D solution for a problem $T(x,y)$ is known, then the error associated to the finite element solution for this problem $T_{FE}(x,y)$ can be written as:

$$E(x,y) = T(x,y) - T_{FE}(x,y) \tag{5}$$

One can note that the error varies over the solution domain.

Global error estimation

Global error estimation procedures:

- need to know *a-priori* the exact solution;
- use some norm of the error over the domain. Example:

$$L_2 norm : \left\| E \right\|_{L_2} = \left[\int_\Omega E_2 dA \right]^{\frac{1}{2}} \tag{6}$$

- evaluate this integral over each element and sum it over all elements.

For elliptic boundary value problems:

$$\left\| E \right\|_{L_2} = Ch^p \tag{7}$$

where:

- C is a constant;

- h is a parameter that depends on mesh size. It is related to some characteristic element dimension;
- p is an integer. It depends on the order of the interpolating functions.

If the equation in vector form is

$$[L]\{u\} = \{b\} \tag{8}$$

Where *[L]* is an adjoint linear operator, then:

$$\|E\|_{L_2} = \left[\int_\Omega \{E\}^T [L]\{E\}\, dA\right]^{\frac{1}{2}} \tag{9}$$

Possible refinements to make $\|E\| \to 0$ are:

- h- refinement. It is performed decreasing the element dimensions;
- p- refinement. It is performed increasing the order of the interpolating functions;
- r- refinement. Remeshing is done by repositioning the nodes, for same h and p.

Local error estimation

If the exact solution is not known a local error estimation procedure can be adopted. One example of this procedure is the local error estimation based on the interpolation error.

One-dimensional problem

The following development is done, for simplicity, for a one-dimensional problem.

Expansion in Taylor series about a point:

$$E(x) = E(\bar{x}) + \frac{dE}{dx}|_{\bar{x}}\,(x-\bar{x}) + \frac{1}{2}\frac{d^2E}{dx^2}|_{\bar{x}}\,(x-\bar{x})^2 + \cdots \tag{10}$$

Where the higher order terms for x are neglected in a vicinity of $\bar{x}$. Take $\bar{x} = x_M$, the point in one element where error is a local maximum. Then $\frac{dE}{dx}(x_M) = 0$. Figure 16 illustrates the case.

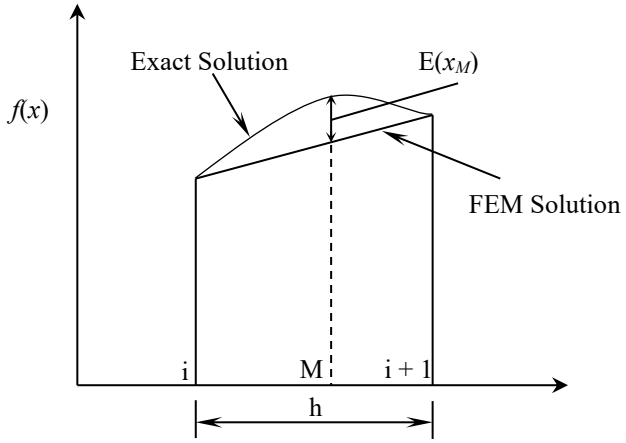

Figure 16: FEM solution error - adapted from (Huebner et al., 2008)

Assume that the FE solution is exact at the nodes. This is valid for $\frac{d^2T}{dx^2} = Q$ (and, in particular, for Laplace's equation, which is this equation when Q = 0). But this is only approximate for other equations.

For $x = x_i$:

$$0 = E(x_i) = E(x_M) + \tfrac{1}{2}\tfrac{d^2E}{dx^2}|_{x_M}\,(x_i - x_M)^2 \Rightarrow E(x_M) = -\tfrac{1}{2}\tfrac{d^2E}{dx^2}|_{x_M}\,(x_i - x_M)^2 \tag{11}$$

For $x = x_{i+1}$:

$$0 = E(x_{i+1}) = E(x_M) + \tfrac{1}{2}\tfrac{d^2E}{dx^2}|_{x_M}\,(x_{i+1} - x_M)^2 \Rightarrow E(x_M) = -\tfrac{1}{2}\tfrac{d^2E}{dx^2}|_{x_M}\,(x_{i+1} - x_M)^2 \tag{12}$$

Where either $|x_i - x_M| \le \frac{h}{2}$ or $|x_{i+1} - x_M| \le \frac{h}{2}$. This leads to

$$|E|_{(e)} \le \frac{1}{8}\left|\frac{d^2E}{dx^2}\right|_{x_M} h^2 \tag{13}$$

which is an estimate for the interpolation error at element (e). As $|\frac{d^2E}{dx^2}|_{x_M}$ is unknown, it is approximated by

$$\left|\frac{d^2E}{dx^2}\right|_{x_M} \cong \left|\frac{d^2T_{FE}}{dx^2}\right|_e \tag{14}$$

This is not anymore an estimate of the error, but just an error indicator. If, in particular, T satisfies Laplace's equation, then

$$\frac{d^2E}{dx^2} = \frac{d^2T}{dx^2} - \frac{d^2T_{FE}}{dx^2} = -\frac{d^2T_{FE}}{dx^2} \tag{15}$$

Because $\frac{d^2T}{dx^2} = 0$. In this case

$$\left|\frac{d^2E}{dx^2}\right|_{x_M} = \left|\frac{d^2T_{FE}}{dx^2}\right|_{x_M} \tag{16}$$

But even in this case, Equation 14 is still just an approximation as $|\frac{d^2T_{FE}}{dx^2}|_{x_M}$ is in this equation considered to be the same (constant) for the entire element (e).

Two-dimensional problem

Similarly, for a two-dimensional problem:

$$|E|_{(e)} \le \frac{1}{8}\left(|\frac{\partial^2 T_{FE}}{\partial x^2}|_{x_M} + 2|\frac{\partial^2 T_{FE}}{\partial x \partial y}|_{x_M} + |\frac{\partial^2 T_{FE}}{\partial y^2}|_{x_M}\right)h^2 \tag{17}$$

From the above equation, it can be seen that 2nd derivatives of FE solution have to be computed, for error estimation. A procedure to smooth the gradient to compute these derivatives with good accuracy is called gradient recovery.

Gradient recovery

If FE solution is linear, then nodal 2nd derivatives are evaluated from a weighted average of element derivatives surrounding the node. The weighting factors are the element areas.

From $\left\{T^{(e)}\right\}$ it can be written:

$$\left(\frac{\partial T}{\partial x}\right)^{e} = \left\lfloor \frac{\partial N}{\partial x} \right\rfloor \{T\}^{(e)} \tag{18}$$

The derivatives are now written in an average sense

$$\left(\frac{\partial T}{\partial x}\right)^{e}_{AVE} = \lfloor N \rfloor \left\{\frac{\partial T}{\partial x}\right\}^{(e)}_{AVE} \tag{19}$$

to find $\left\{\frac{\partial T}{\partial x}\right\}^{e}$. It can now be written:

$$\int_{\Omega^{(e)}} \{N\} \lfloor N \rfloor dA \left\{\frac{\partial T}{\partial x}\right\} = \int_{\Omega^{(e)}} \{N\} dA \frac{\partial T}{\partial x}^{(e)} \tag{20}$$

This is a system of equations from which the vector of nodal derivatives $\left\{\frac{\partial T}{\partial x}\right\}^{(e)}$ can be obtained. The same approach can be used for the 2nd derivatives. From $\left\{\frac{\partial T}{\partial x}\right\}^{(e)}$:

$$\left(\frac{\partial^2 T}{\partial x^2}\right)^{e} = \left\lfloor \frac{\partial N}{\partial x} \right\rfloor \left\{\frac{\partial T}{\partial x}\right\}^{(e)} \tag{21}$$

2nd derivatives can now be evaluated in this same average sense:

$$\int_{\Omega^{(e)}} \{N\} \lfloor N \rfloor dA \left\{\frac{\partial^2 T}{\partial x^2}\right\} = \int_{\Omega^{(e)}} \{N\} dA \frac{\partial^2 T}{\partial x^2}^{(e)} \tag{22}$$

This is a system of equations from which the vector of nodal 2nd derivatives $\left\{\frac{\partial^2 T}{\partial x^2}\right\}^{(e)}$ can be obtained. Figures 17 and 18 illustrate the smoothing process to obtain the refined gradient from the FE solution.

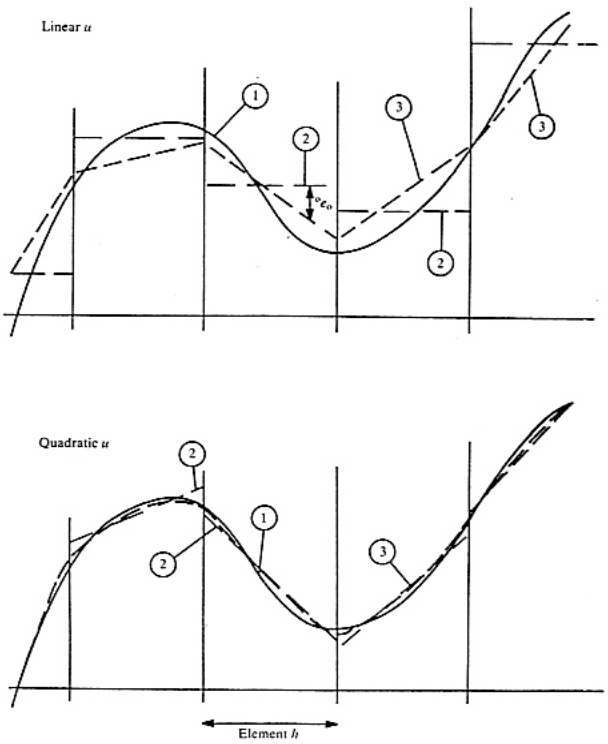

Why projection gives higher order approximation (1) σ Exact solution. (2) $\hat{\sigma}$ FEM solution = least square approximation to σ (discontinuous). (3) σ^* projected solution = least square approximation to $\hat{\sigma}$ (continuous high order)

Figure 17: Higher order approximation for the gradient - adapted from (Olgierd C. Zienkiewicz & Taylor, 1994)

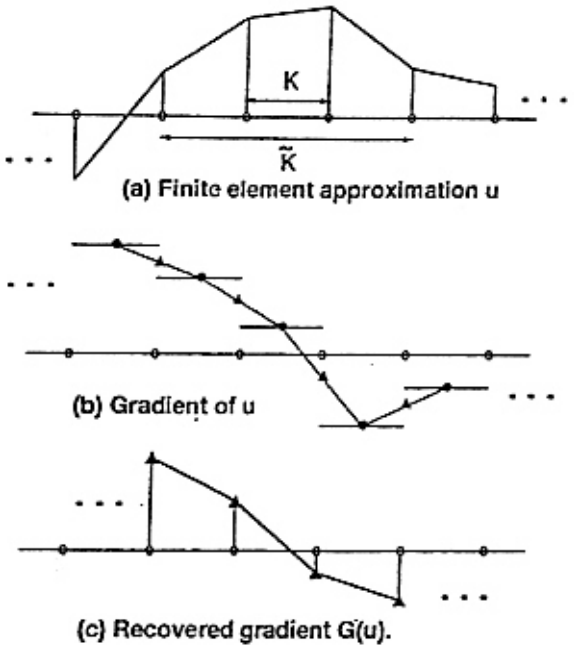

Construction of recovery operator $G_X = G$ from piecewise linear approximation in one dimension.

Figure 18: Construction of recovered gradient - adapted from (Ainsworth & Oden, 1997)

3.1.2 Error Estimates and Adaptive Finite Element Refinement

This section follows the discussion as presented in (Huebner et al., 2008) and in (Olgierd C. Zienkiewicz & Taylor, 1994). Error estimators are used in adaptive remeshing. The goal is to have constant error throughout the domain, or to have the error uniformly distributed throughout the mesh.

- 1-D: find h such that

$$h^2 \left| \frac{d^2T}{dx^2} \right| = Constant \tag{23}$$

- 2-D: find eigenvalues λ_1, λ_2 and corresponding eigenvectors $\mathbf{x}_1$, $\mathbf{x}_2$ of the matrix

$$\begin{vmatrix} \frac{\partial^2 T}{\partial x^2} & \frac{\partial^2 T}{\partial x \partial y} \\ \frac{\partial^2 T}{\partial x \partial y} & \frac{\partial^2 T}{\partial y^2} \end{vmatrix} \tag{24}$$

such that

$$h_1^2 |\lambda_1| = h^2 |\lambda_2| = Constant \tag{25}$$

Where h_i is the element size in the direction of the eigenvector $\mathbf{x}_i$ corresponding to the eigenvalue λ_i. With this, an h refinement process is obtained. Figure 19 illustrates the process.

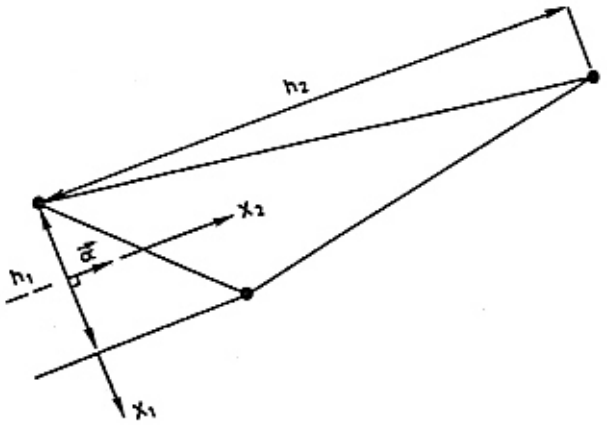

Figure 19: Resizing the mesh - adapted from (Huebner et al., 2008)

Errors and adaptivity

The general procedure is

(a) Find the error, i.e., the *a-posteriori* estimate. For an elasticity problem , the errors could be:
   - in displacement: $e_u = u_{Exact} - u_{FE}$
   - in stress: $e_\sigma = \sigma_{Exact} - \sigma_{FE}$

(b) Use this information on the error to refine the approximation. Refinement methods could be *h*-, *p*-, *hp*- or *r*-. Adaptive refinement process is used for optimal results. Figure 20 illustrates the refinement process.

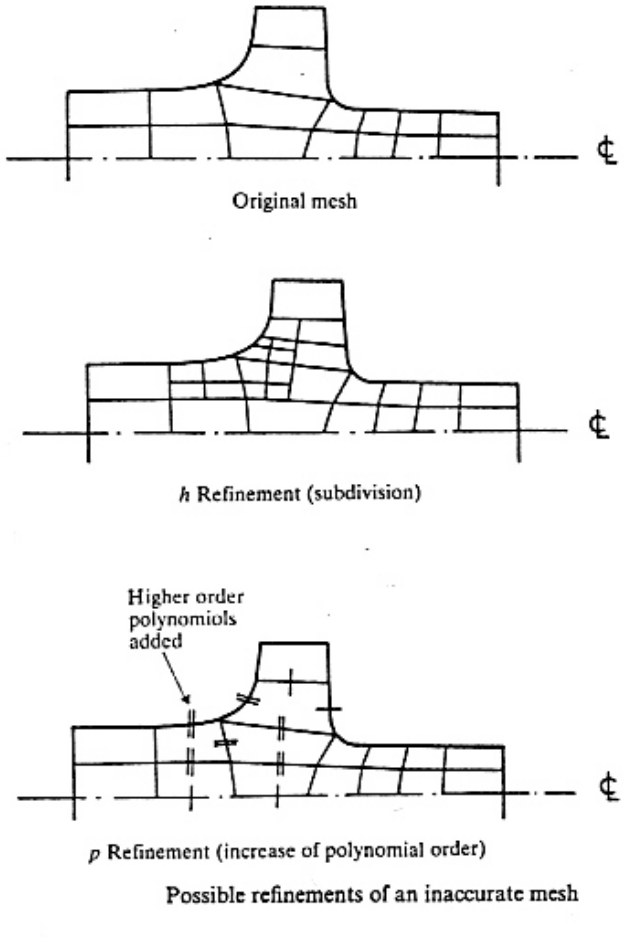

Figure 20: h- and p- refinements -adapted from (Olgierd C. Zienkiewicz & Taylor, 1994)

Error norms and convergence rates

Let $Lu + P = 0$ and $\sigma = D\varepsilon$ be the equations for elasticity problem. Different norms can be defined:

• Energy norm:

$$\|e\|^2 = \int_\Omega e^T L e d\Omega = \int_\Omega (u_{Exact} - u_{FE})^T L (u_{Exact} - u_{FE}) d\Omega \int_\Omega (\sigma_{Exact} - \sigma_{FE})^T D^{-1} (\sigma_{Exact} - \sigma_{FE}) d\Omega \tag{26}$$

• L_2 norm for displacement error:

$$\|e_u\|_{L_2}^2 = \int_\Omega (u_{Exact} - u_{FE})^T (u_{Exact} - u_{FE}) d\Omega \tag{27}$$

• L_2 norm for stress error:

$$\|e_\sigma\|_{L_2}^2 = \int_\Omega (\sigma_{Exact} - \sigma_{FE}) T (\sigma_{Exact} - \sigma_{FE}) d\Omega \tag{28}$$

Total error in the entire domain is the sum of the errors in all elements.

$$\|e\|^2 = \sum_{i=1}^{m} \|e\|_i^2 \tag{29}$$

Convergence rate is the slope of the curve error (in non-dimensional form) and the number of degrees of freedom of the FEM mesh used. The biggest this slope, the faster convergence is attained with the same refinement. Figures (21) and (22) illustrate the differences in convergence rates when there is a singularity. This example shows that there is a need for highly refined meshes in a vicinity close to a singularity.

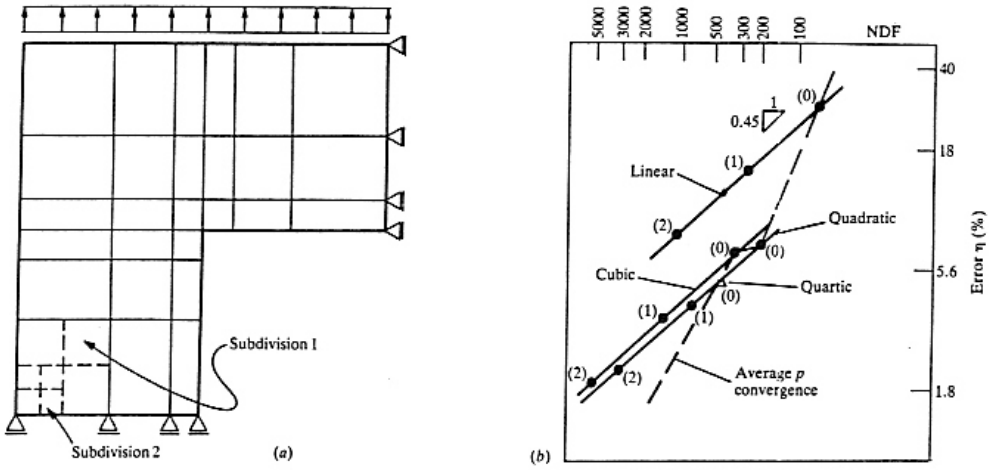

Analysis of an L-shaped domain with singularity. h convergence for various p values. Plane stress $E = 1$, $\nu = 0.3$. (a) Initial mesh (0) and uniform subdivisions (i). (b) % error (η) versus NDF (number of degrees of freedom)

Figure 21: L-shaped domain with singularity (Olgierd C. Zienkiewicz & Taylor, 1994)

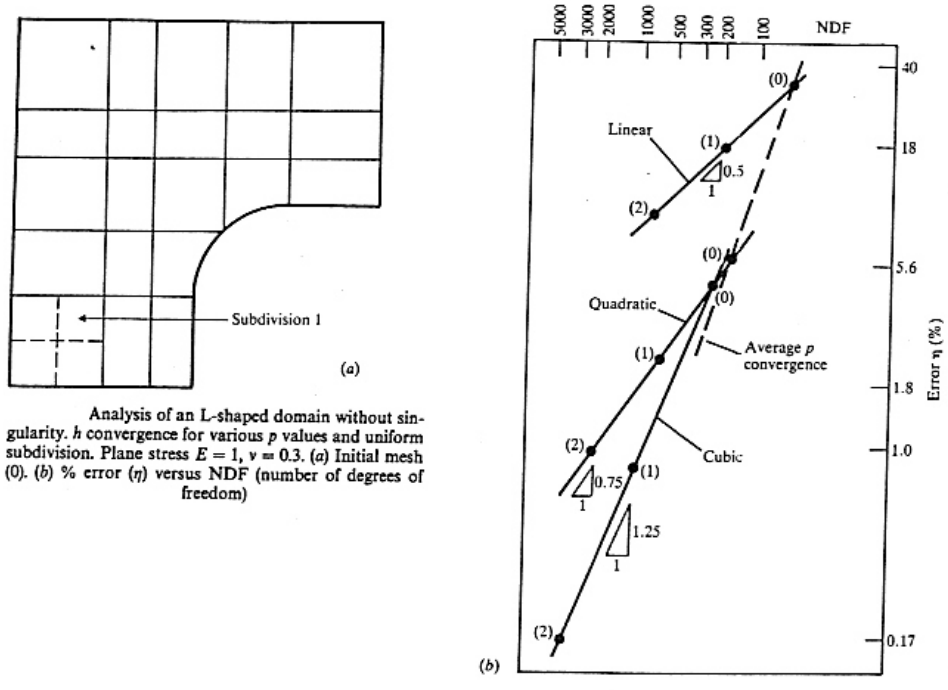

Analysis of an L-shaped domain without singularity. h convergence for various p values and uniform subdivision. Plane stress $E = 1$, $\nu = 0.3$. (a) Initial mesh (0). (b) % error (η) versus NDF (number of degrees of freedom)

Figure 22: L-shape domain without singularity (Olgierd C. Zienkiewicz & Taylor, 1994)

3.1.3 *a-posteriori* Error Estimation in Finite Element Analysis

This section follows the discussion as presented in (Ainsworth & Oden, 1997).

3.1.3.1 Status and scope

- earliest estimates
  - *a-priori* : for example, errors ~ Ch^p
  - opredictor corrector algorithms, as for ODE's
  - error η_k on energy norm on element: explicit algorithm; basis for adaptivity
  - complementary energy (global)
  - element complementary plus equilibrated boundary data
  - element residual (plus equilibrated boundary data)
- 1980's
  - *ad-hoc* estimators, for example, based on interpolation. Used in CFD; not accurate for boundary layer problems
  - recovery based methods (smoothed gradients) (superconvergent patch recovery method)
  - extrapolation (global / hierarchical)
- 1990's
  - application to general problems
- current
  - robustness of estimators
  - limits on their performance

3.1.3.2 Reference elements

Standard elements:

$$\mathbf{K} = \{(x, y) : 0 \le \mathbf{x} \le 1; 0 \le \mathbf{y} \le 1 - \mathbf{x}\} (triangle)$$

$$\mathbf{K} = \{(\mathbf{x}, \mathbf{y}) : -1 \le \mathbf{x} \le 1; -1 \le \mathbf{y} \le 1\} (quatrilateral)$$

Polynomial spaces of degree p $\in N$: P_k

Finite element space:

$$x = \left\{ v \in C(\Omega) : v|_k = \mathbf{v} \circ F_k^1 \text{forsome} \mathbf{v} \in P_k \text{forall} k \in P \right\} \tag{30}$$

3.1.3.3 Model problem

Elliptic BVP: $-\Delta u + cu = f(x)$ in Ω, with BC: $\frac{\partial u}{\partial n} = q$ on Γ_N ; $u = 0$ on Γ_D .

Variational form: $B(u, v) = L(v)$, $\forall v \in V$,

Where $V = \{v \in H^1(\Omega) : v = 0 \text{ on } \Gamma_D$

$$B(u, v) = \int_\Omega (\nabla u \cdot \nabla v + cuv) dx \qquad l(v) = \int_\Omega fv dx + \int_{\Gamma_N} gv ds \tag{31}$$

FE approximation: $u_x \in X$ such that $B(u_x, v_x) = L(v_x)$

Error: $e = u - u_x$; $e \in V$ Residual equation:

$$B(e,v) = B(u,v) - B(u_x,v) = L(v) - B(u_x,v) \qquad \forall v \in V \tag{32}$$

Orthogonality condition:

$$B(e,v_x) = 0, \forall v_x \in X \tag{33}$$

3.1.3.4 Estimators based on gradient recovery

In this approach, u_x is post-processed to obtain more accurate representations of the gradient $G(u_x)$.

An estimate of the error is $G(u_x) - \nabla u_x$.

This estimator makes no use of information from original problem. In Section 3.1.1 this procedure was explained with more detail.

3.1.3.5 Explicit a posteriori estimators

Here, a residual equation similar to Eq. 28 is obtained using integration by parts.

$$\int_k (\nabla e \cdot \nabla v + cev)dx = \int_k rvdx + \int_{\partial k} v(n_k \cdot \nabla u - n_k \cdot \nabla u_x)ds \tag{34}$$

Where: k is the element;

∂k is the boundary;

n_k is the unit exterior normal;

and the residual is: $r = f + \Delta u_x - cux$. Solution is bounded:

$$\|e\|_k \le C_1 \|r\|_{L_2(k)} + C_2 \|n_k \cdot \nabla e\|_{L_2(\partial k)} \tag{35}$$

Where C_1 and C_2 are non-negative constants. If flux on ∂k is replaced by a suitable approximation, a bound on the error is found. This leads to the implicit error residual method.

Error estimate in energy norm

Upper bound on discretization error for the above bilinear model problem

$$\|e\|^2 \le C \sum_{k \in P} \left\{ h_k^2 \|r\|_{L_2(k)}^2 + \frac{1}{2} h_k \|R\|_{L_2(\partial k)}^2 \right\} = C \sum_{k \in P} \eta_k^2 \tag{36}$$

Where

- $r = f_\Lambda u_x - Cu_x$ in k is the interior residual
- $R = g - \frac{\partial u_x}{\partial n_k}$ on ∂k on Γ_N is the boundary residual
- η_k^2 is the local error indicator in energy norm

Error estimate in L_2 norm

The upper bound is:

$$\|e\|_{L_2(\Omega)}^2 \le C \sum_{k \in P} \left\{ h_k^4 \|r\|_{L_2(k)}^2 + \frac{1}{2} h_k^3 \|R\|_{L_2(\partial k)}^2 \right\} = C \sum_{k \in P} \eta_{L_2(k)}^2 \tag{37}$$

Where $\eta_{L_2(k)}^2$ is the local error indicator in L_2 norm

Equivalence of estimators

There should be C such that

$$\sum_{k\in P}\eta_k^2 \le C\|e\|^2 \tag{38}$$

Two sided bound for the error:

$$\frac{1}{C}\|e\|^2 \le \sum_{k\in P}\eta_k^2 \le C\|e\|^2 + \sum_{k\in P} h_k^2 \|f-\pi_P f\|_{L_2(k)}^2 + \sum_{\gamma\in\Gamma_N} h_k \|g-\pi_P g\|_{L_2(\gamma)}^2 \tag{39}$$

The effect of numerical quadrature

Actual error is different from η_k^2. Also, r_k and R_k are finite dimensional approximations on actual data.

3.1.3.6 Implicit a posteriori estimators

The implicit error residual method is obtained by replacing the flux on ∂k in Eq. 34 by a suitable approximation. In this case, a bound on the error is found.

Error residual problem must be solved over k to determine error estimator $\|\phi_k\|$.

To get rid of C_1 and C_2 a local BVP has to be solved for the error:

$$\int_k (\nabla\phi_k\cdot\nabla v + c\phi_k v)dx = \int_k rv dx + \int_{\partial k} v(g_k - n_k\cdot\nabla u_x)ds \tag{40}$$

Where:

- g_k = approximation of flux on ∂k
- $\|\phi_k\|^2 = \int_k (\nabla\phi_k{}^2 + c\phi_k^2)dx$
- an infinite-dimensional space is approximated by a finite dimensional sub-space
- boundary flux $n_k\nabla u$ must be approximated in some effective way
- if $c=0$, solution may not exist unless:

$$\int_k r dx + \int_{\partial k}(g_k - n_k\cdot\nabla u_x)ds = 0 \tag{41}$$

Subdomain residual method

- homogeneous essential boundary data over subdomains of Ω
- requires the exact solution of the local problem over the subdomain
- the method is seldom used
- integrating by parts leads to $\|e\| < C\sum_{k\in P}\eta_k^2$, which is an explicit estimator in energy norm.

Element residual method

- uses a larger space than the original FE subspace x
- replaces the original problem by a number of independent local problems posed over each k
- BC for elements in the interior of Ω will interfere on existence of solution. For instance, homogeneous essential BC does not guarantee existence of solution. In fact, in this case only for very particular problems the solution will exist.

3.1.3.7 The equilibrated residual method

This approach evaluates implicit error estimates in which boundary fluxes are specially constructed so that problem is well posed.

Let η_k be the local error estimate. Let η be the global error estimate. Then

$$\eta = \left\{ \sum_{k \in P} \eta_k^2 \right\}^{\frac{1}{2}} \tag{42}$$

General property for a successful error estimator.

$$C_1 \|e\| \leq \eta \leq C_2 \|e\|. \tag{43}$$

Where is the global error in energy norm.

Effectivity indices:

$$\text{global} : \frac{\eta}{\|e\|} \qquad \text{local} : \frac{\eta_k}{\|e\|} \tag{44}$$

This section reviewed issues of error estimation for the finite element method. Different types of error measures were discussed. Error estimators based on error norms or residuals are helpful in adaptive remeshing. To obtain an error estimator suited for further stochastic treatment, the procedures for error estimation need to be adapted or modified in order for the error estimate to be allowed to assume either positive or negative values. Error estimators are needed that represent directly the errors in the response quantity of interest, and not errors obtained from energy norms related to this quantity. Section 4.1 describes several types of error estimators adapted to give directly the desired information of error in stress for the elasticity problem.

3.2 Error Estimators in Boundary Element Methods (BEM)

This section is based on new error estimation and adaptivity approaches for BEM, presented in (Jorge, Ribeiro, et al., 2003), for 2D potential-BEM, and in (Jorge et al., 2005), for 2-D elastostastics BEM. These approaches were originally presented in the PhD Dissertation (Jorge, 2002) at Vanderbilt University.

3.2.1 Introduction

Boundary integral equation (BIE) formulations are exact representations of a boundary value problem (BVP), but errors may appear in the discretization process leading to the boundary element method (BEM). To evaluate these local errors, two error estimator approaches are presented. An adaptive mesh refinement procedure using these local error estimators is also presented.

To solve the BIE numerically, the boundary is divided into elements. The collocation boundary element method (BEM) is a discretization of the BIE so that the solution is only valid at a finite number of boundary collocation points. For the other boundary points, an approximation is written using interpolating functions. Several sources of error exist in BEM problems. First, the discretized boundary may not represent the original one anymore. Second, the polynomial interpolation is only an approximation of the variable inside the element. Third, the continuity of the boundary elements may not allow the

smoothness requirements for the boundary in the original BIE to be satisfied exactly. Fourth, numerical integration using Gaussian quadrature is only an approximation of the integral being evaluated. Local and global contributions for the error due to an element can be estimated so that refinements of the mesh of the discretized problem can be performed in order to minimize these errors. A global error estimator can be used to determine the need for refinement, while a local error estimator can be used to determine which portions of the boundary require refinement, in an adaptive process.

This section briefly gives some background on existing error estimation approaches and algorithms for the collocation Boundary Element Method (BEM). This brief review includes error estimators for BEM in two different representations: symmetric and collocation. Two different error estimator approaches for the collocation BEM are considered in detail, for 2-D potential problems. The first approach is a local error estimator based on a gradient recovery procedure, wherein the smoothed or recovered functions are rates of change of the boundary variables in the local tangential direction.

The gradient recovery approach as used in the Finite Element Method (Huebner et al., 2008) (Olgierd C. Zienkiewicz & Taylor, 1994) (Ainsworth & Oden, 1997) considers the evaluation of the gradient in global coordinates, allowing for continuous derivatives of the field variable in the fixed global directions. On the other hand, in the BEM the variables of interest are written in local coordinates, so that the flux is the boundary variable associated to the outward local normal derivative of the potential. The potential is continuous throughout the boundary, while the flux and the tangential derivative of the potential may be discontinuous, such as in the case where the boundary is not smooth. The recovery procedure of the tangential derivatives in BEM shall allow these discontinuities to appear in the formulation. The adopted approach was to include double nodes at corners for the recovery approach.

The second error estimator approach is associated to an external problem formulation and gives both a local and a global measure of the error, depending on an appropriate choice of the external point where the equation is applied. The potential should vanish at points located in the exterior of the domain due to the fact that the swept angle that appears in the boundary integral formulation is zero. Nonzero values indicate that the formulation is in error. By collocating the external point close to the boundary, the influence of the nearby elements in the error estimator will be dominant, so that the information on the error can be considered to be local.

These two error estimator approaches represent a post-processing step, after the BEM solution is already known. No information on the exact solution is required for both error estimators. The two error estimators are computed for a 2-D potential problem containing a singularity, so that a comparison is made between both error estimators for comparable boundary meshes. The consistency with mesh refinement is also compared for both error estimators.

3.2.2 Current Error Estimators for Collocation and Symmetric BEM

Several types of a posteriori error estimators for BEM have been proposed in the literature. A review can be found in (S. Liapis, 1994). These error estimators include various versions of element residual methods, flux projection estimators, extrapolation error estimators and estimators measuring the sensitivity of the numerical solution to a shift in the collocation point. In (Kelly et al., 1987) a global error estimator is proposed.

In (Liang et al., 1999) local error estimators are proposed based on dual BIE formulations. In (Paulind et al., 1996) and (Menon et al., 1999) a *pointwise* error estimator is proposed, based on the difference between two formulations, the standard formulation and the hypersingular formulation, obtained by differentiation of the first one. This approach is applied to Symmetric-Galerkin BEM formulation in (Glaucio H. Paulino & Gray, 1999). An error estimator for the direct collocation method in the elastostatics problem is proposed in (Denda & Dong, 1999). In this case, a comparison with an equivalent representation of the same problem, obtained for the exterior domain, is done. Upper and lower bounds of the error are found using a residual approach in (Jou & Liu, 1999). Nodal sensitivities are used in (G. H. Paulino et al., 1997). Other nodal sensitivities to variations in node location are found in (Shi et al., 1995) and (Guiggiani, 1996). Other error estimators are proposed in (Varfolomeyev et al., 1998) (Zhan & Yokoyama, 1997) (Karafiat, 1997) (Stergios Liapis, 1996) (Charafi & Wrobel, 1997) (Chao & Lee, 1999) (Zhao, 1998) (Ammons & Vable, 1998).

Some current approaches for error estimators or error indicators already available in other BEM formulations can be adapted or transposed to the collocation BEM formulation. Usually, the error estimator approaches deal with the discretization error, looking for an optimal adaptive procedure for mesh refinement, if a local error measure is available. The approaches for error estimators and adaptivity for the collocation BEM can be grouped as follows.

Gradient recovery

Using a local average approach, an updated or more accurate gradient could be obtained. This average could be an element average or a domain average. If a domain average is used, then the gradient could be evaluated in some interior region in the vicinity of the boundary, and then a limit to the boundary could be done. The difference between this refined gradient and the actual gradient as found for a certain mesh would be a measure of the error. The components of the gradient are the normal and the tangential derivatives. The tangential derivative is obtained in a post-processed manner, by taking the derivative of the shape functions with respect to the intrinsic variable ξ, while the normal derivative is written in terms of the shape functions themselves. For the usual polynomial shape functions, the tangential derivative is written in a representation that has one degree less than the normal derivative. So, another possibility, which would be simpler, would be the recovery of only the tangential derivative, so that the gradient components (normal and tangential) would now be written with shape functions of same order. A measure of the error could be the difference between the refined and the actual tangential derivatives. This simpler approach would be better adapted to the parts of the boundary where the tangential derivative varies very fast, and its representation, with shape functions of one degree less, is inaccurate. On the other hand, for parts of the boundary where the normal derivative is changing very fast, as could be the case, for example, if the radius of curvature of that part of the boundary is small, then the contribution of the normal derivative to the error might be significant and could not be neglected *a-priori*.

Average in the norm

The numerical solution is the exact solution plus some error. The error satisfies the equation modeling the problem. If numerical solution is not known, the numerical solution for a refined mesh could be adopted as the ”exact“ solution for the purpose of finding this difference. Errors in displacement and traction (in the elastostatics problem)

or in potential and flux(in the potential problem) can be evaluated for all nodal points. Local (in the element) and global (in the entire boundary) averages of this error could be written, in the L_2 norm sense or in some energy norm, and a local relative error in this norm could be obtained. This relative error could be used to guide adaptive mesh refinement. The error in one variable (say, traction or flux) could be dominant with respect to the error on the other variable (say, displacement or potential). Another procedure could be to first find the error in the tangential derivatives from the error in displacement (or in potential), and then evaluate the error in some norm sense, the norm being some average of the tangential and normal derivatives. The same as before, local (element) and global measures of the error shall be obtained, so that a relative error is assessed in the element. This alternative procedure could be adopted in conjunction with the tangent derivative recovery, to have both tangential and normal derivatives written with shape functions of the same order, before the error norm is evaluated.

Sensitivity analysis

A sensitivity analysis could be performed in two ways, leading to two different sensitivity measures. The first measure is related to regularization sensitivity. The singular or hypersingular kernels in certain BIEs can be regularized before a numerical procedure to solve the BIE is implemented. Simple solutions may be imposed in this regularization procedure to obtain self-regular formulations for the BIEs. The sensitivity measure would be on the response to variations in the simple solution being imposed in the self-regular formulation of the integral representation of the problem. If these simple solutions are considered as a truncated Taylor series expansion about some point, then small variations about this point could be considered when higher order terms where included in this series expansion. For example, for the self-regular potential-BIE formulation, with local coordinates ζ_i, the general format of the variation about the simple constant potential solution would be to include the Taylor expansion first order term, which means to substitute $\phi(x)$ by $\left[\emptyset(x) + \frac{\partial \emptyset}{\partial \zeta_i}\Big|_x \zeta_i\right]$.

Similarly, in the self-regular gradient-BIE formulation, the variation about the simple linear potential solution would be to include the Taylor expansion second order term, which means to substitute $\left[\emptyset(x) + \frac{\partial \emptyset}{\partial \zeta_i}\Big|_x \zeta_i\right]$ by $\left[\emptyset(x) + \frac{\partial \emptyset}{\partial \zeta_i}\Big|_x \zeta_i + \frac{1}{2}\frac{\partial^2 \emptyset}{\partial {\zeta_i}^2}\Big|_x {\zeta_i}^2\right]$.

The variations in the self-regular displacement and traction formulations in the elastostatics problem would have similar approaches.

The second measure is related to nodal sensitivity. The sensitivity of the response to variations of location of nodes could be evaluated. Small variations of the position of the central node could be done. To evaluate this sensitivity, two approaches are possible: allowing the element size to change (Lagrangian approach) or imposing the change in position of the node to occur in the same deformed shape of the element, i.e. without changing its length (Eulerian approach).

Difference between two equivalent formulations

The exact solution for the BVP as written in one integral representation shall satisfy any other possible different integral representation of the same BVP. When a numerical solution is found for some discretization of one formulation, this solution can be plugged into the discretized form (with same discretization) of the other possible formulation. As

the numerical solution is not exact, the identities in the discretized form of this second formulation will not be satisfied. The difference will be a measure of the error in the discretization of both formulations. For example, for a closed domain, the exterior problem representation is equal to zero in both the potential and in the elastostatics problems. So, any difference from zero could be related to the discretization error. As the fundamental solutions are functions of the distance between source and field points, one representation in which the exterior point is very close to the boundary might give a different error measure than another external formulation in which the exterior point is considered far away from the boundary. If different exterior points are considered, different external formulations may be obtained. The error measure might be sensitive to the external point position, for some particular problem. Another possibility is to obtain an equivalent formulation by taking derivatives of an existing formulation. Derivatives taken in different directions are all different equivalent formulations of the same problem. All scalar equations that are components of the vector equation obtained in some representation, are different equivalent formulations and can be used for this error measure purpose. This is the case in the gradient formulation, which was transformed into the flux formulation by taking the component of this equation in one direction. So, the component of this equation in the other direction (say, tangential) is an equivalent formulation that can be used. The same applies to the various components of the vector equation in the elasticity problem.

Various equivalent formulations could be used, for some specified boundary discretization. For example, for the potential problem, a comparison could be done between the potential-BIE and the gradient-BIE formulations. As the gradient-BIE formulation is a vector equation, one component of this equation, say, the flux equation, could be retained. The decomposition of the gradient equation in a different direction will lead to a different, but equivalent, equation, because the derivative of the potential equation was taken in a different direction. Other possible comparisons could be between the potential formulation and potential formulation for an exterior problem, or between the gradient formulation and the gradient formulation for an exterior problem. Again, as the gradient formulation is a vector equation, all scalar components of this equation are valid equivalent formulations.

Similar comparisons for the elastostatics problem could also be done, for example, between the displacement-BIE and the traction-BIE formulations. As the traction formulation is a vector equation (the projection of the tensor of stresses in one direction) any component of this equation can be retained. The traction equation in a different direction will lead to a different, but equivalent, equation, because the derivative of the displacement equation was taken in a different direction. Other possible comparisons could be between the displacement formulation and the displacement formulation for an exterior problem, or between the traction formulation and the traction formulation for an exterior problem. As before, as the traction formulation is a vector equation, all scalar components of this equation are valid equivalent formulations.

Adaptivity

When a local measure of the discretization error, in one element, is available, it could be compared to an average global measure of this error. If the relative error is bigger than 1 for a certain element, a refinement shall be applied to this element. Adaptive refinement of the mesh could be done by adopting either *h*-refinement or *p*-refinement procedures.

In the *h*-refinement procedure, the element where the local error is big is divided into two small elements (usually it is divided into two equal elements). In the *p*-refinement procedure, the degree of the shape functions used to represent the variables in this element is increased. For this *p*-refinement procedure, the use of hierarchical shape functions would be advantageous, because computations already done for the coarse mesh will be kept and don't need to be done again in the refined mesh.

3.2.3 Proposed Error Estimators for Potential-BEM

Two error estimators for BEM are proposed, one based on the gradient recovery approach and the other based on the error on the external formulation. These error estimators are post-processing approaches that give qualitative indicators of the local errors on the boundary solution for any BEM formulation and for a certain boundary discretization into a particular mesh. These error estimators are suitable to be used for the collocation BEM, where other error estimators such as the ones obtained using energy norms may not be available.

3.2.3.1 The gradient recovery approach

The following discussion will be limited to potential theory in 2D, but the ideas can be adapted to the 3D problem and to the elasticity theory. The idea of recovery of derivatives is borrowed from error estimators for finite element methods, where to compute some error indicators it was necessary first to obtain expressions for the derivatives of the finite element solution. Even small errors in the finite element solution could lead to large errors or inaccuracy in the derivatives of the solution, evaluated in a post-processing manner by taking derivatives of the shape functions. Smoothed or refined approximations for the derivatives were developed so that the error indicators depending on these derivatives would be more credible. A procedure to smooth the gradient to compute these derivatives with good accuracy is called gradient recovery (Huebner et al., 2008) (Olgierd C. Zienkiewicz & Taylor, 1994) (Ainsworth & Oden, 1997). The derivatives are evaluated from a weighted average of element derivatives surrounding the node. The weighting factors are the element areas. The FEM procedure is illustrated for a one-dimensional problem, for simplicity. For each element (e), the first derivatives are first expressed in terms of the derivatives of the shape functions N and of the nodal values of the potential solution $\{\phi\}^{(e)}$ as:

$$\left(\frac{\partial \phi}{\partial x}\right)^{e} = \left\lfloor \frac{\partial N}{\partial x} \right\rfloor \{\phi\}^{(e)} \tag{45}$$

The derivatives are now written in an average sense

$$\int_{\Omega^{(e)}} \{N\} \lfloor N \rfloor dA \left\{\frac{\partial \phi}{\partial x}\right\} = \int_{\Omega^{(e)}} \{N\} dA \frac{\partial \phi}{\partial x}^{(e)} \tag{46}$$

where the goal is to find the vector of smoothed or recovered nodal derivatives $\{\partial\phi/\partial x\}^{e}$. For that, an equivalence equation can now be written in a region $\Omega^{(e)}$ surrounding an element *(e)* as:

$$\int_{\Omega^{(e)}} \{N\}[N] dA \left\{\frac{\partial \phi}{\partial x}\right\} = \int_{\Omega^{(e)}} \{N\} dA \frac{\partial \phi}{\partial x}^{(e)} \tag{47}$$

The element equations as in Eq. (47) are then assembled for the entire domain Ω. A system of equations is obtained from which the vector of smoothed nodal derivatives $\{\partial \phi / \partial x\}^{(e)}$ can be obtained. An important feature in this procedure is that the x-coordinate belongs to a global coordinate system, so that not only the potential field at the nodes $\{\phi\}^{(e)}$ is continuous in Ω, but also all the elements of the smoothed gradient components $\{\partial \phi / \partial x\}^{(e)}$ vector in a general problem are continuous in Ω too, so long as linear or higher order elements are used.

This post-processing approach to find error estimators from gradient recovery can be adapted to a BEM problem, after the solution is known for all nodes on the boundary. Consider first an element *(e)* of the boundary region in which the gradient is being recovered. Let ϕ be the potential, $\partial\phi/\partial s$ be the tangent derivative of ϕ and $q = \partial\phi/\partial n$ be the flux. From the BEM solution, the nodal values $\phi_i^{(e)}$ and $q_i^{(e)}$ are known. Both the flux q and the tangential derivative $\partial\phi/\partial s$ are allowed to be discontinuous at boundary points where the normal unit vector is not unique. The tangent and normal unit vectors are uniquely defined only locally in the interior of a boundary element. Usual BEM solutions allow for these discontinuities to occur, and the flux solution on the boundary is given both as a function of the node number i and of the element number *(e)* so that on a certain element i the flux on the element before the node $q_i^{(e)}$ might be different form the flux for the element after the node $q_i^{(e+1)}$. The same discontinuities will apply for both the original and the recovered or smoothed values of the tangential derivative of the potential $\partial\phi/\partial s$ at the same boundary nodes where the flux is discontinuous.

To be able to write a system of equations similar to the one obtained with the FEM procedure as outlined above, continuity would be required for the derivatives of the potential. But the derivatives of the potential would be continuous only in a global coordinates system, and not in local coordinates systems along the boundary curve, if the boundary has corners. The approach adopted in this work was to introduce double nodes at all the discontinuity points, such as the corner nodes on the boundary. Elements with zero length connect these double nodes, so that no local or global contribution for the error from these fictitious elements is obtained. It must be pointed out that the gradient recovery approach is a post-processing procedure that is completely independent from the BEM method that was used to obtain the boundary solution. The original BEM method may or may not use double nodes, and this is irrelevant for the post-processing procedure, because the double nodes being introduced here came from the fact that discontinuities exist in the values of q and $\partial\phi/\partial s$ on these corner nodes locations, and not due to the original BEM procedure to evaluate the boundary solution, that remains unchanged.

The solution at any point inside the element is $\phi^{(e)}(\xi) = \sum_{i=1}^{m} N_i(\xi)\phi_i^{(e)}$ and $q^{(e)}(\xi) = \sum_{i=1}^{m} N_i(\xi) q_i^{(e)}$, where ξ is the intrinsic coordinate and m is the number of element nodes corresponding to the polynomial interpolation being used, such as $m = 2$ for linear elements, $m = 3$ for quadratic elements, etc. Taking derivatives with respect to the intrinsic coordinate gives

$$\frac{d\phi^{(e)}(\xi)}{d\xi} = \sum_{i=1}^{m} \frac{dN_i(\xi)}{d\xi} \phi_i^{(e)} \quad ; \quad \frac{dq^{(e)}(\xi)}{d\xi} = \sum_{i=1}^{m} \frac{dN_i(\xi)}{d\xi} q_i^{(e)} \tag{48}$$

These derivatives can now be written with polynomial shape functions one degree higher as

$$\frac{d\phi^{(e)(*)}(\xi)}{d\xi} = \sum_{i=1}^{m} N_i(\xi) \frac{d\phi_i^{(e)(*)}}{d\xi} \quad ; \quad \frac{dq^{(e)(*)}(\xi)}{d\xi} = \sum_{i=1}^{m} N_i(\xi) \frac{dq_i^{(e)(*)}}{d\xi} \tag{49}$$

where $d\phi_i^{(e)(*)}/d\xi$ and $dq_i^{(e)(*)}/d\xi$ are the sets of nodal values of the corresponding derivatives, equivalent in a local averaging sense, to the original ones, $d\phi_i^{(e)}/d\xi$ and $dq_i^{(e)}/d\xi$. The element equivalence is enforced by setting that both formulations for the derivatives give same element integrals, defined by

$$\begin{aligned} I_\phi^{(e)} &= \int_S^{(e)} \{N\} \frac{d\phi_i^{(e)}(\xi)}{d\xi} J(\xi,s) dS = \int_S^{(e)} \{N\} \frac{d\phi_i^{(e)(*)}(\xi)}{d\xi} dS \\ I_q^{(e)} &= \int_S^{(e)} \{N\} \frac{dq_i^{(e)}(\xi)}{d\xi} J(\xi,s) dS = \int_S^{(e)} \{N\} \frac{dq_i^{(e)(*)}(\xi)}{d\xi} dS \end{aligned} \tag{50}$$

where $\frac{d\phi_i^{(e)}(\xi)}{d\xi} J(\xi,s) = \frac{\partial \phi_i^{(e)}(s)}{\partial s}$, $J(\xi,s)$ being the Jacobian of the transformation between the real element (with coordinate s) and the standard element (with the intrinsic coordinate ξ). The derivatives of $\phi^{(e)(*)}$, $q^{(e)}$ and $q^{(e)(*)}$ follow similar transformation of coordinates. The integration is performed on S which is the element length in 2-D or the element area in 3-D. If the element for integration is now written as $dS = J(\xi,s)d\xi$, all terms in the integrands are now only function of the intrinsic variable ξ, and all element integrations are now performed for $\xi \in [-1,1]$, for the usual Lagrangian interpolating functions.

The element equations as in Eq. (50) are then assembled for the entire boundary S. A system of equations is obtained from which the vectors of smoothed nodal derivatives $\{\partial \phi_i / \partial s\}^{(e)}$ and $\{\partial q_i / \partial s\}^{(e)}$ can be obtained. It must be pointed out that the system matrix for the coefficients of the recovered or smoothed quantities is not singular, and admits an inverse, after all elements are assembled, including the zero-length elements that link the double nodes.

Several approaches could be envisaged to use the assembly of the element integrals as obtained in Eq. (50). By assembling the element integrals of the type $I_\phi^{(e)}$ only, an expression for the local error related to the tangent derivative of ϕ could be obtained. Similarly, by assembling the integrals of the type $I_q^{(e)}$ only, an expression for the local error related to the tangential derivative of the flux q could be obtained, noting that the flux is the normal derivative of the potential ϕ. A more elaborate expression for the error related to both the tangential and the normal derivatives of the potential could be obtained by combining both integrals. In this case, normalizing or scaling the integrals first, before

adding or combining them, might be necessary, so that they will be of the same order of magnitude.

In any of these approaches, the error is already normalized with respect to the size of the element, the normalization factor being the Jacobian $J(\xi, s)$ that appeared naturally in the formulation when the chain rule was applied for the derivatives of the transformation equations from local variables to intrinsic element variables. So the obtained the quantity of interest is a measure of the relative error, already normalized with respect to the element size, and not a measure of the error that could be dependent on the size of the element.

The approach follows several steps. The first step is to solve the system of equations corresponding to the integral (or to the combination of integrals) chosen, obtaining the equivalent set of nodal values for the derivatives. For any point with generic coordinate *S* in the element, a difference will exist between the derivative as written in the original system and the derivative using the recovered equivalent nodal values. By construction, these differences will add to zero if the entire boundary is considered, because adding for all positions *S* is the same as integrating in the entire boundary, obtaining again the equivalence equation that was enforced. A quadratic expression for a residual is proposed such that the differences between the derivatives point by point are first squared and then added to obtain an expression for the local error. The proposed residuals are, then, functions of the position *S* within the element:

$$r_{\emptyset}^{(e)}(s) = \left[\frac{\partial \emptyset^{(e)(*)}}{\partial s}(s) - \frac{\partial \emptyset^{(e)}}{\partial s}(s)\right]^2 \quad ; \quad r_q^{(e)}(s) = \left[\frac{\partial \emptyset^{(e)(*)}}{\partial s}(s) - \frac{\partial q^{(e)}}{\partial s}(s)\right]^2 \tag{51}$$

Local error expressions in the original elements can now be defined as:

$$E_{\phi}^{(e)} = \frac{1}{S^{(e)}}\int_{S^{(e)}} r_{\phi}^{(e)}(s)dS^{(e)} \qquad ; \qquad E_q^{(e)} = \frac{1}{S^{(e)}}\int_{S^{(e)}} r_q^{(e)}(s)dS^{(e)} \tag{52}$$

where $S^{(e)}$is the total size, or length, of the element, appearing as the scaling factor equivalent to the Jacobian that would appear if the integration were performed with respect to the intrinsic variable ξ.

The residuals in an element *(e)* at the position *s*, obtained from the two sources of error, $r_{\phi}^{(e)}(s)$ and $r_q^{(e)}(s)$ can be combined to give a unique information about the local error in the element, coming from both the tangential and the normal derivatives of the potential.

As the order of magnitude of the quantities involved may vary, these residuals are proposed to be normalized with respect to the average values of the quantities in the element, before they are added to obtain a unique residual, now normalized, for the element.

The average values can be obtained directly from the equivalence equation, Eq. (50) as

$$\begin{aligned}\left.\frac{\partial \emptyset^{(e)}}{\partial s}\right|_{AVE} &= \frac{1}{S^{(e)}}\int_{S^{(e)}} \frac{\partial \emptyset_i^{(e)}}{\partial s}(s)dS^e = \frac{1}{S^{(e)}}\int_{S^{(e)}} \frac{\partial \emptyset_i^{(e)(*)}}{\partial s}(s)dS^e \\ \left.\frac{\partial q^{(e)}}{\partial s}\right|_{AVE} &= \frac{1}{S^{(e)}}\int_{S^{(e)}} \frac{\partial q_i^{(e)}}{\partial s}(s)dS^e = \frac{1}{S^{(e)}}\int_{S^{(e)}} \frac{\partial q_i^{(e)(*)}}{\partial s}(s)dS^e\end{aligned} \tag{53}$$

The normalized residuals are then defined as:

$$r_{\emptyset}^{(e)}(s)|_{norm} = \left[\frac{\frac{\partial \emptyset^{(e)(*)}}{\partial s}(s) - \frac{\partial \emptyset^{(e)}}{\partial s}(s)}{\left.\frac{\partial \emptyset^{(e)}}{\partial s}\right|_{AVE}}\right]^2 \quad ; \quad r_q^{(e)}(s)\big|_{norm} = \left[\frac{\frac{\partial \emptyset^{(e)(*)}}{\partial s}(s) - \frac{\partial q^{(e)}}{\partial s}(s)}{\left.\frac{\partial q^{(e)}}{\partial s}\right|_{AVE}}\right]^2 \tag{54}$$

so that a single residual for the element *(e)* at the position *s* and the resulting local error element can now be defined as

$$r^{(e)}(s) = r_{\phi}^{(e)}(s)|_{norm} + r_q^{(e)}(s)|_{norm} \quad ; \quad E^{(e)} = \frac{1}{S^{(e)}}\int_{S^{(e)}} r^{(e)}(s)dS^{(e)} \tag{55}$$

It has to be pointed out that the residuals were normalized with respect to the average values of the corresponding variables, and also with respect to the size of the elements, so that these residuals are now related only to the local error due to the corresponding source, either the tangential derivative or the normal derivative of the potential.

It may occur that one source of error might be dominant, so that the other residual could be negligible in a certain problem. Numerical experiments have to be performed to establish relationships between these residuals, or conditions in which one of them, if any, could be discarded without loss in the accuracy of the error estimator.

In the current work, only the error obtained from the recovery of the tangential derivative of the potential, denoted as $Error_{\phi}$, is evaluated. Thus, in this gradient recovery approach, the smoothed or recovered function is not the gradient itself, but its component in the locally tangent direction, because this component is not obtained from the integral equation directly, but from the tangential derivative of the potential.

The reason for not considering the error from the recovery of the flux in this first study is that the tangential derivative of the potential is being approximated, using isoparametric elements, by a polynomial that is one degree less then the polynomial that approximates the normal derivative of the potential, which was obtained directly in the solution of the boundary integral equation. The smoothed tangential derivative and the original normal derivative are, then, approximated using polynomials of the same degree.

The recovery procedure could be refined in a future work, so that the rate of change in tangential direction of the normal derivative could be smoothed too. With this refinement in the gradient recovery procedure, a comparison could be performed between the normal and tangential contributions for the element error. This refinement is proposed but not implemented in this work, as the tangential derivative of the potential, being written with a polynomial with one degree less than the flux, appears to be the component of the gradient that gives the most significant contribution for the total element error. (Jorge, Ribeiro, Cruse, et al., 2001) shows that accurate results for the potential and the flux were obtained for coarse graded meshes where the tangential derivatives of the potential were better approximated.

A global error estimator can now be defined simply by $E_{Global} = \sum_{e=1}^{N} E^{(e)}$, where N is the number of boundary elements, so that an average error for the entire boundary and the normalized local element errors can be defined respectively as:

$$E_{AVE} = \frac{1}{N}E_{Global} = \frac{1}{N}\sum_{e=1}^{N} E^{(e)} \quad ; \quad E^{(e)}|_{norm} = \frac{E^{(e)}}{E_{AVE}} \tag{56}$$

so that this normalized local error indicator can now be used in an adaptive procedure. If $E^{(e)}|_{norm} > 1$ then the local error in the element is bigger than the average, and a mesh refinement is needed, either changing the size of the elements in this boundary region to smaller ones (h- refinement) or increasing the order of the polynomial interpolant in the element (p- refinement). If $E^{(e)}|_{norm} \cong 1$, the local error has an average value and no refinement is needed. If $E^{(e)}|_{norm} < 1$, no refinement is needed, either. In this case, in fact, the local error being small shows that the element size is already small enough and it could be made bigger without much loss in the solution accuracy.

3.2.3.2 The external domain approach

Usually, the error estimator approaches deal with the discretization error, looking for an optimal adaptive procedure for mesh refinement, if a local error measure is available. Existing ideas, approaches and error estimators for collocation BEM are the starting point for the error estimators to be proposed. From these ideas, the difference between two equivalent formulations is seems to be one of the easiest to be adopted, due to its simplicity. The exact solution for the BVP as written in one integral representation shall satisfy any other possible different integral representation of the same BVP. When a numerical solution is found for some discretization of one formulation, this solution can be plugged into the discretized form (with same discretization) of the other possible formulation. As the numerical solution is not exact, the identities in the discretized form of this second formulation will not be satisfied. The difference will be a measure of the error in the discretization of both formulations.

For example, for a closed domain, the exterior problem representation is equal to zero in both the potential and in the elastostatics problems. So, any difference from zero could be related to the discretization error. As the fundamental solutions are functions of the distance between source and field points, one representation in which the exterior point is very close to the boundary might give a different error measure than another external formulation in which the exterior point is considered far away from the boundary. If different exterior points are considered, different external formulations may be obtained. The error measure might be sensitive to the external point position, for some particular problem. Two equivalent formulations can be used, for some discretization, for the potential problem: evaluate the solution in the boundary with a potential formulation and then check the expected vanishing of the results of the potential formulation for an exterior problem.

So, an error estimator is implemented for the potential problem, based on the fact that the potential vanishes at external points. In the potential formulation for an exterior problem, a numerical solution at the boundary is first obtained for the discretized mesh using the collocation BEM or any other BEM formulation. This boundary solution is then substituted on the exterior form of Green's identity given by

$$0 = -\int_S \phi\,(s)\vec{\nabla}\ln\left(\frac{1}{r(s,y)}\right)\cdot\vec{n}(s)dS + \int_S \vec{\nabla}\,\phi(s)\cdot\vec{n}(s)\ln\left(\frac{1}{r(s,y)}\right)dS \;\; \forall y \in \bar{R} \quad (57)$$

As it was discussed in Section 3.2.2, other choices of integral representations could also have been adopted for the exterior equation. By implementing this methodology to other exterior problem equations, optimal choices for this equation could be looked at.

The exterior point $y \in \bar{R}$ is proposed to be located at a distance to the boundary (the distance from the exterior point to the closest point on the boundary) that is 1/4 of the size of the element closest to this exterior point. This distance is measured in the direction normal to the element. This distance was chosen to avoid the quasi-singularity problem that may appear if the external point is too close to the boundary and also to avoid round-off error that may appear in the computations of very small fundamental solutions when the exterior point is too far away from the boundary. It has to be noted that other choices for this position could have been adopted, and numerical experiments could have been performed to determine optimum minimal distances for different cases.

3.2.3.3 Implementation of the proposed Error Estimators

A numerical example is performed to demonstrate the implementation of the two proposed error estimators (Jorge, Ribeiro, & Fisher, 2001). This example was proposed by Motz (Jaswon et al., 1978). The problem consists of a rectangular domain, as shown in Fig. 23 (a). The flux is singular at point O in the element where the potential is prescribed.

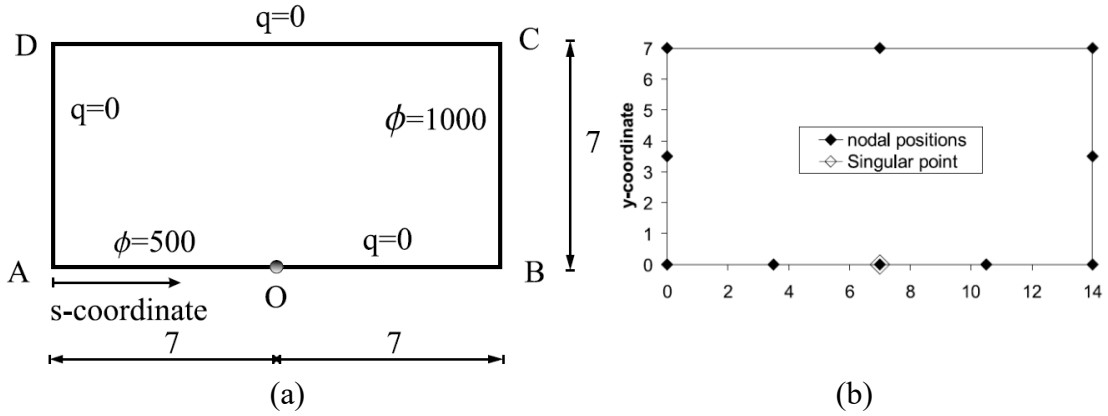

Figure 23: The Motz problem: (a) a singularity is created at point O by the boundary conditions; (b) the coarse mesh: 10 elements - adapted from (Jorge, Ribeiro, et al., 2003)

All BEM results were obtained with the code BETIS from (París & Cañas, 1997), which uses linear elements. Two meshes are implemented to compare the error estimators. The first mesh is coarse and has only 2 elements in each linear segment in which a specific boundary condition is prescribed. Then, a finer mesh is studied in which there are eight elements on the side where the flux is known to have a discontinuity. Figure 23 (b) illustrates the coarse mesh that was implemented.

The implementation of the tangent derivative recovery for linear elements is detailed as follows. A standard linear element has two end nodes with corresponding shape functions $N_1(\xi) = (1-\xi)/2$ and $N_2(\xi) = (1+\xi)/2$ for $\xi \in [-1,1]$. The Jacobian for this 1-D straight element is $J(\xi, s) = \partial\xi/\partial s = 2/L^{(e)}$, where $L^{(e)}$ is the length of the boundary element *(e)*, so the element of integration is $dS^{(e)} = \left(L^{(e)}/2\right)d\xi$. The original and the recovered (denoted by (*)) tangent derivatives of the potential are written for the element *(e)* so that the equivalence in the element can be enforced as follows.

$$\int_{-1}^{1} \begin{Bmatrix} N_1(\xi) \\ N_2(\xi) \end{Bmatrix} \lfloor N_1(\xi) \quad N_2(\xi) \rfloor \frac{L^{(e)}}{2} d\xi \begin{Bmatrix} \frac{\partial \phi_1}{\partial s}^{(e)(*)} \\ \frac{\partial \phi_2}{\partial s}^{(e)(*)} \end{Bmatrix} \tag{58}$$
$$= \int_{-1}^{1} \begin{Bmatrix} N_1(\xi) \\ N_2(\xi) \end{Bmatrix} \frac{L^{(e)}}{2} d\xi \frac{2}{L^{(e)}} \lfloor N_1{}'(\xi) \quad N_2{}'(\xi) \rfloor \begin{Bmatrix} \phi_1^{(e)} \\ \phi_2^{(e)} \end{Bmatrix}$$

Now all element matrices given by Eq. (58) can be assembled for both the coarse and the refined meshes. By solving the assembled system of equations, the vector of nodal values for the smoothed tangential derivatives of the potential $\partial \phi_i^{(*)} / \partial s$ is obtained. The assembled matrices are sparce. The vector of element interpolations is now obtained as

$$\left\{ \frac{\partial \phi^{(i)(*)}}{\partial s}(\xi) \right\} = \left(\frac{1-\xi}{2} \right) \frac{\partial \phi_i^{(*)}}{\partial s} + \left(\frac{1+\xi}{2} \right) \frac{\partial \phi_{i+1}^{(*)}}{\partial s} \tag{59}$$

The residuals r_ϕ^i are now evaluated for each element as the square of the differences between the smoothed solution obtained in Eq. (59) and the original non-smoothed solution.

$$r_\phi^i(\xi) = \left[\frac{\partial \phi^{(i)(*)}}{\partial s}(\xi) - \frac{2}{L^i} \lfloor N_i{}'(\xi) \quad N_{i+1}{}'(\xi) \rfloor \begin{Bmatrix} \phi_i \\ \phi_{i+1} \end{Bmatrix} \right]^2 \tag{60}$$

so the element errors R_ϕ^i, the average error E_{AVE} and the normalized element errors $E_\phi^i = R_{\phi_{norm}}^i$ are found as

$$R_\phi^i = \int_{-1}^{1} r_\phi^i(\xi) d\xi \qquad E_{AVE} = \frac{1}{N} \sum_i R_\phi^i \qquad E_\phi^i = \frac{R_\phi^i}{E_{AVE}} \tag{61}$$

where the element errors E_ϕ^i can now be compared with the local element errors E_{EXT}^i, obtained from the external error approach. Figure (24) shows the results for the normalized local error estimators for both the coarse and the fine meshes. The horizontal axis of the four plots corresponds to the s- coordinate of the middle of each element along the boundary.

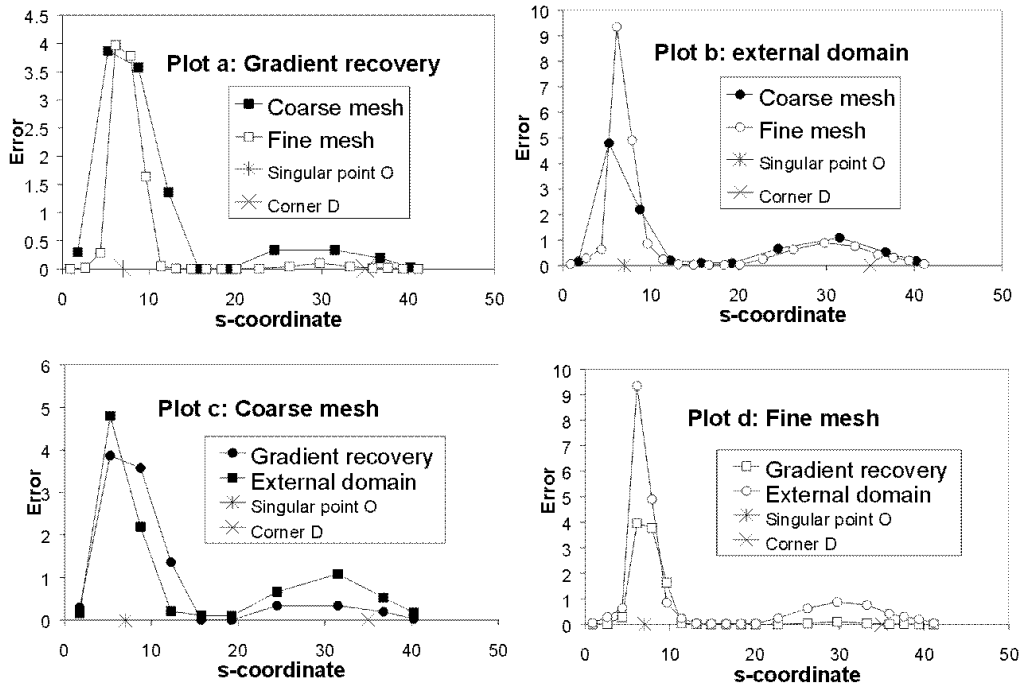

Figure 24: Error estimator results. (a) and (b): Influence of mesh refinement for each estimator. (c) and (d): Comparison between estimators for each mesh. - adapted from (Jorge, Ribeiro, & Fisher, 2001)

Plot (a) shows the results for the error on the tangential derivative of the recovered gradient $Error_{\phi}$ while plot (b) shows the results for the error obtained using the exterior domain formulation $Error_{EXT}$. The boundary region that shows the highest values for the normalized error in both cases is the region that contains the elements adjacent to the singular point O, as expected. The error results were qualitatively consistent with the mesh refinement. Plots (c) and (d) compare the error estimators for the coarse and the refined meshes, respectively. Both error estimators indicate the same region about the singular point O with highest values for the normalized error.

Also, the boundary region immediately before corner node *D* presents relatively high secondary errors for both estimators. These errors appear to be related to the fact that this region corresponds to the boundary corner the farthest distance away from any boundary region where the potential is prescribed.

It must be pointed out that the element before the singular point has the potential prescribed as constant. So, any contribution for the error could only come from the error in the flux, in this element. Similarly, the element after the singular point has the flux prescribed as constant. So, any contribution for the error could only come from the error in the potential, in this element. This means that both error estimators were capable of recovering the local information of the total error regardless of the cause of the error being the boundary potential or the boundary flux.

Although the adopted gradient recovery procedure does not explicitly recover the errors from the tangential derivative of the flux, high values for the error that could only be related to the local flux were encountered in an element adjacent to the singular point. An

explanation for this behavior is that the gradient recovery procedure is based on an algorithm that includes all the boundary elements. The recovery of the tangential derivative of the potential is not made independently for each element, in a local basis. Instead, a unique value for the smoothed or recovered nodal values of the tangential derivative of the potential is only obtained when all the element matrices are assembled and the solution for the obtained system of equations is calculated. The redistribution of the tangential derivatives of the potential throughout the boundary appears to implicitly account for the local error in the flux.

3.2.4 Proposed Error Estimators for Elastostatics-BEM

New Error Estimators based on Gradient Recovery and External Domain Approaches were extended to 2D Elastostatics Problems in (Jorge et al., 2005). These error estimator approaches were derived for 2D potential problems in (Jorge, Ribeiro, et al., 2003), and the extension of these error estimators for a problem with a different integral formulation highlights their generality of use.

Error estimators based on residuals and error norms, similar to the approaches available in the finite element method (FEM), have been used for symmetric BEM formulations, but the error estimators literature is scarce for the collocation BEM formulation. Reviews for error estimation and adaptivity methods for BEM can be found in (S. Liapis, 1994) and in (Kita & Kamiya, 1994) (Kita & Kamiya, 2001).

The two local error estimator approaches presented in this work can be used for both Galerkin and collocation BEM formulations. The first approach involves a gradient recovery procedure, wherein the smoothed or recovered functions are rates of change of the boundary variables in the local tangential direction. The gradient recovery approach is commonly used in the finite element method (Ainsworth & Oden, 1997) and considers the evaluation of the gradient of the field variable in global coordinates, with continuous derivatives of this field variable in fixed global directions.

On the other hand, in the BEM the variables of interest are written in local coordinates, the displacements are continuous throughout the boundary, while the tractions and the tangential derivatives of the boundary variables may be discontinuous, such as at points where the boundary is not smooth or where the boundary conditions are discontinuous.

The second error estimator approach is associated with an external problem formulation and gives both a local and a global measure of the error depending on the external point where the equation is applied. (Denda & Dong, 1999) presented an error estimator for elasticity based on the strain energy in the exterior region. In the current work, the error estimator is obtained using directly the error in the displacements and in the stresses obtained from the exterior problem. Displacements and stresses should vanish at points located in the exterior of a closed domain, and consequently, nonzero values indicate errors. If the external evaluation point is near the boundary, the influence of the nearby boundary elements in the error estimate will be dominant, and the error information assumes a local characteristic. To eliminate any influence of the choice of the global directions on the values of the stress error estimates, the stresses at the exterior point are first combined into stress invariants, the mean stress and the octahedral stress, before any error information is evaluated. In (Jorge et al., 2005), the two error estimators were computed for two 2D elastostatics problems, one of which contains a singularity. A comparison was made between global and local error estimates, and the error consistency

with mesh refinement is also compared. Some details are shown in the following subsections.

3.2.4.1 The gradient recovery approach

The concept of recovery of derivatives for error estimation originated with finite element methods, in which error indicators were derived from derivatives of the computed finite element solution. A procedure to smooth the gradient to compute these derivatives with good accuracy is called gradient recovery (Ainsworth & Oden, 1997). The derivatives are evaluated from a weighted average of element derivatives surrounding a node. The weighting factors are the element areas.

This post-processing approach to estimate error from gradient recovery was adapted by the authors to 2D potential BEM problems in (Jorge, Ribeiro, et al., 2003). An important feature in this procedure when applied to FEM is that the derivatives of the field variables (displacements) are taken with respect to a global coordinate system. Thus, not only are the field variables continuous at the domain nodes, but also the smoothed gradient vectors in a general elastostatics problem are continuous. On the other hand, when the gradient recovery procedure is applied to BEM, the tangential and normal directions are written in local coordinates, and discontinuities in the tangential derivatives need to be allowed in both the original and the recovered tangential derivatives of the density fields (boundary displacements and tractions).

To write a system of equations similar to the one obtained with the FEM procedure, continuity would be required for the derivatives of the densities. The approach adopted in (Jorge, Ribeiro, et al., 2003) and extended in this work is to introduce double nodes at all the discontinuous points, such as the corner nodes on the boundary. Elements with zero length connect these double nodes, so that no local or global contribution for the error from these fictitious elements is incurred. The concept of double nodes to account for discontinuities in the tractions when obtaining the boundary solution is well known in the BEM literature (París & Cañas, 1997) but is not used in this work.

The double nodes introduced here originate from discontinuities in the values of the tangential derivatives of the densities at corner nodes in the post-processing algorithm to obtain the element errors and not from the original BEM procedure to evaluate the boundary solution.

The basic boundary integral equation for the elastostatics problem (Wendland & Cruse, 1990), gives the displacement $u_j(x)$ as a function of boundary integrals. This displacement-BIE, can be written, for an homogeneous domain Ω as:

$$C_{ji}(p)u_i(p) = \int_{\partial\Omega} \Psi_{ji}(p,Q)t_i(Q)dS(Q) - \int_{\partial\Omega} T_{ji}^{\psi}(p,Q)u_i(Q)dS(Q) \qquad (62)$$

where $Q \in \partial\Omega$. The functions Ψ_{ji} and T_{ji}^{ψ} are associated with fundamental solutions of the Navier equation, and C_{ji} is associated with the location of the collocation point p, as an interior, exterior, or boundary point. The integrals in Eq. (62) provide a constraining equation for the boundary variables when evaluated for $p \in \partial\Omega$, in which case C_{ji} depends on the boundary smoothness at the point.

Four different densities must be considered when writing a boundary integral equation for 2D elastostatics: the two components of the displacements, $u_1 = u$ and $u_2 = v$, and

the two components of the tractions, $t_1 = SG$ and $t_2 = TAU$. In this work, recovery of the tangential derivatives of each density is made independently, so that separate element error information is obtained for each of the four boundary densities. In a later step, the element residuals are combined into element errors that contain information from the recovery of the tangential derivatives of all four densities.

In what follows, a boundary density is denoted by ϕ ($\phi = u, v, SG$ or TAU) and its tangential derivative by $\partial\phi/\partial s$. The solution at any point inside the element *(e)* is

$$\phi^{(e)}(\xi) = \lfloor N \rfloor \{\phi\}^{(e)} = \sum_{i=1}^{m} N_i(\xi)\phi_i^{(e)}$$

where ξ is the intrinsic coordinate and m is the number of element nodes corresponding to the polynomial interpolation being used. The symbols $\lfloor \cdots \rfloor$ and $\{\cdots\}$ denote row and column vectors, respectively. Taking derivatives with respect to the intrinsic coordinate gives

$$\left(\frac{\partial\phi}{\partial s}\right)^{(e)} = \left(\frac{\partial\phi}{\partial\xi}\right)^{(e)}\left(\frac{\partial\xi}{\partial s}\right)^{(e)} = \left\lfloor\frac{\partial N}{\partial\xi}\right\rfloor\{\phi\}^{(e)}\left(\frac{\partial\xi}{\partial s}\right)^{(e)} \tag{63}$$

where $J(\xi, s) = (\partial\xi/\partial s)^{(e)}$ is the Jacobian of the transformation between the real element (with coordinate s) and the standard element (with the intrinsic coordinate ξ). These derivatives can be written with polynomial shape functions of one degree higher order as

$$\left(\frac{\partial\phi}{\partial s}\right)^{(e)*} = \lfloor N \rfloor \left\{\frac{\partial\phi}{\partial s}\right\}^{(e)*} \tag{64}$$

where $\{\partial\phi/\partial s\}^{(e)*}$ is the set of nodal values of the corresponding derivatives, equivalent in a local averaging sense, to the original ones, $\{\partial\phi/\partial s\}^{(e)}$. The element equivalence is enforced by requiring that both formulations for the derivatives give same element integrals, defined by

$$I_\phi^{(e)} = \int_{S^{(e)}} \{N\}\left(\frac{\partial\phi}{\partial s}\right)^{(e)*} ds = \int_{S^{(e)}} \{N\}\left(\frac{\partial\phi}{\partial\xi}\right)^{(e)} J(\xi, s)\, ds \tag{65}$$

where the integration is performed on $S^{(e)}$, which is the element length in 2D or the element area in 3D. If the element under integration is now written as $ds = J(s,\xi)d\xi$, where $J(s,\xi) = \partial s/\partial\xi = 1/J(\xi, s)$, all terms in the integrands are only functions of the intrinsic variable ξ, and all element integrations are performed for $\xi \in [-1,1]$, for the usual Lagrangian interpolating functions.

The element equations in Eq. (65) are then assembled for the entire boundary S, leading to an expanded system of equations that includes the original elements and the new zero-length elements at the double nodes.

A simple procedure is implemented in this work to account automatically for these new zero-length elements when assembling the system of equations. The procedure consists of three steps. In the first step, a test is performed at each node i, for discontinuities in the tractions or in the normal unit vector between the elements that share the node. A corner locator variable is set to a value of one wherever a corner is located or a discontinuity in traction exists.

The second step is to renumber the current nodes and elements to include the zero-length elements at the located "corner" nodes. A new augmented connectivity matrix is thus created relating node/element numbering, including the added zero-length elements. With this procedure, single values for the tractions and for the tangential derivatives of both the displacements and the tractions can be assigned to each node in the augmented system. An assembled system of equations is thus obtained from which the vectors of smoothed nodal derivatives $\{\partial\phi/\partial s\}^{(e)}$ can be obtained in this augmented system. The system matrix for the coefficients of the recovered or smoothed quantities is not singular and admits an inverse after assembling all elements.

The third step is to evaluate the element errors still in the augmented system and then renumber backwards the nodes/elements to their original numbering, by excluding the zero-length elements, so that only the error information of the original elements is retained.

The recovery of all four densities ($\phi = u, v, SG$ or TAU) is implemented in this work so that error estimators are obtained separately from the smoothed tangential derivatives of the displacements and of the tractions, and also a combined error estimator is obtained when the individual contributions from the tangential derivatives of the various densities are added. A scaling parameter is introduced so that the individual contributions are scaled before being added. Additional details for the implementation of the tangential derivative recovery for linear elements are described in (Jorge et al., 2005).

3.2.4.2 The external domain approach

The external domain error estimator approach is based on the difference between two equivalent formulations. The exact solution for one integral representation a problem satisfies any other possible different integral representation of the same problem. When a numerical solution is found for one formulation, this solution can be substituted into the discretized form (with same discretization) of the other possible formulation. Because numerical solutions are not exact, the identities in the discretized form of this second formulation will not be satisfied. The difference is a measure of the discretization error of both formulations.

The external domain approach uses the fact that, for a closed domain, the exterior boundary integral representations for both the displacements and the stresses equal zero in the elastostatics problem. Thus, any difference from zero can be related to the discretization error. Because fundamental solutions are functions of the distance between source and field points, one representation in which the exterior point is very close to the boundary might give a different error measure than the case in which the point is far away from the boundary. If different exterior points are considered, several external formulations may be obtained.

This error measure, estimated from the residual of the integral equation held at the outer source point, is sensitive to the external point position for non-trivial problems. For small but finite distances to the boundary, the estimator gives a local measure of the discretization error, but if the distance to the boundary becomes too small, errors associated to the location of the source point, coming from the numerical evaluation of the near-singular integrals, might become significant.

To implement the procedure, first a numerical solution at the boundary is obtained for the discretized mesh using a collocation BEM formulation. This boundary solution is then

substituted into the discretized integral representations for the interior displacements and stresses, and finally these displacements (u and v) and stresses (σ_x, σ_y and τ_{xy}) are evaluated at an exterior point $y^{(e)}$ in a close vicinity to a boundary element *(e)*. An external error estimator for the total displacement ($Ext: D$) is constructed as

$$E_{Ext:D}^{(e)} = \left[u\left(y^{(e)}\right)^2 + v\left(y^{(e)}\right)^2\right]^{1/2} \tag{66}$$

External error estimators can be defined from the stresses at the exterior point, as well. To eliminate any influence of the choice of global directions on the values of the stress error estimates, the stresses at the exterior point are combined into stress invariants to obtain error estimators. Two external errors estimators are adopted in this work: the octahedral stress ($Ext: T$) and the mean stress ($Ext: M$), given by

$$E_{Ext:T}^{(e)} = \frac{\sqrt{2}}{3}\left[\sigma_x^2 - \sigma_x\sigma_y + \sigma_y^2 + 3\tau_{xy}^2\right]^{1/2}$$
$$E_{Ext:M}^{(e)} = \left(\sigma_x + \sigma_y\right)/2 \tag{67}$$

with σ_x, σ_y and τ_{xy} evaluated at the exterior point $y^{(e)}$. The mean and octahedral stresses were chosen because they are independent stress invariants. Naturally, if the numerical boundary solution is exact, all external error estimators are zero.

The exterior evaluation point $y^{(e)}$ is located at a distance from the boundary (the distance from the exterior point to the closest point on the boundary) that is a fraction α of the size of the nearest boundary element *(e)*. This distance is measured from the element center in the normal direction to the element at this point.

In this work, numerical experiments are done with various values of the fraction α in order to evaluate the most appropriate location for the external point y. The closer the external point to the boundary, the more "local" the error information is.

On the other hand, if the external point is too close to the boundary, numerical errors may appear due to quasi-singularities.

The external domain error estimators can also be combined to obtain a more general error estimator ($Ext: D + T + M$) with error information from both external displacements and stresses. The individual contributions for element error are also scaled before adding, with the scaling factors defined as the average boundary total displacement $(u^2 + v^2)^{1/2}$ and total traction $(SG^2 + TAU^2)^{1/2}$, respectively.

An implementation of the proposed error estimators was presented in (Jorge et al., 2005), for the element errors $E_{Ext}^{(e)}$ for various values of the fraction α. Comparisons were also made between $E_{Ext}^{(e)}$ and $E_{GR}^{(e)}$ to show the consistency of the local information given by these estimates with mesh refinement.

One must point out that the external domain error estimator can be used only for domains in which an exterior region exists. For example, if using a traction-BIE without a multiregion approach for the case of a crack embedded in an infinite elastic body, no exterior region could be defined in which the evaluation point would be at a finite distance from the boundary.

In this case, the external domain error estimator could not be used, while the gradient recovery approach can always be used, for closed or open boundaries, and for finite or infinite domains.

3.2.4.3 A final note on the proposed Error Estimators for elastostatics BEM

Error estimators based on gradient recovery and external solution have shown consistency with mesh refinement and have given similar qualitative results. The error estimators were also proven to be useful to compare the efficiency of different types of mesh refinement (such as the *r*- and *h*-refinement schemes) for a particular problem.

The error estimator using the gradient recovery approach presents a more general characteristic as this formulation does not rely on an "optimal" choice of an external parameter, such as in the case of the external domain error estimator. Also, the external domain error estimator can be used only for domains in which an exterior region exists, while the gradient recovery approach can be used on a broader range of elastostatics problems.

4 Model Validation Under Uncertainty: Consistent Error Estimators and Bayesian Approaches

This section is based on research work in errors estimators in the context of modeling and simulation for design under uncertainty (Jorge et al., 2002), performed under the supervision of Dr. Sankaran Mahadevan, head of the multidisciplinary NSF-IGERT program (Multidisciplinary Doctoral Studies in Reliability and Risk Engineering and Management). The research objectives comprised:

- Review of error estimators for finite element methods.
- Coding of two error error estimators for the 2-D displacement-FEM. The first estimator is based on a gradient recovery procedure; the second estimator is based on the lack of inter-element stress continuity for the discretized results.
- Study the correlation / consistency between different error estimators, including both estimators coded (see previous item) and two other estimators previously obtained: error estimator based on Richardson extrapolation (uses two meshes: coarse and fine) and maximum error bound for the error (based on second derivatives).
- Outline a global-to-local approach for validation as follows: globally, the error estimator is investigated for consistency with the measured error or with other available estimators. Then, weak local regions are chosen to construct a reliability model to validate the numerical code.

A new model validation approach has been developed (Zhang & Mahadevan, 2003) (Rebba et al., 2006) (Mahadevan, 2002), in which error estimators from the discretized model were combined into an appropriate stochastic response surface approach, and a Bayesian approach for hypothesis testing was subsequently used, leading to decisions on acceptance/rejection of the model. The methods were demonstrated for application to the probabilistic life prediction of a composite helicopter rotor hub component, shown in Fig. (25).

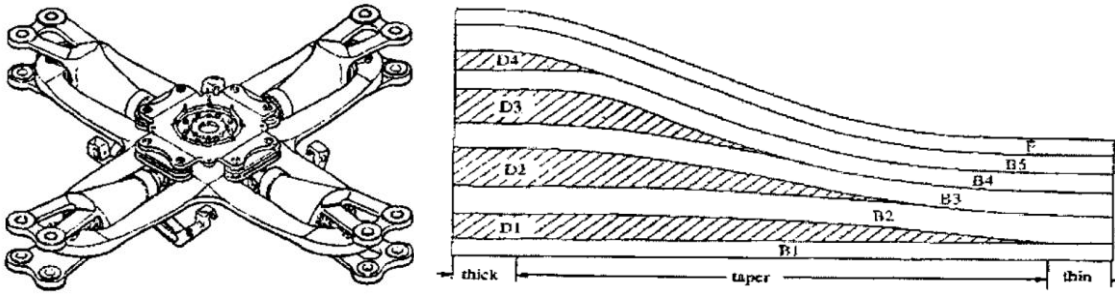

(a) (b)

Figure 25: (a) Rotor hub assembly (b) Half of the symmetric section of tapered composite test specimen - adapted from (Mahadevan, 2002)

In (Jorge et al., 2002), the consistency of different error estimators evaluated from different response quantities was investigated. Mean and octahedral stresses at a particular location were used as response quantities to obtain independent error estimates. Consistency between predicted weak locations of the structure was also investigated. The gradient recovery and the stress continuity error estimators were shown to be highly correlated and to indicate similar weak regions for the structure, while error estimators based on Richardson extrapolation and maximum error bound didn't shown similar consistency.

Also in this work, model validation results were investigated for consistent and nonconsistent error estimators, using conventional and stochastic response surface methods (RSM). Stochastic RSM was shown to be a more accurate model (for the response quantity of interest) than conventional RSM. Also, model validation results were found to be consistent (i.e., the probability of rejecting the code was similar) for consistent error estimators using the stochastic RSM.

For related research work in these topics see also (Rebba et al., 2003) (Rebba, 2005) (Rebba & Mahadevan, 2006b) (Rebba et al., 2006) (Rebba & Mahadevan, 2006b) (Rebba & Mahadevan, 2006a).

4.1 Consistent Error Estimation Strategy for Model Validation

4.1.1 Introduction

A 3-step methodology for numerical model validation under uncertainty is presented in this paper, in which a) a consistent error estimator is selected; b) an appropriate response surface method is constructed for the error function to replace the numerical model; and c) a Bayesian approach is used for decisions on model acceptance. This section concentrates on the strategy for the choice and use of appropriate error estimators for model validation purposes.

The details of the proposed methodology are included in subsection 4.1.2. For the purpose of illustrating the consistent error estimator strategy, the discussion in this work uses a displacement-based finite element model for a 2D elastostatics problem. Surveys of the extensive literature existing on error estimation for finite element methods can be found in (Noor & Babuška, 1987) (Olgierd C. Zienkiewicz & Taylor, 1994) (J. Tinsley Oden & Demkowicz, 1989) (Zhu, 1997) (Ainsworth & Oden, 1997). Mostly, the literature deals with discretization error, and the development of methods for estimating modeling error

has appeared very recently (J. Tinsley Oden & Vemaganti, 2000) (J. Tinsley Oden et al., 2003).

Adaptive mesh refinement is a common application of error estimators (O. C. Zienkiewicz & Zhu, 1991) (Verfürth, 1994) (Zhu & Zienkiewicz, 1997). For that purpose, error approaches usually include the evaluation of error norms and / or some type of residuals (J. T. Oden et al., 1990) (Ainsworth & Oden, 1993) (I. Babuška et al., 1995). Usually, residuals, norms and other quantities used for error estimation are not explicit variables of a code. Instead, residuals are usually obtained after numerical manipulations of the code variables, and thus they cannot be measured directly. In this work, error estimators are sought that provide local error information on variables obtained explicitly from the code, so that these variables can be studied as response quantities of interest, for further stochastic treatment.

Four existing discretization error estimator approaches are investigated in this work, for their usefulness for further stochastic treatment of the error. The first error estimator is based on Richardson's extrapolation (Richards, 1997), in which the local error is evaluated from the differences between the response quantities obtained for two different meshes. The second error estimator gives in fact not an estimate, but just an upper bound for the magnitude of the error, and is called the maximum error bound error estimator (Huebner et al., 2008). This maximum error bound is obtained by evaluating second derivatives of the smoothed numerical solution. The third error estimator procedure is based on inter-element continuity requirements for the stress field, not satisfied by the finite element solution (O. C. Zienkiewicz & Zhu, 1987). The fourth error estimator is based on a gradient recovery procedure (O. C. Zienkiewicz & Zhu, 1987) (O. C. Zienkiewicz & Zhu, 1992a) (O. C. Zienkiewicz & Zhu, 1992b). The recovery of displacement derivatives is rewritten as stress recovery, using Hooke's law. The error estimators used in this work are detailed in subsection 4.1.3.

The key feature in the approach is the study of the consistency of some error estimator with respect to other available information. In this work, the available information is represented by other independent error estimator approaches and / or error estimators obtained for other independent response quantities. The error estimators are investigated for consistency in Section 4.1.4.

Model validation can be performed also by comparing the numerical information with some available measured / experimental results. The procedure to investigate error consistency is analogous, with the error estimator results being compared with the experimental results, in this case. The consistency of the error estimators with respect to measurement results (if available) is studied using the same global-to-local methodology, but comparisons between measurement and numerical results can be made only in regions were measurement results are available.

The consistent error estimator approach (first step of the 3-step approach) is detailed in subsection 4.1.4. Depending on the choice of the error estimator and response quantity, the model validation criterion could lead to different decisions of accepting or rejecting the model. The strategy adopted in this work is to choose different error estimators and check for the consistency of the error throughout the domain being modeled. For a particular problem, a measure of the consistency between the available error estimators can be obtained by the correlation between the 2D plots of the local error estimates. Similarly, this correlation study can be performed between estimated error results and the

measured error, if some information from measurements of the physical problem is available. Typical results for the errors are included in subsection 4.1.4, below.

The response surface methods (RSM) and the Bayesian approach used in this work (for the time-independent case without statistical uncertainty in the model) are detailed in subsection 4.2, below. The Bayesian approach is applied to obtain Bayes factors, needed for model-acceptance decisions. The obtained model-acceptance decisions are compared in subsection 4.2, below, for the cases of the conventional and stochastic RSMs and also for the cases of consistent and non-consistent error estimators.

4.1.2 A 3-Step Methodology for Numerical Model Validation under Uncertainty

The proposed methodology for numerical model validation under uncertainty consists of three steps. In the first step, a global-to-local strategy is used to locate regions with high error values and to choose an error estimator that consistently represents the discretization error in these regions of interest.

For a particular problem being modeled, local error estimators could be evaluated for different response quantities. Also, different error estimation approaches could be adopted for the same response quantity. Also, different locations in the domain being modeled could be chosen to generate the prior estimates of model failure probability. Depending on so many choices for the error estimator, the Bayesian model validation could lead to different decisions of accepting or rejecting the model, for different error estimators, response quantities and locations.

The strategy adopted in this work is to check for the consistency of the distributed error throughout the domain being modeled, for different error estimators. The correlation between 2D plots for the local error obtained from different estimators is used in this work as a measure of the consistency of the estimator.

From the correlation between the estimators, an error estimator is chosen based on its global consistency when compared with the other available error sources.

Different error estimators are compared by means of 2D dispersion plots. Also compared are the errors obtained from different response quantities. By using 3D plots, errors are shown to indicate weak regions of the structure, where high errors coexist with high, unacceptable, values of the response quantity. Consistent error estimators are highly-correlated, and thus are expected to identify and locate similar weak regions. A certain number of representative points are selected from these weak regions.

The second step constructs a metamodel for the error at the selected points using response surface techniques, to estimate the statistical distribution of the prediction error for the finite element model. The statistical distribution of the model error at a particular location is used to compute prior estimates of model failure probability, to be used in Bayesian model validation.

Finally, Bayesian hypothesis testing-based model validation procedure can be applied for the selected critical locations, and decisions of accepting or rejecting the model are made based on the Bayes factor computed at the critical locations. The Bayesian approach (third step of the 3-step approach) has been developed earlier in (Zhang & Mahadevan, 2003), for time-independent and time-dependent cases, and for cases with or without statistical uncertainty in the model.

The obtained Bayes factors were used as acceptance/rejection criteria for the model. This Bayesian approach is extended in this work to metamodels corresponding of response surfaces representing the chosen consistent estimator of the numerical error at the selected points.

Basically, first the approach looks for error estimator consistency from a global point of view. Then, weak regions are located where the Bayesian approach is applied, so model validation is considered from a local perspective, only at regions where important errors were found.

The goals are to establish enough confidence on the error estimator first, and then to use the error information to reduce the number of points where model validation will be tested.

4.1.3 Estimators of Discretization Error for Model Validation

Errors in the prediction of a certain response quantity are expected to exist when using approximate numerical models. Different error estimators can be envisaged for a particular problem. The current work focuses on a strategy for the choice and use of appropriate error estimators for model validation purposes.

Some error estimators well suited for adaptive refinement provide estimates that are always positive. This is the case, for example, of error estimators based on residuals. In this work, the envisaged stochastic distribution of the error may be able to assume either positive or negative values, as the numerical model over-predicts or under-predicts the average response quantity in the element.

Some of the error estimators in this work were derived so that they can assume positive or negative values, to allow further stochastic treatment for the error.

Four error estimator approaches are investigated in this work:

- error estimator based on Richardson's extrapolation (Richards, 1997);
- maximum error bound error estimator (Huebner et al., 2008);
- error estimator based on lack of inter-element stress continuity (O. C. Zienkiewicz & Zhu, 1987); and
- gradient recovery error estimator (O. C. Zienkiewicz & Zhu, 1987) (O. C. Zienkiewicz & Zhu, 1992a) (O. C. Zienkiewicz & Zhu, 1992b).

These estimators were selected because they are able to provide error information for variables explicitly obtained from the code, without the need to indirectly obtain other quantities such as the residuals. These code variables can be understood as response quantities, for further stochastic treatment of the error.

For the elastostatics problem being studied, all estimators provide local error information for the stresses. Stress invariants can be written so that the stress information is recast in terms of scalar quantities, independent of the directions. The mean stress and the octahedral stress are used for this purpose. Because in 2D these two stresses are independent quantities, error estimators based on mean stress and on octahedral stress are also independent.

After the various distributions of element errors are obtained, relationships between the different error indicators, or between an error indicator and the measured error, can be obtained. In subsection 4.1.4, 2D plots are adopted, to study the 2D dispersion or

correlation of those error measures. Linear regression can be used to quantify this correlation. Points in the 2D plot are generated from local error information at the various elements. As far as the spatial error distribution is concerned, each element error is associated with a point corresponding to the element centroid.

A square plate with a hole in the center subjected to uniform distributed loading is considered as a numerical example. One quarter of the plate is modeled, as shown in Fig. (26). The plate is discretized using a mesh of 133 nodes, with constant strain triangular elements (CST), i.e., elements with linear distribution for the displacements. A second mesh with 280 nodes is considered for the Richardson extrapolation error estimator.

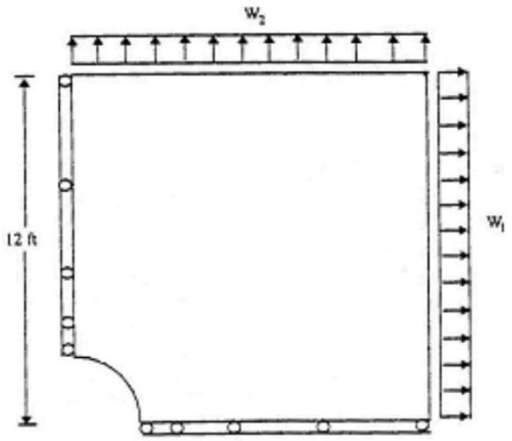

Figure 26: Plate with a central hole under uniform distributed loading - adapted from (Jorge et al., 2002)

4.1.3.1 Richardson extrapolation error estimator

In the Richardson extrapolation for estimating the error in grid refinement, consider an analysis code that predicts the output response f as

$$f = f_{h=0} + g_1 h + g_2 h^2 + g_3 h^3 + \ldots \tag{68}$$

where $f_{h=0}$ is the exact solution or the continuum value given for the mesh size $h = 0$. The functions g_1, g_2, g_3, etc., are independent of the grid size. Assuming a second order solution and computing the response at two different mesh sizes h_1 and h_2, with h_1 being the size of the finer mesh, neglecting higher order terms in the above expansion and solving for $f_{h=0}$,

$$f_{h=0} \cong f_1 + \frac{f_1 - f_2}{r^2 - 1} \tag{69}$$

where the grid refinement ratio $r = \dfrac{h_2}{h_1}$ and f_1, f_2 are the solutions at two mesh sizes. By generalizing the Richardson extrapolation for a p^{th} order method,

$$f_{h=0} \cong f_1 + \frac{f_1 - f_2}{r^p - 1} \tag{70}$$

The ordered error estimate, given by ($f_{h=0}$ - f_1), is a good approximation of the discretization error. The order of convergence p can be obtained from the equation:

$$p = \ln\left(\frac{f_3 - f_2}{f_2 - f_1}\right) / \ln(r) \tag{71}$$

where f_3 is the solution with the finest grid size.

4.1.3.2 Maximum error bound

If the exact solution for a problem in two dimensions, f(x, y) is known, then the error associated with the finite element solution $f_{fem}(x, y)$ can be written as (Verfürth, 1994):

$$E(x, y) = f(x, y) - f_{fem}(x, y) \tag{72}$$

Thus the error varies across the domain. If the exact solution is not known, local error estimation based on interpolation error is adopted. To illustrate the derivation of the local maximum error bound, a one-dimensional case is shown subsection 3.1.1, for simplicity (see also Fig. (16), above). For a two-dimensional problem,

$$E(e) \cong \frac{1}{8}\left(\left|\frac{\partial^2 f_{fem}}{\partial x^2}\right|_{x_M} + 2\left|\frac{\partial^2 f_{fem}}{\partial x \partial y}\right|_{x_M} + \left|\frac{\partial^2 f_{fem}}{\partial y^2}\right|_{x_M}\right) h^2 \tag{73}$$

4.1.3.3 Error based on inter-element continuity for stresses

An error estimation procedure for displacement-based FEM was developed by (O. C. Zienkiewicz & Zhu, 1987) to obtain energy norms of errors derived from the lack of inter-element stress continuity. In this work, instead of evaluating element residuals that are always positive, an average value for the element error is pursued, which can assume either positive or negative values.

The usual C^0 continuity assumption for the displacements in displacement-based finite element formulations results in a stress field that is continuous inside the elements, while discontinuous in the interface between elements. Except for problems with physical discontinuities, such as cracks in fracture mechanics problems, the usual linear elastostatics problems deal with stress fields that are physically continuous. Thus, differences between stress values evaluated at an inter-element node, from the various elements sharing this node, represent local error indicators.

To construct an element-based measure for the stress error at a node, the average stress at this node, as evaluated from all elements sharing the node, is taken as a better approximation for the nodal stress. Thus, the stress error vector at node n of element i is given by

$$\Delta\sigma_n^i = \sigma_n^i - \sigma_n^{ave} \tag{74}$$

where σ_n^i represents a stress component (either σ_x, σ_y or τ_{xy}) at node *n* of element *i*, and the corresponding averaged stress is evaluated as

$$\sigma_n^{ave} = \frac{\sum_{i=1}^{N_e^n} \sigma_n^i}{N_e^n} \tag{75}$$

where N_e^n is the number of elements sharing node *n*. An element error for each stress quantity is constructed as the element average of the nodal contributions. For that, the stress error is interpolated inside element i using appropriate shape functions.

$$\Delta\sigma_i(x,y) = \lfloor N_n(x,y) \rfloor \{\Delta\sigma_n^i\} \tag{76}$$

The element error for each stress quantity is obtained from the stress error average.

$$E_\sigma^i = \frac{1}{S^i} \iint_{S^i} \Delta\sigma_i(x,y)dxdy \tag{77}$$

In this work, the stress error is interpolated with the same shape functions used for the interpolation of the displacements. In other words, the stress error is interpolated inside each element with shape functions one degree higher than the shape functions necessary to interpolate the original stress components. In the case that $\Delta\sigma_i(x,y)$ is interpolated with linear shape functions, the element error in Equation (77) reduces to the stress error at the element centroid *G*

$$E_\sigma^i = \Delta\sigma_i(x_G, y_G) \tag{78}$$

The resulting element error has dimensions of stress, and in terms of spatial error distribution, this error can be associated with a point in the domain corresponding to the centroid of the element. Also, different from (O. C. Zienkiewicz & Zhu, 1987), the error is not obtained from an energy norm expression. The goal here is to obtain estimates that can assume positive or negative values, to allow further stochastic treatment for the error. The stress tensor components are direction-dependent quantities. To obtain scalar quantities to be used as response quantities, the stress tensor invariants can be evaluated. In this work, the mean stress (σ_m) and the octahedral stress (τ_o) are adopted as response quantities, as they are independent invariants obtained from the stress tensor.

$$\sigma_m = \frac{\sigma_x + \sigma_y}{2} \tag{79}$$

$$\tau_o = \frac{\sqrt{3}}{2}[\sigma_x^2 - \sigma_x\sigma_y + \sigma_y^2 + 3\tau_{xy}^2]^{1/2} \tag{80}$$

Thus, from Equation (77) (general case) or from Equation (78) (linear interpolations for the stress errors), the element stress errors can be obtained as $E_{\sigma_m}^i$ and $E_{\tau_o}^i$. Thus, independent error estimators are obtained from the two independent response quantities, mean stress and the octahedral stress.

4.1.3.4 Error based on a gradient recovery approach

The procedures of error estimation using stress or gradient recovery were introduced by (O. C. Zienkiewicz & Zhu, 1987) and are detailed in subsection 3.3.1, above. In this procedure, element residuals are obtained from differences between smoothed and non-

smoothed derivatives of the field variables. In the current work, instead of evaluating element residuals that are always positive, an average value for the element error is pursued, which can assume either positive or negative values.

Nodal smoothed derivatives are evaluated from a weighted average of element derivatives surrounding the node. The weighting factors are the element areas. The derivative of the finite element solution in the element can be written using derivatives of the shape functions. The derivatives are written in an average sense to find the vector of nodal smoothed derivatives. An element equivalence between smoothed and non-smoothed derivatives is written and a system of equations is obtained by assembling the element equations, from which the vector of nodal smoothed derivatives is obtained.

Also, similar to the inter-element continuity error procedure, the response quantities of interest are two independent stress invariants, the mean stress and the octahedral stress. To obtain a better approximation of nodal stresses, the first step is to apply the gradient recovery approach to displacement derivatives. Smoothed nodal values for the displacement derivatives are obtained by imposing the smoothed solution to be equivalent to the original solution in an average sense. The obtained nodal values for the smoothed displacement derivatives are converted into smoothed strains which are subsequently converted into stresses by means of Hooke's law. Then, a better approximation for the mean and octahedral stresses is obtained from Equations (79) and (80). Finally, the stress error vector at node *n* of element *i* is given by

$$\Delta\sigma_n^i = \sigma_n^i - \sigma_n^{i*} \tag{81}$$

where σ_n^i represents a stress component (either σ_x, σ_y or τ_{xy}) at node *n* of element *i*, and the smoothed stresses are denoted by an asterisk (*). Then, similar to the inter-element continuity error procedure, the element error is obtained by Equation (77), for both the mean and the octahedral stresses. Thus, two independent local error estimators, one for each response quantity, are obtained using the recovery procedure for the displacement derivatives.

The gradient recovery error estimator was coded for 2D elastostatics problems modeled by displacement-based FEM. The FEM code uses CST constant strain triangular elements with linear distribution of displacements. The recovery of the four types of derivatives $\frac{\partial u}{\partial x}$, $\frac{\partial u}{\partial y}$, $\frac{\partial v}{\partial x}$, and $\frac{\partial v}{\partial y}$ is performed independently. Also, to obtain the smoothest solution for the displacement derivatives, element matrices obtained from the equivalence equation are assembled for the entire domain, and not only for a region surrounding a node.

4.1.4 Consistency of the Error Estimators

The four error estimators presented in this work are investigated for consistency. The correlation between different error estimator results for the response quantity is investigated. Also investigated is the correlation between error results for the same error estimator and different response quantities.

4.1.4.1 Consistency between error estimators for the same response quantity

Different error estimation approaches can lead to different local error estimates for a given response quantity. Consistency through different error estimators is investigated for the two response quantities used in this work: mean stress and octahedral stress in the region of interest. Figure 27 shows the good agreement between the errors in mean stress from two different error estimation approaches: gradient recovery and lack of inter-element continuity in stress. The points present a very good correlation, with ρ=0.9927, showing that the gradient recovery error estimator is consistent with the inter-element continuity error estimator for the response quantity considered.

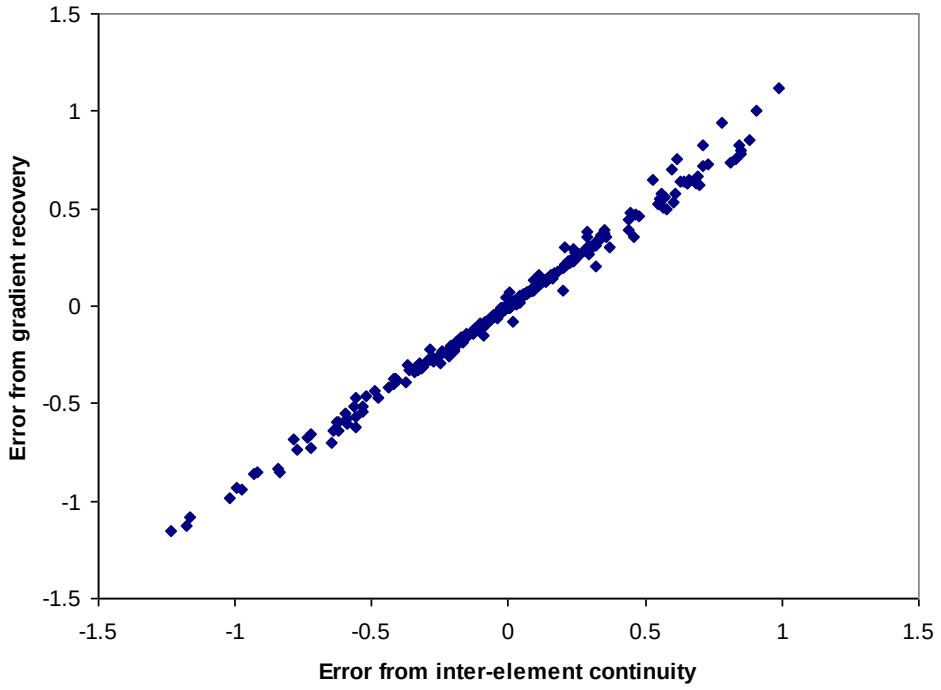

Figure 27: Errors in Mean Stress from two different error estimation approaches. Each point corresponds to an element centroid. Mesh of 280 nodes - adapted from (Jorge et al., 2002)

The four error estimators for the octahedral stress were compared two by two, to investigate the correlation between the pairs of estimators. Figures 28 (a) to (f) show the various plots, including the regression equation and the *R*-squared parameter obtained from linear regression.

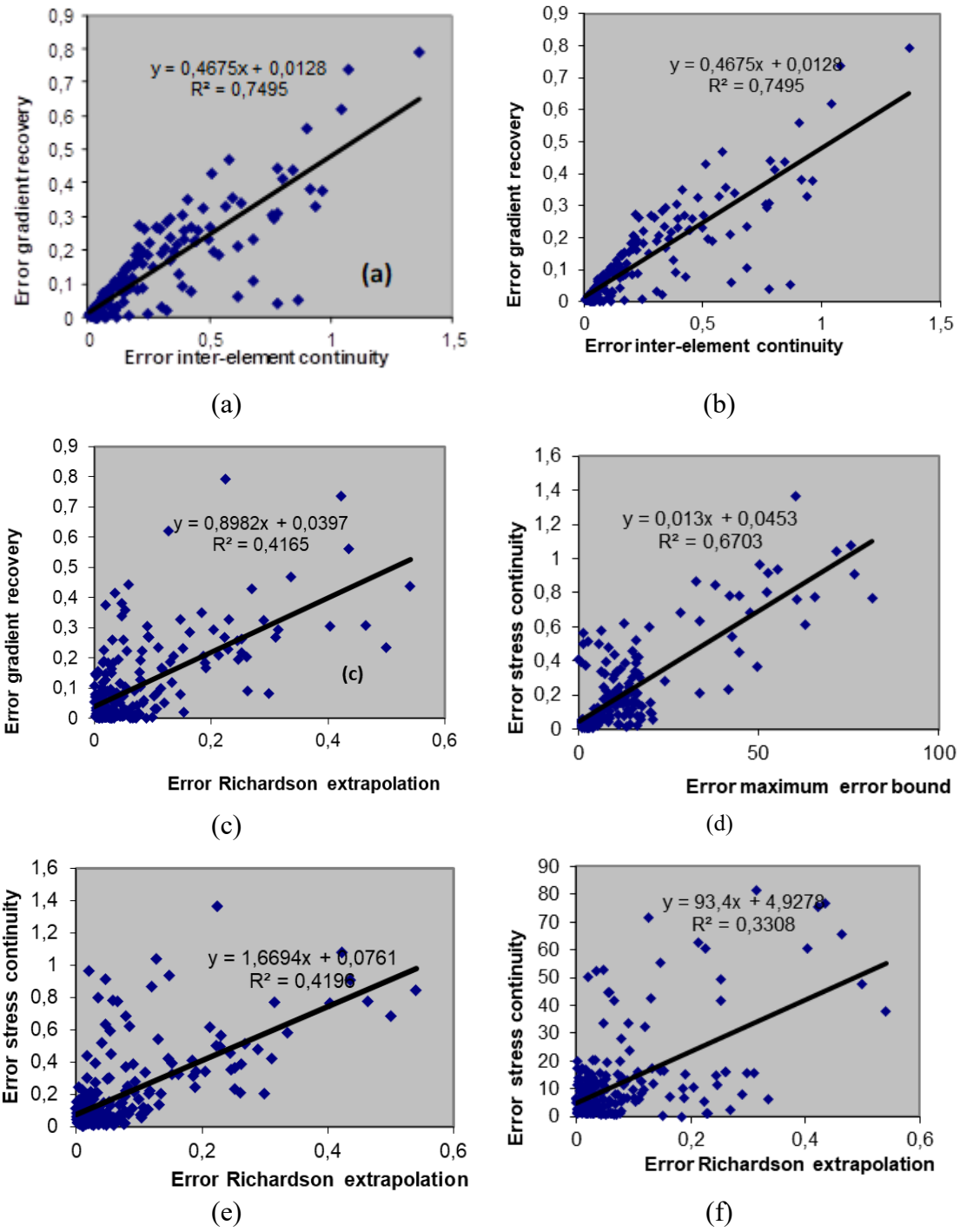

Figure 28: error estimators for the octahedral stress, 133-node mesh (a) Gradient recovery vs. stress continuity; (b) Gradient recovery vs. maximum error bound; (c) Gradient recovery vs. Richardson extrapolation; (d) Stress continuity vs. maximum error bound; (e) Stress continuity vs. Richardson extrapolation; (f) Maximum error bound vs. Richardson extrapolation - adapted from (Jorge et al., 2002)

From the six cases, the diagram for gradient recovery and stress continuity presents the best correlation, with ρ = 0.8657. When the comparison is done including either Richardson extrapolation or maximum error bound error estimators, the plots present poorer correlation coefficients.

Table 1 summarizes the results for the correlation.

Table 1: octahedral stress error estimators correlation - adapted from (Jorge et al., 2002)

Estimators being compared	Correlation coefficient ρ
Gradient recovery versus stress continuity	0.8657
Gradient recovery versus maximum error bound	0.7049
Gradient recovery versus Richardson extrapolation	0.6454
Stress continuity versus maximum error bound	0.8187
Stress continuity versus Richardson extrapolation	0.6478
Maximum error bound versus Richardson extrapolation	0.5752

The poor correlation results shown in Table 1 whenever either Richardson extrapolation or maximum error bound is included in the 2-D plot, helps demonstrate the lack of consistency when comparing these error estimators to any other estimator among those evaluated in this work.

4.1.4.2 Consistency between response quantities for the same error estimator

The consistency of different (and independent) error estimators evaluated from different response quantities is investigated. For example, the mean stress and the octahedral stress at a particular point are independent stress invariants and can be used to obtain independent error indicators. Figure 29 shows the plot of the errors from the gradient recovery approach as evaluated for the two response quantities of interest, the mean stress and the octahedral stress. The points present a reasonably good correlation, with ρ = 0.8512, showing that the gradient recovery error estimators are consistent for the two independent response quantities considered.

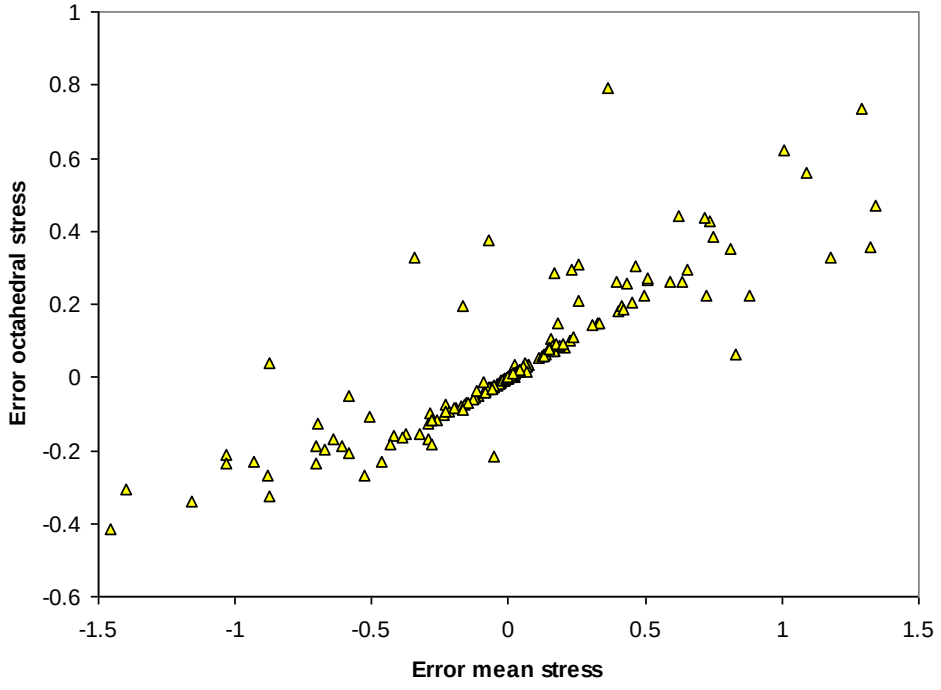

Figure 29: Stress errors from gradient recovery for two independent quantities. Points are associated with element centroids. Mesh with 133 nodes - adapted from (Jorge et al., 2002)

4.1.4.3 Consistency of weak locations for response quantities and error estimators

The consistency between predicted weak locations of the structure is investigated. Weak locations are expected to be consistent for different (but consistent) error indicators. Also, predicted weak locations should be consistent with experimentally measured weak locations. In case weak locations are not consistent, an issue remains to be investigated, namely, to verify if the error indicators were able to predict this inconsistency.

Figure 30 shows the plot of the errors in mean stress (from the lack of inter-element continuity in stresses) versus the mean stress values at element centroids. The points present a very correlation, with $\rho = 0.9641$, showing that these errors are consistent with the variable values. High values of the errors were found at locations with high stress values.

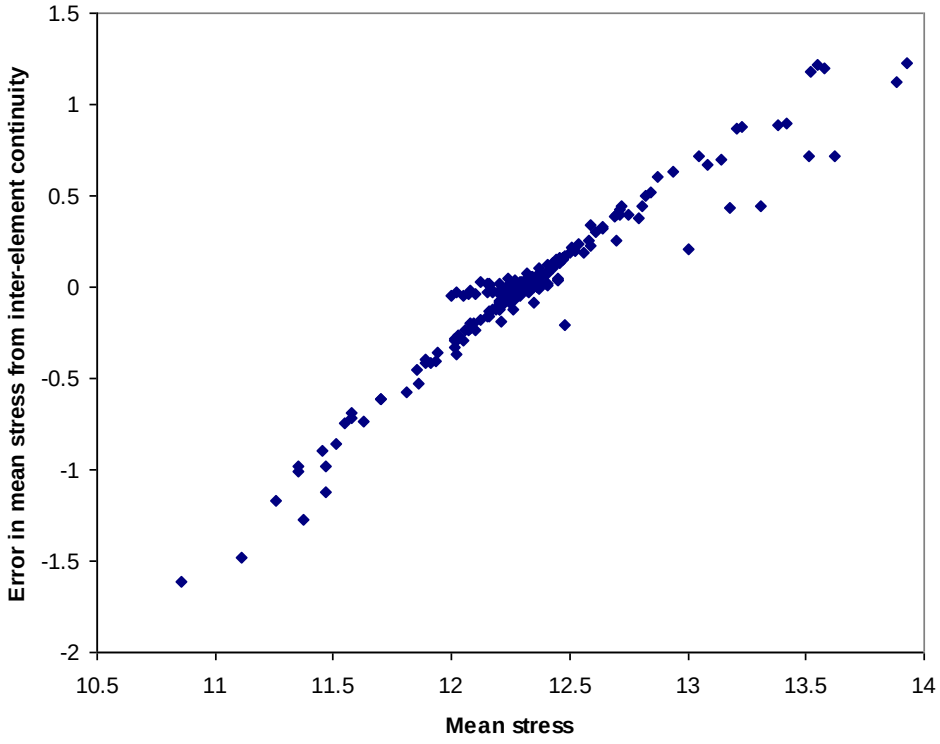

Figure 30: Error in mean stress (from the lack of inter-element continuity in stresses) versus mean stress values at element centroids. Mesh with 133 nodes – adapted from (Jorge et al., 2002)

Figure 31(a) shows the plot of the errors due to the lack of inter-element continuity in the octahedral stresses versus the Cartesian coordinates of the plate. The locations for the points with high errors are consistent with the locations with high values for the octahedral stress itself, as shown in Figure 31(b). The gradient recovery error estimator (not shown) gives similar results.

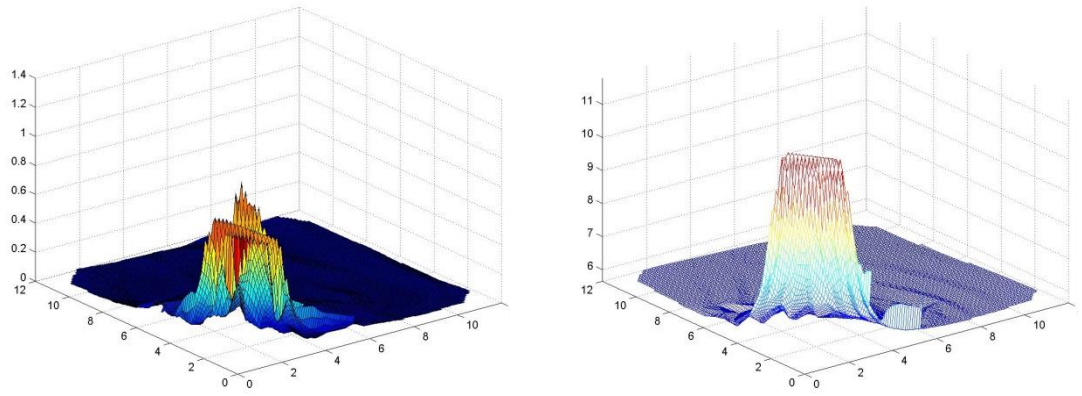

(a) (b)

Figure 31: Consistency of weak locations of the plate. (a) Errors in Octahedral Stress from lack of inter-element stress continuity. (b) Octahedral Stress – adapted from (Jorge et al., 2002)

In this problem, the region close to the circular hole corresponds to high values of both a response quantity and the discretization error relative to this quantity.

4.1.4.4 Consistency between error estimators and model validation

An important issue that needs to be addressed is to verify the desired correlation between error consistency and model validation consistency. If error indicators are consistent, the corresponding model validation results are expected to be consistent, too. In other words, the probability of rejecting the code is expected to be similar in the case of two consistent error indicators. Furthermore, the decisions to accept/reject the model are also expected to be similar. This issue is addressed in subsection 4.2, below.

4.1.5 Global-to-Local Approach for Using Consistent Error Estimators in Model Validation

Error estimators quantify the local discretization error. With random inputs to the finite element model, the output becomes a random quantity. Thus the prediction error is a random variable, whose statistics combined with Bayesian hypothesis testing (I. Babuška et al., 1995) lead to a model validation criterion. However, the choice of the error estimator may control the acceptance or rejection of the model to some extent.

One estimator may imply that the model is valid but another estimator may imply the opposite. Also, the error in model predictions may vary over the domain. A consistent error estimator is needed for model validation, so that error predictions for two different but consistent estimators are equivalent.

A global-local approach for using consistent errors for model validation can be envisaged as follows: globally, an error indicator for a particular response quantity is investigated for consistency with other available error estimators or with a measured error, if available. Then, local weak regions are identified, where the error is large and the values of the response quantity are also large. One or more points can be selected in this ‘’weak’’ region so that a metamodel for the error at this location can be constructed using response surface methods.

Finally, the Bayesian approach can be applied at the chosen points in the weak region, to obtain a minimum value for the Bayes factor, to be used for model validation. The Bayesian approach is applied in subsection 4.2, below, for two metamodels, one constructed using conventional response surface methods (RSM) and another using stochastic RSM. Also, the Bayesian approach is applied in subsection 4.2, below, for metamodels obtained using consistent and non-consistent error estimators.

4.1.6 Some Remarks on Consistent Error Estimators

Error consistency can be qualitatively demonstrated by means of 2D dispersion plots. A statistical model to measure error consistency is useful to quantify this consistency. In this work, the evaluation of the regression parameters from the 2D plots was performed with this purpose.

Typical consistency results are obtained by comparing the correlation between different error estimators and also by comparing errors from different response quantities. In this work, two error estimators didn't show consistent behavior (Richardson extrapolation and maximum error bound) while two other estimators (inter-element continuity and gradient recovery) presented a good correlation, for a give response quantity. Also, two different response quantities were shown to be reasonably correlated (the mean and the octahedral stress)

From this approach, one or more weak locations are selected to apply the Bayesian approach on subsection 4.2, below. Consistent error estimators lead to the same decisions in terms of the choice of the weak regions of the structure.

Consistency of the error estimators with respect to measurement results (if available) can also be studied using the same global-to-local methodology. Comparisons between measurement and numerical results can be made only in regions were measurement results are available.

4.2 Combining Error Estimators and Bayesian Hypothesis Testing in a Model Validation procedure

4.2.1 Introduction

In subsection 4.1, a 3-step methodology for numerical model validation under uncertainty is presented, in which

a) a consistent error estimator is selected;
b) an appropriate response surface method is constructed for the error function to replace the numerical model; and
c) a Bayesian approach is used for decisions on model acceptance.

Also, subsection 4.1 concentrates on the strategy for the choice and use of appropriate error estimators for model validation purposes. The consistent error estimator approach (first step of the 3-step approach) is detailed in subsection 4.1, wherein four error estimator approaches were investigated: error estimator based on Richardson's extrapolation (Richards, 1997), maximum error bound error estimator (Huebner et al., 2008), error estimator based on inter-element stress continuity requirements (O. C. Zienkiewicz & Zhu, 1987), and error estimator based on a gradient recovery procedure (O. C. Zienkiewicz & Zhu, 1987) (O. C. Zienkiewicz & Zhu, 1992a) (O. C. Zienkiewicz & Zhu, 1992b).

These local error estimators were applied to two independent response quantities: the octahedral stress and the mean stress. The error estimator based on inter-element continuity for stress and the gradient recovery error estimator were shown to be consistent for a given response quantity. Also, the two response quantities were shown to be consistent for a given error estimator.

The Bayesian approach for model validation (third step of the 3-step approach) was introduced in (Zhang & Mahadevan, 2003). This approach requires the knowledge, or at least an estimate, of the statistical distribution of the error in the computational model. This information is used to compute a prior estimate of model failure probability, an essential quantity in Bayesian model validation. The error estimators used in deterministic finite element analysis need to be extended to stochastic analysis for systems with uncertainties. To attain this objective, two possible approaches would be Monte Carlo simulation and response surface methods (RSM).

In this subsection, response surface models are employed for computational efficiency in predicting the stochastic distribution of error. The conventional RSM, as well as a stochastic collocation point-based RSM are explored to obtain prior error distribution to be used in the Bayesian approach. The error in predicting the response is obtained in terms of the input random variables and the distribution of this error is used to calculate the Bayes factor, an estimator of model validity.

Finally, in this subsection, only the Bayesian approach for the time-independent case without statistical uncertainty in the model is applied, to obtain the Bayes factors needed for model-acceptance decisions. The obtained model-acceptance decisions are compared for the cases of the conventional and stochastic RSMs and also for the cases of consistent and non-consistent error estimators.

4.2.2 Stochastic Distribution of Error

For a certain problem, the output of the model is given by some function of response quantities. In the 2D plate presented in subsection 4.1, the octahedral and the mean stress are local response quantities obtained from the finite element model. These response quantities are evaluated at certain locations, either the nodes or the element centroids, depending on the error estimator.

Due to physical, model and data uncertainty, the obtained response quantity at a certain location is not a single value but follows a statistical distribution. The type of distribution depends on the statistics of the input random variables, and also on how these uncertainties propagate through the model to become uncertainties in the response quantity.

The uncertainties in the response need to be quantified using probabilistic methods. One possible approach to quantity these uncertainties would be to perform Monte Carlo simulation. For that, statistical parameters are assigned to the input quantities, and the response is obtained by repeating the finite element analysis for a large sample input parameters. For the plate problem, the loads are the random inputs of the model. The scatter in the response can be used to estimate the scatter in error. In order to determine the type of distribution for the response, we need typically, a large number of finite element runs. For complex finite element models, this could be practically impossible and very time intensive, and is not pursued in this work.

For computational efficiency, a sufficiently accurate computational model may be used to replace the finite element model. The variabilities in the input variables are propagated to the output through this computational model. Various methods are available to carry out such uncertainty analysis. Available uncertainty propagation models can be classified into three categories:

(a) analytical methods;
(b) sampling based methods; and
(c) response surface methods.

The selection of the method depends on the nature of model used for predicting the output. In this subsection, response surface-based methods are used to predict the output of the response quantity at a certain location and determine the distribution of the error in this predicted output. The error estimators discussed in subsection 4.1 can be extended to estimating the error in the prediction of the response in stochastic analysis, in which the response is written in terms of input random variables by a response surface technique. Thus, the error calculated is stochastic and its distribution can be easily obtained by simulating the input random variables.

4.2.3 Response Surface Methods

Response surface methods (Pike et al., 1988) consist in selecting different values of input parameters, running the computer or simulation model to get samples of response, and then fitting a closed-form model which acts as a surrogate to the actual input-output relationship. The new adopted surrogate model or metamodel can be used to predict the response and carry out the uncertainty analysis. In this subsection, two stochastic response surface based methods are investigated, specifically, conventional response surface method (CRSM) and stochastic response surface method (SRSM). The details in implementation of the two methods are discussed below.

4.2.3.1 Conventional Response Surface Method

The basic idea in using the response surface is to propagate the uncertainties in the input parameters to the output response. The full-scale complex physical model of interest e.g. finite element model or the exact model can be replaced by a response surface equation, consisting of the input parameters, with data obtained from an appropriate design of experiments. This model can describe the variability in the response. A simple second order response surface model in terms of the input variables xi is given by

$$y(x) = b_o + \sum_j b_j x_j + \sum_i \sum_j b_{ij} x_i x_j \tag{82}$$

For the implementation of the response surface methodology to the plate problem defined in subsection 4.1, the coefficients of the above equation are estimated from a factorial design, using the statistics for the load variables given in Table 2.

Table 2: Statistics of the input variables - adapted from (Jorge et al., 2002)

Variable	Type	Parameters
W_1	Normal	(12, 2.4) kips/in
W_2	Normal	(12, 2.4) kips/in

Sample points for fitting the conventional RSM are obtained when the response quantity (in this work, the error in the mean stress or in the octahedral stress at the chosen location) is evaluated for W_1 and W_2 assuming the following values: low=12-3*2.4=4.8, average=12, and high=12+3*2.4=19.2.

4.2.3.2 Stochastic Response Surface Method

The metamodel or response surface could also be constructed in a different way. A stochastic response surface method is proposed here with the objective of providing a better response surface, which is accomplished by approximating both the input and output of the system with uncertainties through series expansions of standard random variables. Each of the input random variables may be expressed as a function of standard normal variables ξ_i, because of mathematical tractability. For example, a normal random variable can be expressed in terms of its parameters as $\mu + \sigma\xi$. A uniform random variable bounded between a and b is expressed as $a + \frac{b-a}{2}\left(1 + erf\left(\frac{\xi}{\sqrt{2}}\right)\right)$. The output can be approximated by a polynomial chaos expansion, given by:

$$y = a_o + \sum_{i_1=1}^{n} a_{i_1}\Gamma_1(\xi_{1_1}) + \sum_{i_1=1}^{n}\sum_{i_2=1}^{i_1} a_{i_1 i_2}\Gamma_2(\xi_{i_1},\xi_{i_2}) + \sum_{i_1=1}^{n}\sum_{i_2=1}^{i_1}\sum_{i_3=1}^{i_2} a_{i_1 i_2 i_3}\Gamma_3(\xi_{i_1},\xi_{i_2},\xi_{i_3}) + ... \quad (83)$$

where y is the output and $\Gamma_p(\xi_{i_1},...,\xi_{i_p})$ are muti-dimensional Hermite Polynomials of degree p given by

$$\Gamma_p(\xi_{i_1},...,\xi_{i_p}) = (-1)^p e^{\frac{1}{2}\xi^T\xi} \frac{\partial^p}{\partial\xi_{i_1}...\partial\xi_{i_p}} e^{-\frac{1}{2}\xi^T\xi} \quad (84)$$

where ξ is a vector of independent standard normal variables $\{\xi_{i_k}\}_{k=1}^{p}$. The series could be truncated to a finite number of terms. The accuracy of the computational model depends on the order of the expansion. Additional transformations are necessary if the variables are correlated. The unknown coefficients may be estimated by various methods. One approach is to use the Galerkin method to minimize the residual obtained by requiring the residual to be orthogonal to the approximation space (Ghanem & Spanos, 1991). Another approach is to use the collocation method (Isukapalli & Georgopoulos, 1999). Here the model outputs are selected at a set of collocation points to estimate the coefficients. These collocation points can be the roots of the Hermite polynomial of a higher order. In this case, this way of estimating coefficients will capture points from regions of high probability (Tatang et al., 1997). Compared to the conventional response surface method , the stochastic response surface method has several advantages. The first advantage is that the polynomial chaos is a mean square convergent series expansion. This series is optimal in the Fourier sense, as it minimizes the mean square error from truncation after a finite number of the terms in the series (Ghanem & Spanos, 1991).

When the inputs are expressed as functions of standard normal variables and the number of the standard normal variables is defined as "number of the degrees of the freedom" in input uncertainty, the output are deterministic function of the the model inputs, so they have the same number of degrees of the freedom with respect to uncertainty. Polynomial chaos in terms of the standard normal variables provides a complete orthogonal basis for

the L^2 space (space for second order random function). Therefore any random function in the space can be represented by the polynomial chaos basis with corresponding coefficients. The second advantage is that the error from the truncation in the polynomial chaos series can be quantified. Thus, the accuracy of the metamodel itself can be quantified. This metamodel error will be accounted for in the response surface error. The third advantage is that polynomial chaos is a Hermite polynomial of random variables. The roots af the Hermite polynomial provide efficient collocation points to evaluate the model output and to compute the coefficients in the response surface. In general, the stochastic response surface method is founded on a solid mathematical basis and it is expected to provide a more accurate response surface model for predicting the response than the model from conventional RSM.

4.2.4 Bayesian Approach for Model Validation

When evaluating model uncertainty, if several possible models exist to describe a phenomenon, a Bayesian approach can be used to include all the candidate models by assigning a model weight (the probability of each model being correct) and integrating the effects of all models. When there is observation/data available, the model weights may be updated and shifted to the more appropriate model. This approach has been applied to probability distribution type uncertainty and linear regression model uncertainty problems in statistics (Edwards, 1984) (Soares, 1989) (Draper, 1995) (Volinsky et al., 1997), and was recently used to account for mechanical model uncertainty (Zhang & Mahadevan, 2000). The Bayesian approach can be adapted to problems in which there is only one model available, either due to the complexity of the problem, or because of the limited resources for model implementation. The Bayesian hypothesis testing uses assumptions on the prior distribution under the alternative hypothesis (Jeffreys, 1961).

A methodology for the problem of acceptance testing of mechanical reliability computation models, based on the concepts of Bayesian hypothesis testing was proposed in (Zhang & Mahadevan, 2003), for both time-independent and time-dependent problems, and also for problems both with and without statistical uncertainty. An outline of the Bayesian approach (only the case of time-independent problem without statistical uncertainty in the model) is reproduced below from (Zhang & Mahadevan, 2003), for clarity. First, consider two models M_i and M_j, with prior probabilities to be the correct model denoted by $P(M_i)$ and $P(M_j)$. By Bayes' rule, when an event/data Y is observed, the relative posterior probabilities of two hypotheses are obtained as:

$$\frac{P(M_i|observation)}{P(M_j|observation)} = \left[\frac{P(observation|M_i)}{P(observation|M_j)}\right]\left[\frac{P(M_i)}{P(M_j)}\right] \tag{85}$$

The data-dependent term in the first set of square brackets on the right hand side of Eq. (85) is called the "Bayes factor" (Jeffreys, 1961). This Bayes factor can be viewed as the "weighted" likelihood ratio of M_i to M_j and hence can be interpreted solely in terms of comparative support of the data for the two models. The data are said to favor M_i relative to M_j if the Bayes factor exceeds one, that is, if the observed data is more likely under hypothesis M_i than it is under hypothesis M_j. To make use of the Bayes' rule and Bayes factor in the case where only one model M is available, an alternative model M_a is constructed to represent the case in which the model M is not correct.

For the case without statistical uncertainty, the failure probability x of an engineering system predicted by model M is a deterministic value denoted by x_0. It can be considered as a null hypothesis, under which the density of the parameter x is sharply concentrated at x_0. To make use of Bayes' rule, we need to constitute an alternative hypothesis. Assume that there is no prior information about x. Therefore, the uniform distribution between [0, 1] is taken as $P(x|M_a)$, the prior distribution under the alternative hypothesis. In the Bayesian framework, the distribution of x may be taken to be the weighted summation of the prediction of the two models:

$$P(x) = P(x|M)P(M) + P(x|M_a)(1-P(M)) \tag{86}$$

where $P(M)$ is the prior probability that we believe model M is correct. Assuming $P(M)=a$, Eq. (86) may also be written as

$$P(x) = \begin{cases} a & (x = x_0) \\ (1-a)dx & (x \neq x_0) \end{cases} \tag{87}$$

where $x = x_0$ if the model M is correct and $x \neq x_0$ if the model M not is not correct. If n experiments are undertaken, and k failures are observed out of n samples, the probability of this result is:

$$P_n(k) = \binom{n}{k} x^k (1-x)^{n-k} \tag{88}$$

And the Bayes factor is obtained as

$$B = \frac{P(data|M)}{P(data|M_a)} = (n+1)\binom{n}{k} x^k (1-x)^{n-k} \tag{89}$$

Thus in this reliability prediction problem, Bayes factor B is a function of k and n, and is independent of the prior probability of the model being correct. The Bayes factor B in Eq. (89) attains its maximum at $x = k/n$ (Zhang & Mahadevan, 2003). Using the above-mentioned criterion for the Bayes factor, a decision can be made to reject or accept the model M. In what follows, several Bayes factors are evaluated, using prior error distribution obtained from response surface models. These RSM are metamodels for the error of the plate problem, defined in subsection 4.1. One quarter of the plate is modeled, generating corners between the interior hole and the lines representing the axis of symmetry. The discretization error in stress of the finite element model at a location near these corners is selected to be modeled using RSM.

With the availability of the distribution and the parameters for the prior error E, the probability that the computational model will fail to predict accurately or the error exceeding a desired value can be computed. In this work, this desired value is assumed to be 3% of the average value of the predicted stress. Thus, the prior estimate of the probability of failure of the model using one of the possible error estimators is given by x= $P(-0.03\ \sigma < E < 0.03\ \sigma)$.

4.2.4.1 Comparison of Bayes factors for different response surface methods

A 2D elastostatics problem was defined in subsection 4.1, consisting of a plate with a hole submitted to external loading. For the plate problem being studied, the region of

interest is one of the corners of the central hole. The octahedral stress at the centroid of the element closest to this corner is the response quantity of interest, and the error in this quantity is evaluated using the gradient recovery (GR) error estimator and the inter-element stress continuity (SC) error estimators. These estimators were shown previously to be consistent error estimators. The local GR and SC error results for the octahedral stress are modeled using conventional and stochastic response surface methods, and the Bayes factors from both cases are compared. The first-order conventional response surface for the error E in the response quantity of interest is given by

$$E = a_o + a_1 W_1 + a_2 W_2 \tag{90}$$

In this work, the input load variables are written in terms of standard normal variables ξ_1, ξ_2 as: $W_1 = 12 + 2.4\xi_1$ and $W_2 = 12 + 2.4\xi_2$, so that these conventional response surfaces can be written directly in terms of the corresponding standard normal variables for the input variables. The local error in the region of interest is written for the conventional response surface using the GR and SC error estimators as

$$\begin{aligned} E_C^{\,GR} &= a_{o_C}^{\,GR} + a_{1_C}^{\,GR}\xi_1 + a_{2_C}^{\,GR}\xi_2 \\ E_C^{\,SC} &= a_{o_C}^{\,SC} + a_{1_C}^{\,SC}\xi_1 + a_{2_C}^{\,SC}\xi_2 \end{aligned} \tag{91}$$

2-factorial experimental design is done, obtaining nine sample points, shown in Table 3.

Table 3: Sample points for fitting the conventional RSM. and are the gradient recovery and the stress continuity error estimates in the octahedral stress in the element centroid closest to the corner of the hole – adapted from (Jorge et al., 2002)

Point	ξ_1	ξ_2	w_1	W_2	$E_C^{\,GR}$	$E_C^{\,SC}$
1	-3	-3	4.8	4.8	0.1529	0.3658
2	3	3	19.2	19.2	0.6116	1.463
3	-3	3	4.8	19.2	0.8351	2.06
4	3	-3	19.2	4.8	2.054	3.188
5	0	0	12	12	0.3823	0.9145
6	0	-3	12	4.8	1.106	1.743
7	-3	0	4.8	12	-0.6515	0.9829
8	0	3	12	19.2	-0.3715	1.04
9	3	0	19.2	12	1.339	2.22

Polynomial regression is subsequently performed to fit these sample points into the corresponding curves. In this case, linear fitting is adopted, with equations given by:

$$\begin{aligned} E_C^{\,GR} &= 0.606433333 + 0.203783333\xi_1 - 0.124316667\xi_2 + \varepsilon_C^{\,GR} \\ E_C^{\,SC} &= 1.553022222 + 0.19235\xi_1 - 0.040766667\xi_2 + \varepsilon_C^{\,SC} \end{aligned} \tag{92}$$

where $\varepsilon_C^{\,GR}$ and $\varepsilon_C^{\,SC}$ are the residual errors of the regression model adopted, which follow normal distribution with zero mean values and standard deviations of 0.441936688333333 and 0.622834690092593, respectively. Also, the R^2 values for these linear-fit equations are 0.537131 and 0.358417, respectively, showing the poor fit of this set of data. The first-order stochastic response surfaces for the errors $E_S^{\,GR}$ and $E_S^{\,SC}$ are written, respectively, in terms of the standard normal variables, as

$$\begin{aligned} E_S^{\,GR} &= a_{o_S}^{\,GR} + a_{1_S}^{\,GR}\xi_1 + a_{2_S}^{\,GR}\xi_2 \\ E_S^{\,SC} &= a_{o_S}^{\,SC} + a_{1_S}^{\,SC}\xi_1 + a_{2_S}^{\,SC}\xi_2 \end{aligned} \tag{93}$$

The samples for the linear regression are shown in Table 4. These collocation points are obtained as roots of the Hermite polynomial of one degree higher than the polynomial expansion being used. There are 25 possible points to be generated, for each root of the Hermite polynomial. The first nine points are adopted to generate the linear regression model. These points correspond to the nine roots closest to the origin. The remaining points can be used to generate a more accurate linear model for comparison purposes.

Table 4: Sample points for fitting the stochastic RSM. and are the gradient recovery and the stress continuity error estimates in the octahedral stress in the element centroid closest to the corner of the hole – adapted from (Jorge et al., 2002)

Point	ξ_1	ξ_2	w_1	w_2	E_S^{GR}	E_S^{SC}
1	1	1	14.4	14.4	0.4587	1.097
2	1	0	14.4	12	0.7025	1.316
3	1	-1	14.4	9.6	0.9442	1.591
4	0	1	12	14.4	0.1355	0.8039
5	0	0	12	12	0.3823	0.9145
6	0	-1	12	9.6	0.6259	1.139
7	-1	1	9.6	14.4	-0.1942	0.7466
8	-1	0	9.6	12	0.05853	0.6406
9	-1	-1	9.6	9.6	0.3058	0.7316
10	1	$\sqrt{3}$	14.4	16.16	0.2782	0.9952
11	1	$-\sqrt{3}$	14.4	7.84	1.12	1.814
12	0	$\sqrt{3}$	12	16.16	-0.0481	0.8244
13	0	$-\sqrt{3}$	12	7.84	0.8028	1.345
14	-1	$\sqrt{3}$	9.6	16.16	-0.3841	0.9154
15	-1	$-\sqrt{3}$	9.6	7.84	0.4845	0.8942
16	$\sqrt{3}$	1	16.16	14.4	0.6939	1.383
17	$\sqrt{3}$	0	16.16	12	0.9363	1.639
18	$\sqrt{3}$	-1	16.16	9.6	1.177	1.932
19	$\sqrt{3}$	$\sqrt{3}$	16.16	16.16	0.5148	1.232
20	$\sqrt{3}$	$-\sqrt{3}$	16.16	7.84	1.353	2.161
21	$-\sqrt{3}$	1	7.84	14.4	-0.4466	0.889
22	$-\sqrt{3}$	0	7.84	12	-0.1842	0.6295
23	$-\sqrt{3}$	-1	7.84	9.6	0.06859	0.5233
24	$-\sqrt{3}$	$\sqrt{3}$	7.84	16.16	-0.6477	1.119
25	$-\sqrt{3}$	$-\sqrt{3}$	7.84	7.84	0.2497	0.5975

Polynomial regression is subsequently performed to fit these sample points into the corresponding curves.

In this case, linear fitting using the first nine points is adopted, with equations given by:

$$\begin{aligned} E_S^{GR} &= 0.379914 + 0.322545\xi_1 - 0.245983333\xi_2 + \varepsilon_S^{GR} \\ E_S^{SC} &= 0.9978 + 0.3142\xi_1 - 0.135683333\xi_2 + \varepsilon_S^{SC} \end{aligned} \tag{94}$$

where ε_S^{GR} and ε_S^{SC} are the residual errors of the regression model adopted, which follow normal distribution with zero mean values and standard deviations of 0.0000116068675925925 and 0.0143696230555556, respectively. Also, the R^2 values for these linear-fit equations are 0.999929465 and 0.890726, respectively, showing the good linear fit for this set of data. The prior estimate for the probability of failure (x) of the model is evaluated for both the conventional and the stochastic response surfaces, for the first order models. In all cases, the maximum allowed error is assumed to be 0.72ksi, which corresponds to 3% of the average predicted mean stress in the location of interest, the corner of the hole. The mean value for the local error in the obtained equations using the error estimates should be zero, corresponding to the case with no external loading. Equations (92) and (94) show that the linear fitting adopted for the error estimators presents a bias from zero. This mean value represents the inability of the error estimator in representing the zero-mean property of the real error. The real error is assumed to have zero mean with same variability than the estimated errors. Thus, to evaluate the probability of failure, the mean value of the error is dropped from Equations (92) and (94). After evaluating the probability of failure, a set of n=10 experiments is conducted. Failure occurs when the predicted and the observed stresses at the location of interest differ more than 3%. Assuming that failure occurs in a number k of these experiments (k=0,…,10), the Bayes factors can be evaluated using Eq. (89). The tests are based on the pass/fail criterion and hence the test data k (number of failures) follows binomial distribution with the parameters n (number of tests) and the probability of failure of the each test given by x. Table 5 shows the results for the probability of failure x and for the corresponding Bayes factors for each value of x.

Table 5: Prior estimates of probability of failure (x) and corresponding Bayes factors (B) for various k values. Probabilities of failure x obtained for the cases of conventional (C) and stochastic (S) RSM, first order model, for the GR and SC estimators of error in the octahedral stress in the region of interest – adapted from (Jorge et al., 2002)

K	B_C^{GR}	B_C^{SC}	B_S^{GR}	B_S^{SC}
	x = 0.3112	x = 0.3741	x = 0.0731	x = 0.0469
0	0.264438	0.101494	5.148984	6.804205
1	1.194732	0.606631	4.060748	3.348203
2	2.429011	1.631625	1.44113	0.74141
3	2.926474	2.600589	0.303079	0.097289
4	2.313818	2.720148	0.041829	0.008378
5	1.25446	1.950997	0.003959	0.000495
6	0.472304	0.971758	0.00026	2.03E-05
7	0.121936	0.331897	1.17E-05	5.7E-07
8	0.020659	0.07439	3.47E-07	1.05E-08
9	0.002074	0.009881	6.08E-09	1.15E-10
10	9.37E-05	0.000591	4.79E-11	5.66E-13

As shown in Table 5, the conventional and stochastic RSM lead to different results in terms of probability of failure. The large difference between the probabilities of failure for the conventional and stochastic RSM can be explained by the poor linear fitting in the conventional RSM case. Thus, only the results of probability of failure for the stochastic response surface case are acceptable. In this case, the Bayes factors for both error estimators evaluated (GR and SC) are consistently higher than 1 for K=0 and K=1, are in close vicinity of 1 for K=2, and are below 1 for K=3 and beyond.

4.2.4.2 Comparison of Bayes factors for consistent error estimators

In this subsection, the Bayes factors are compared for different consistent error estimators applied to different independent response quantities. The stochastic RSM is used to generate response surfaces for two different error estimators, the gradient recovery (GR) error estimator and the error estimator obtained from the lack of inter-element continuity (SC) for the stress. The errors in two independent response quantities, the mean stress and the octahedral stress in the region of interest, are evaluated. The linear expressions for the error using the GR and SC error estimators for the octahedral stress were already obtained in Equations (94). Table 6 shows the GR and SC error data for the mean stress.

Table 6: Sample points for fitting the stochastic RSM. $E_{S,Mean}^{GR}$ and $E_{S,Mean}^{SC}$ are the gradient recovery and the stress continuity error estimates in the mean stress in the element centroid closest to the corner of the hole – adapted from (Jorge et al., 2002)

Point	ξ_1	ξ_2	w_1	w_2	$E_{S,Mean}^{GR}$	$E_{S,Mean}^{SC}$
1	1	1	14.4	14.4	0.8989	0.8027
2	1	0	14.4	12	1.099	1.162
3	1	-1	14.4	9.6	1.298	1.521
4	0	1	12	14.4	0.5494	0.3096
5	0	0	12	12	0.7491	0.6689
6	0	-1	12	9.6	0.9488	1.028
7	-1	1	9.6	14.4	0.1998	-0.1834
8	-1	0	9.6	12	0.3995	0.1758
9	-1	-1	9.6	9.6	0.5992	0.5351
10	1	$\sqrt{3}$	14.4	16.16	0.7524	0.5392
11	1	$-\sqrt{3}$	14.4	7.84	1.445	1.785
12	0	$\sqrt{3}$	12	16.16	0.4029	0.04615
13	0	$-\sqrt{3}$	12	7.84	1.095	1.292
14	-1	$\sqrt{3}$	9.6	16.16	0.05339	-0.4469
15	-1	$-\sqrt{3}$	9.6	7.84	0.7457	0.7986
16	$\sqrt{3}$	1	16.16	14.4	1.155	1.164
17	$\sqrt{3}$	0	16.16	12	1.355	1.524
18	$\sqrt{3}$	-1	16.16	9.6	1.555	1.883
19	$\sqrt{3}$	$\sqrt{3}$	16.16	16.16	1.009	0.9008
20	$\sqrt{3}$	$-\sqrt{3}$	16.16	7.84	1.701	2.146
21	$-\sqrt{3}$	1	7.84	14.4	-0.05646	-0.545
22	$-\sqrt{3}$	0	7.84	12	0.1432	-0.1857
23	$-\sqrt{3}$	-1	7.84	9.6	0.3429	0.1736
24	$-\sqrt{3}$	$\sqrt{3}$	7.84	16.16	-0.2029	-0.8085
25	$-\sqrt{3}$	$-\sqrt{3}$	7.84	7.84	0.4894	0.437

Polynomial regression is performed to fit the sample points for the gradient recovery (GR) and stress continuity (SC) error estimators into the corresponding curves. In this case, linear fittings are adopted, with equations given by:

$$E_{S,Mean}^{GR} = 0.749078 + 0.349567\xi_1 - 0.19965\xi_2 + \varepsilon_{S,Mean}^{GR}$$
$$E_{S,Mean}^{SC} = 0.668856 + 0.493033\xi_1 - 0.3592\xi_2 + \varepsilon_{S,Mean}^{SC} \quad (95)$$

where $\varepsilon_{S,Mean}^{GR}$ and $\varepsilon_{S,Mean}^{SC}$ are the residual errors of the regression model adopted, which follow normal distribution with zero mean values and standard deviations of $3.9\text{x}10^{-8}$ and $5.93\text{x}10^{-9}$, respectively. Also, the R^2 values for these linear-fit equations are both equal to 1, showing the good linear fit for this set of data.

The prior estimate for the probability of failure (x) of the model is evaluated for the first order models for the stochastic response surface. Again, the maximum allowed error is assumed to be 0.72ksi, and a set of n=10 experiments is conducted, with failure occuring in k of these experiments (k=0,…,10). The Bayes factors are evaluated using Eq. (89). Table 7 shows the results for the probability of failure x and for the corresponding Bayes factors for each value of x.

Table 7: Prior estimates of probability of failure (x) and corresponding Bayes factors (B) for various k values. Probabilities of failure x obtained for the gradient recovery (GR) and stress continuity (SC) error estimators, for first order stochastic RSM, for two response quantities: mean and octahedral stress – adapted from (Jorge et al., 2002)

K	$B_{S,Oct}^{GR}$	$B_{S,Oct}^{SC}$	$B_{S,Mean}^{GR}$	$B_{S,Mean}^{SC}$
	x = 0.0731	x = 0.0469	x = 0.0706	x = 0.2333
0	5.148984	6.804205	5.289558	0.772053
1	4.060748	3.348203	4.018106	2.34929
2	1.44113	0.74141	1.373523	3.216906
3	0.303079	0.097289	0.278232	2.610336
4	0.041829	0.008378	0.036987	1.390029
5	0.003959	0.000495	0.003372	0.507568
6	0.00026	2.03E-05	0.000213	0.128707
7	1.17E-05	5.7E-07	9.26E-06	0.02238
8	3.47E-07	1.05E-08	2.64E-07	0.002554
9	6.08E-09	1.15E-10	4.45E-09	0.000173
10	4.79E-11	5.66E-13	3.38E-11	5.25E-06

As shown in Table 7, different (but consistent) error estimators evaluated for different (and independent) response quantities lead to similar results in terms of probability of failure in most of the cases tested. In three of the four cases tested, the Bayes factors for both error estimators evaluated (GR and SC) are consistently higher than 1 for K=0 and K=1, are in close vicinity of 1 for K=2, and are below 1 for K=3 and beyond. Only the case for the SC error in the mean stress presented a higher probability of failure, with different conclusions in terms of Bayes factors. For the majority of the cases tested, similar model acceptance results are obtained with consistent error estimators.

4.2.4.3 Comparison of Bayes factors for non-consistent error estimators

Two error estimators, Richardson extrapolation (R) and maximum error bound (MEB) were previously found to be non-consistent. The octahedral stress near the corner node at the plate hole is used as the output response quantity to be modeled, while the input quantities are the loads W1 and W2 given in Table 1, above. Similarly to the previous subsection, results can be later obtained for the R and MEB error data for the octahedral stress, and are not included in this chapter, at this time.

4.2.5 Some Remarks on Error Estimators and Bayesian Hypothesis Testing in a Model Validation

The results obtained in this preliminary study indicate that:

- stochastic RSM is might be preferable than conventional RSM (more cases need to be studied to confirm this statement);
- consistent error estimators appear to lead to same decisions on model acceptance. On the other hand, non-consistent error estimators might lead to different probabilities of failure of the structure and consequently to different model acceptance decisions. Thus, a key part in the model validation procedure is the appropriate selection of a consistent set of:
  a) weak location;
  b) response quantity; and
  c) error estimator.

4.3 Perspectives for Future work in Error Estimators and Bayesian Hypothesis Testing in Model Validation

The perspectives for future work in error estimators and Bayesian hypothesis testing in Model Validation appear quite promising, and several important topics for future research can be envisaged, such as:

- Selection criteria among error estimators;
- Including measurement error in model validation;
- Extrapolation of validation decision parameters to unmeasured regions;
- Extrapolation of input parameters to regions where data is not available;
- Consistency in model validation decision across various response quantities;
- Incorporate random field nature of error in model validation;
- Quantifying confidence in validation;
- Extension of consistent error estimator technique to time-dependent problems.

5 Perspectives: Validation Techniques in FEM Structural Models

This section presents potential applications in FEM structural modeling that may benefit from the model validation techniques addressed throughout the chapter. Among the selected topics, the reader will find brief discussions on FE model condensation problems, models for structural health monitoring applications in aeronautical structures, modeling of structures obtained via additive manufacturing, and composite modeling for aerospace applications.

5.1 Perspectives for FEM Condensation Models

The recent advances in computer technology have made it possible to build extremely detailed FE models for structural applications. It is not uncommon to come across FE models with hundreds of thousands of degrees of freedom. However, the development of a reliable model often involves validation, updating, or adjustment steps, usually through the correlation of numerical and experimental models. Such experimental models are significantly smaller in size when compared to FE models. There are several methodologies developed over the past few decades that address the problem of reducing the number of degrees of freedom in a numerical model for a variety of purposes.

Figure 32 illustrates numerical and experimental models developed for the structural integrity investigations of the aluminum-aluminum honeycomb sandwich panel used in the construction of the Brazilian Geostationary Satellite. Detailed finite element models were built to study different aspects of the panel structural integrity when subjected to the static, dynamic, and environmental operational loads. Figure 32 (b) shows a small portion of a very detailed 3-D model built with shell elements, with a very large number of degrees of freedom, even for smaller specimens used in the experimental models. Figure 32 (d) presents one typical configuration for an experimental modal analysis that produced a good experimental model with only 136 degrees of freedom (Domingues, 2019). Once the test is carefully conducted with all the required expertise, the experimental model is a much more reliable representation of the real behavior of the panel. However, for detailed design simulations, the more refined model is extremely useful. The task is then to validate the numerical model using the experimental one. In order to allow an efficient correlation of the two models and to adjust or update the numerical model, reduction techniques must be used (Wang et al., 2017). The process of condensing a numerical model will certainly introduce errors that may impose a tremendous challenge that demands the applications of the theory and methodologies discussed in the present chapter in order to minimize possible errors induced by the process of model reduction.

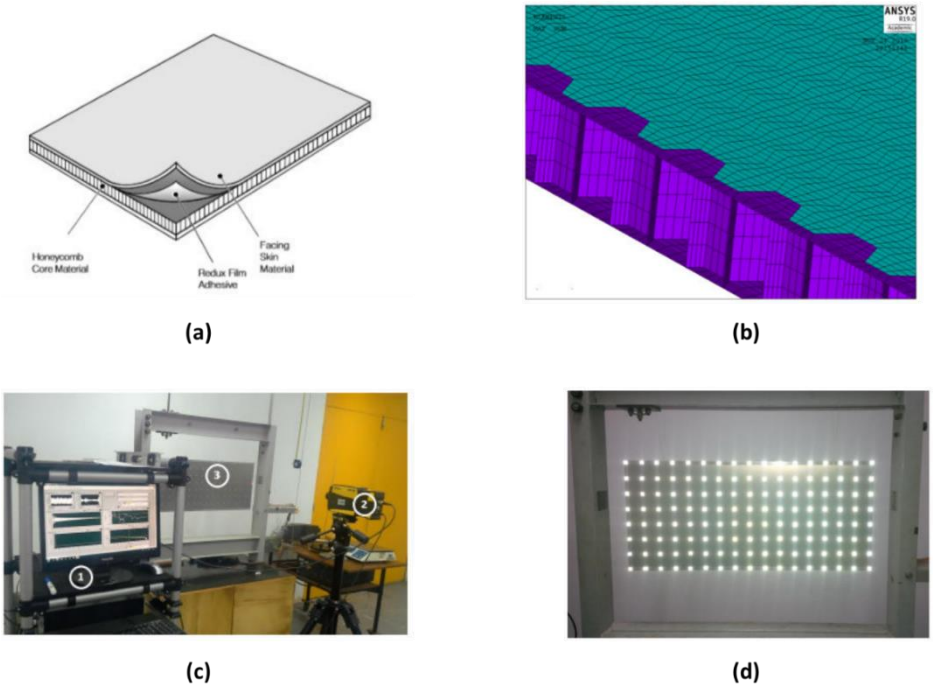

Figure 32: Size differences for numerical and experimental models of a Al-Al honeycomb sandwich panel (a) schematic representations of the panel;(b) detailed finite element model with an order of 10^5 degrees of freedom. (c) experimental apparatus for a modal analysis test; (d) measurement points that generate an experimental dynamic model of 136 degrees of freedom.

5.2 Perspectives for Aeronautical Structures Applications

Structural damage detection methods, sometimes also referred to as Structural Health Monitoring (SHM) methods have received tremendous attention from researchers in the

past few decades. Although some SHM techniques have been implemented in real structures over the years, most practical problems still need further development and offer interesting research challenges and opportunities. The ideal solution of having one general, fully automated, and dependable SHM method which is capable of solving damage problems in a wide variety of structural systems doesn´t seem to be feasible in the foreseeable future. Detecting the presence of damage may be possible with a limited amount of measured physical quantities that may describe the structure status during operation, such as strains, deflections, accelerations, etc. However, due to the intrinsic nature of the problem, the tasks of localizing and quantifying the damage are much more complex and usually will require the inclusion of a dependable, validated model of the structure, usually a numerical model. Such a model will be most likely used in the solution of an inverse problem, it will be evaluated iteratively in some sort of "error" minimization procedure, either classical or heuristic. Therefore, the models need to be, at the same time, reliable and t computationally light. In that sense, the subject of the present chapter is of utmost importance. The next two subsections present potential applications in current research for damage identification in aeronautical structures.

5.2.1 Perspectives for Modeling of Structural Damage Detection/Localization Problems

The problem of localizing damage in aeronautical structures has gained attention in recent years. Many different strategies have been developed in order to solve the corresponding inverse problem. One interesting approach is the use of wavelet transform to treat measurements of the behavior of the potentially damaged structure (Katunin, 2010, 2021). For example, the deflection caused by the operational loads can be monitored to develop an indicator that can reveal the existence and location of changes in the physical characteristics of the structure due to the existence of damaged areas.

Figure 33 illustrates the preliminary results of an ongoing investigation on a discrete wavelet transform (DWT) based method for localizing damage in a beam-like structure, modeled by finite elements. In the depicted example, the beam is discretized with 100 elements and 101 nodes and fixed at both ends. The presence of damage is simulated as a local reduction of stiffness in one single element. Static deflections of the damaged and undamaged beams are calculated for different damage values and locations, and different loading configurations.

A damage indicator was developed using the normalized differences between the calculated coefficients of the DWT of the deflections for the damaged and undamaged beam over its entire length. Several combinations of wavelets and levels of decomposition were tested in order to establish the best candidates for the implementation of the method. The SYM8 wavelet at one level of decomposition was found to be the more suitable choice for implementing the method. The index is computed along the entire FE mesh of the structure capturing the statistical variations of the index in the near vicinity of each node by computing the median and the boxplot height (range from the first and third quartiles) of the normalized differences of the DWT coefficients.

It can be noticed from Figure 33 the potential of the proposed index for damage detection and localization. It should be noted that damage is successfully detected and localized even for small amounts of damage. In such scenarios, the deflection curves of the damaged and the undamaged beams are virtually indistinguishable. The DWT-based damaged index is able to provide a "statistical amplification" of the effect of the damaged

element over the structural behavior of the entire beam. Further investigation of the method is aimed at extending the idea to more complex geometries and including DTW of dynamic responses in the calculation of the statistical damage index.

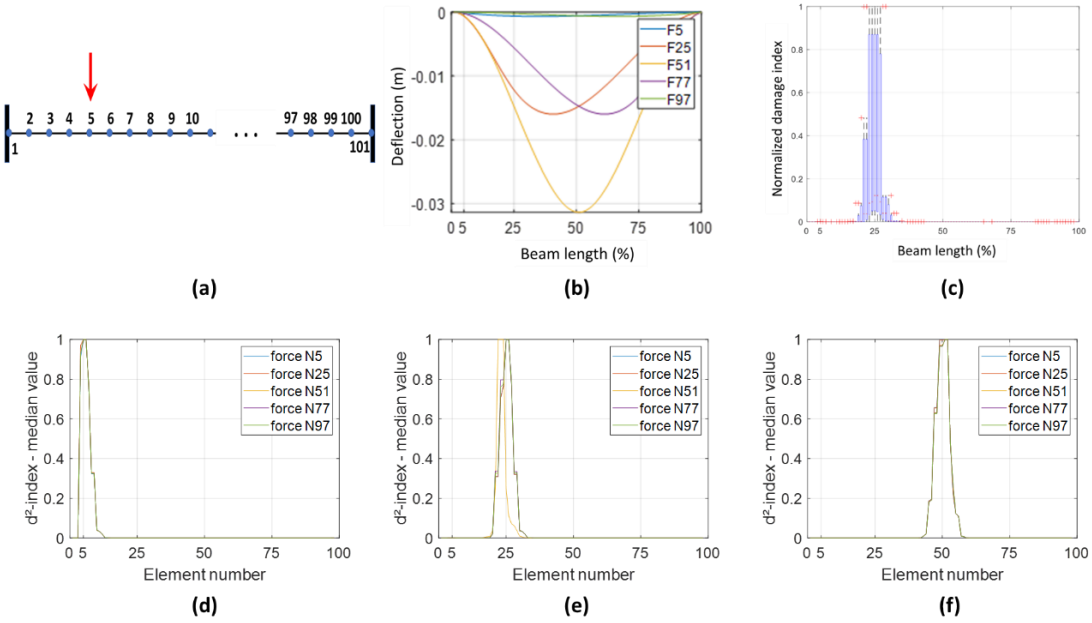

Figure 33: DWT based damage localization in a double clamped beam (a) Mesh with 101 nodes, 100 elements and force at node 5 (b)deflection plots; (c) typical boxplot for 50% damage at 25% beam length; (d), (e), (f) normalized median of damage index for different loading positions and 10% damage at 5%, 25% and 50% of beam length, respectively.

5.2.2 Perspectives for Modeling of Damage Detection/Identification Problems in Structural Aeronautical Fasteners / Joints

Consider the problem of identifying possible failure of fasteners in a structural joint. One possible approach is to monitor the structures in order to evaluate eventual changes in their dynamic behavior (Sinou, 2009). Measured data may be used in the solution of a model-based inverse problem in order to identify potential damage in the joint. Figure 34 depicts the conceptual construction of a simplified, low-fidelity model representing an aircraft wing. The model is intended to be light enough to feed an interactive numerical procedure to solve the inverse problem but must be able to include a mathematical description of both the distributed properties of the wing, in this case using beam finite elements, and the mechanical properties of the joint, modeled as concentrated elastic elements representing the transverse and rotational stiffnesses of the connection. These stiffness parameters can be related to a more detailed model of the joint, which can include geometrical, and material information, as well as torque of a series of bolts, for instance. The model can be used to reproduce the dynamic responses of the wing when submitted to controlled excitations in different positions of its span. The time responses of the structure can be monitored by a series of sensors over the wing. This simplified model is extremely useful for simulations in the development of SHM strategies, allowing for the investigation of types of excitation functions, number and position of exciters and sensors,

selection of damage index candidates based on the ability to evidence damage under uncertainties avoiding false positive and false negative results, etc.

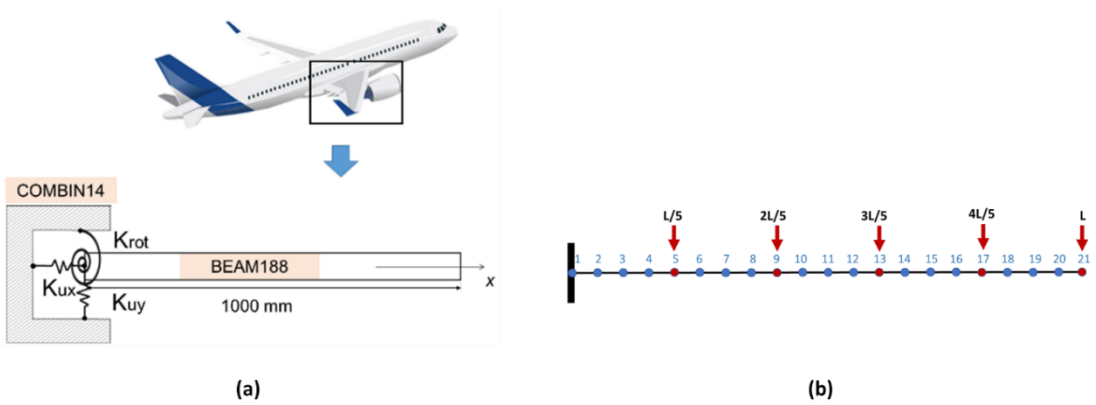

Figure 34: Simplified model of an aircraft wing for SHM procedures. (a) conceptual representation of the joint; (b) finite element mesh with beam elements and representation of excitation pints.

Figure 35 illustrates the study of a damage indication index based on the normalized differences of time responses measured over the wing for damaged and undamaged joints. It can be noticed that for the configurations studied, the damaged index is sensitive to variations in the joint integrity for different combinations of excitation and measurement points, as illustrated by Figures 35 (a) through (c). For all the simulated cases, confidence-bound curves were obtained, correlating the variations in damage index to the loss of torque in a simulated bolted joint. Figure 35 (d) indicates that results show low dispersion of the results for a 95% confidence level, indicating that the proposed strategy is a viable candidate for more detailed studies aiming at a reliable SHM procedure for aeronautical structures with fastened joints.

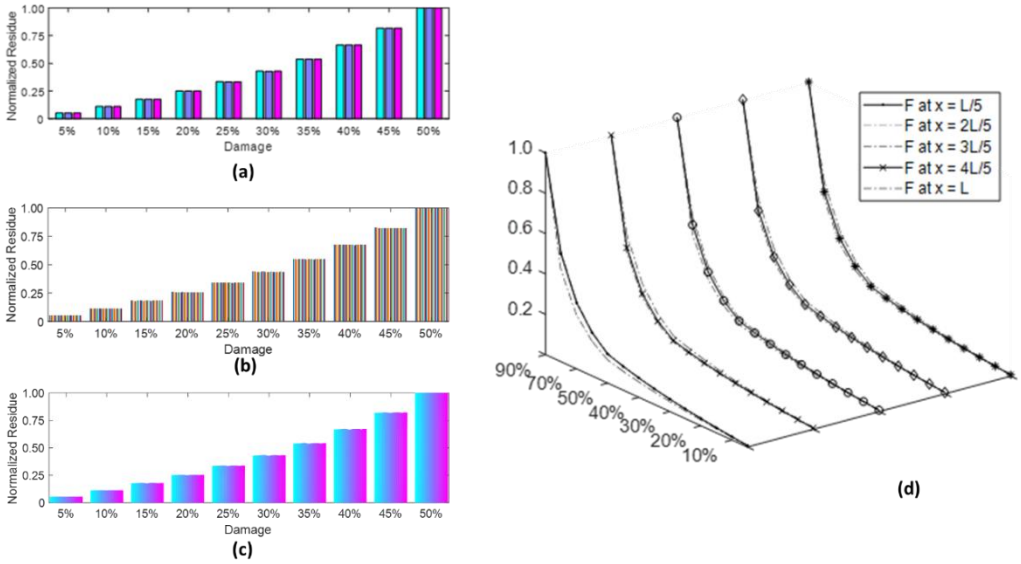

Figure 35: Damage index based on normalized differences of time responses for one excitation point and equally spaced sensors over the wing span (a) 3 sensors; (b) 5 sensors (c) 21 sensors (d) Confidence bound curves for 95% confidence level for all sensor configurations and different excitation points.

5.3 Perspectives in FEM Models for Additive Manufacturing in Aeronautical / Aerospace / Materials Applications

Additive manufacturing (AM), also known as three-dimensional printing, is an innovative manufacturing process based on the deposition of material in a localized manner, originating directly from a CAD/CAE model. This enables the fabrication of complex structures using metallic, ceramic, polymer and hybrid materials. The developed AM process are the technique of Fused Deposition Modeling (FDM) (Gibson et al. 2010), Selective Laser Sintering (SLS), Selective Laser Sintering (SLS), Selective Laser Melting (SLM)) (Gibson et al. 2010, Smith et al. 2014, Smith et al. 2014), and Electron Beam Melting (EBM) (Smith et al. 2017). The current AM technology for metal alloys enables the construction of complex monolithic parts, with high mechanical strength and precision, being possible to be used in operating conditions. In addition, it is important to emphasize that the use of the material is optimized and the production of waste is minimal or often nil, which are positive aspects of the environmental impact of the project. Currently, the negative aspects of the technique are the time and high cost of production; surface quality of the part, and the uncertainties generated by the AM process. Despite being extremely applicable and versatile, AM in metals has brought several challenges in the uncertainties field that must be explored to expand their application in primary structures. Some challenges concerning the MA process can be treated by the methods introduced in this chapter, such as:

- In the influence of manufacturing parameters. The material behavior is sensitive to the set of parameters, such as electron beam power, number of exposures, chamber temperature, layer width among others. Some studies (Lopez et al. 2016 and Hu & Mahadevan 2017) have been addressed the uncertainties associated with mechanical properties due to the aforementioned diversity of manufacturing parameters. Another factor directly affected by manufacturing parameters is the dimensional tolerance of the final part, generally affected by thermal expansion caused by beam power and speed.
- In the computational modeling of the additive manufacturing process. Numerical modeling is attractive in the study of the parameters influence on the final part to be printed. From the analysis of the input parameters for the print, it is possible to evaluate possible final distortions in the geometry, such as the one caused by the beam power responsible for generating thermal expansion and effect of warping in the final geometry (Prabhakar et al. 2015). Figure 36 depicts this type of analysis, where as a next step the behavior of the printed geometry can be numerically evaluated in relation to other engineering problems, such as modal analysis, hysteresis effect, fatigue, among others. The use of numerical simulation makes the experimental AM process more assertive as long as the associated uncertainties are addressed, generating a more efficient and financially viable prototype.

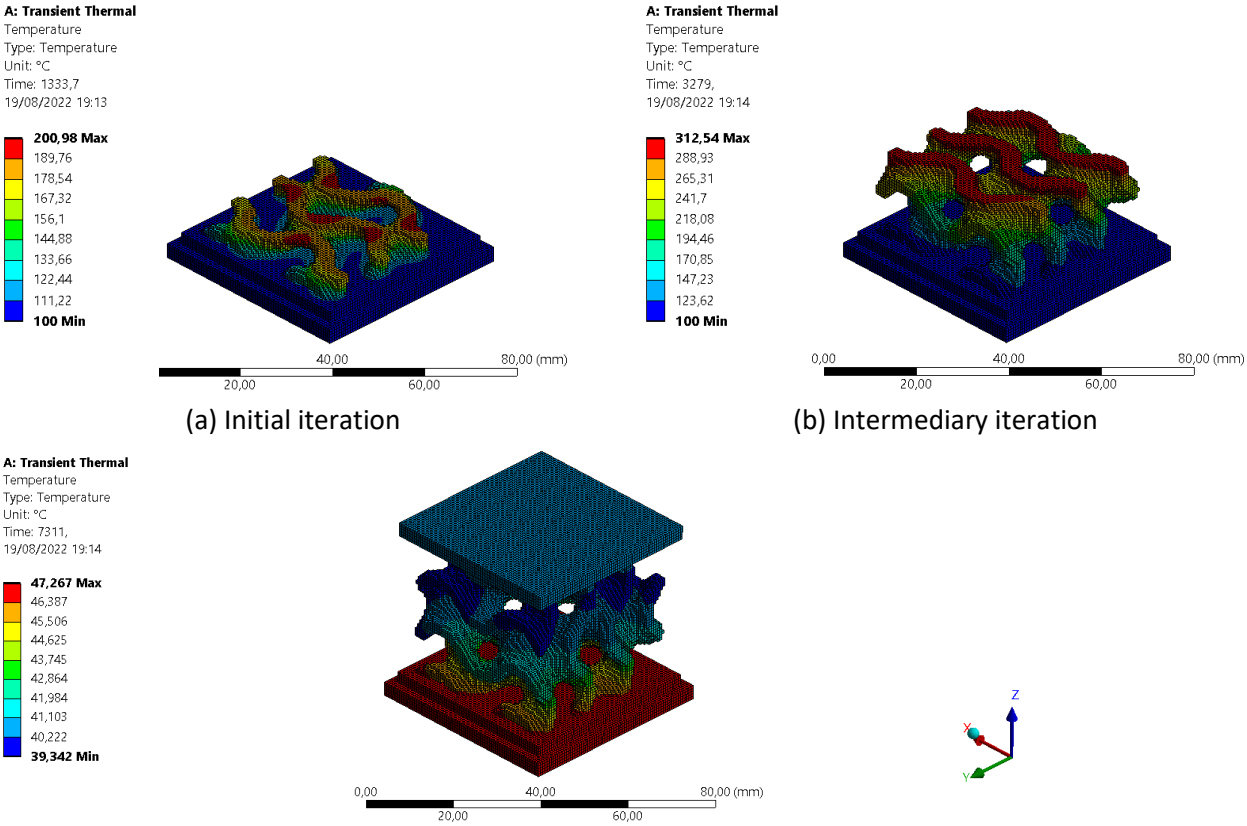

Figure 36: MA modeling by Finite Element Method.

- In the development of complex cellular structures called gyroids. These structures are configuration examples for combinations via MA because of their complexity. This type of structure is indicated for impact absorption (Ramos et al. 2019), being generally manufactured by MA (Figure 37) in aluminum alloys (SLM process). The uncertainties are straight associated in the mechanical performance of the structure, once the geometric parameters such as porosity, width and helix angle affect in the capacity for energy absorption.

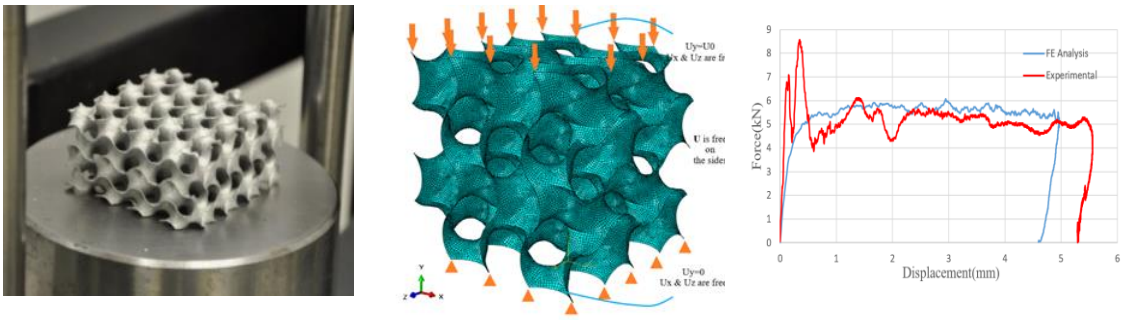

(a) (b) (c)

Figure 37: Gyroid-like cell structure: (a) MA fabricated gyroid structure, (b) numerical model of the structure and, (c) numerical-experimental comparison of gyroid behavior at impact. Ramos et al. (2019).

5.4 Perspectives for Composite Modeling in Aeronautical / Aerospace Applications

The field of studies in composite materials with or without aeronautical application is vast. It is extremely important to address modeling uncertainties in these materials in order to obtain increasingly robust (numerical) models that are faithful to reality.

Some examples and perspectives of application of the methods discussed in this chapter can be cited, namely:

- In the modeling of composite structures in the presence of drop-off ply. These advanced structures are important in the field of composite materials due to their variable thickness. However, interrupting layers can lead to undesirable failure modes (Diniz et al., 2021; Kane et al., 2022; Diniz et al., 2022), as shown in Figure 38(a) and 38(b).
- In the development of materials with high impact absorption capacity. Interest in the use of structural composite materials in components for the automotive and aerospace industry has been increasing considerably in recent years. For this reason, improvements on structural composites crashworthiness are directly related to the human safety in a possible automotive crash and it depends on the energy absorption capability of the composite components (Di Benedetto et al., 2019; Di Benedetto et al., 2021; Di Benedetto et al., 2022), the examples shown in Figure 38(c).
- In the study of aeroelasticity in composite materials. The companies' incessant search for lighter aircraft has led to the use of several new technologies and design solutions in new aircraft models. Two of them have been the use of composites and more flexible structures. However, such structures lead to two main problems: (i) difficulty in identifying damage and defects in composite structures and (ii) very flexible aircraft are more subject to flutter. In view of the new challenges imposed, the present work seeks to assess the influence of structural reduction caused by damage/defects in the flutter speed. (Mendes & Gomes, 2022), as examples shown in Figure 38(d)
- It is also known that the dynamic behaviors of mechanical structures, particularly composite ones, are critical to the effective operation of numerous applications such as automotive, civil and aeronautic industries. With appropriate structural behavior knowledge, failure can be avoided, and undesirable resonance can also be eliminated or even reduced. In this sense, it is extremely important to effectively understand the model and associated uncertainties in the modeling of sandwich structures with a core composed of magnetorheological material (de Souza Eloy *et al.*, 2018; de Souza Eloy *et al.*, 2019, Faria *et al.*, 2020), as examples shown in Figure 38(e).

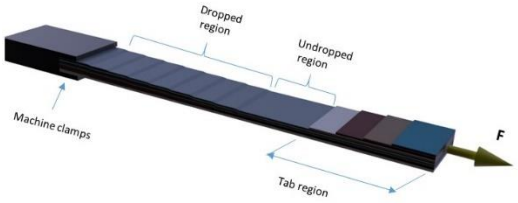

(a) Drop-off modelling
(Kane *et al.*, 2022)

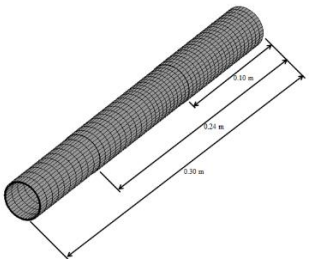

(b) Drop-off modelling in tubes
(Diniz *et al.*, 2022)

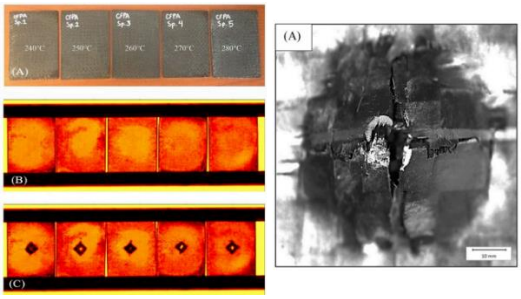

(c) Impact absorption
(Di Benedetto *et al.*, 2019)

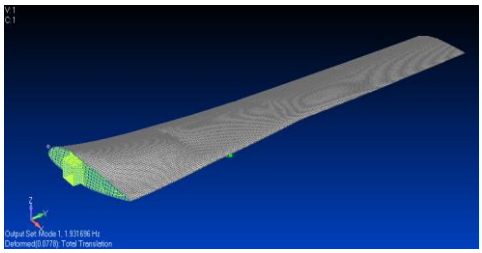

(d) Flutter in composite wings
(Mendes & Gomes, 2022)

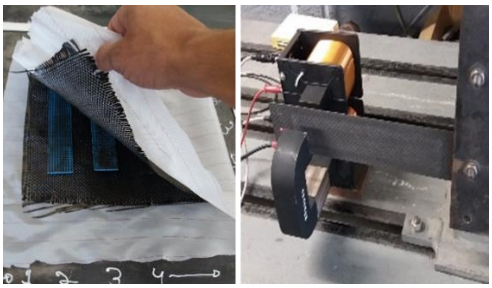

(e) Sandwich composite structure (de Souza Eloy *et al.*, 2018)

Figure 38: Some examples of application perspectives in composite structures.

6 Concluding Remarks

This chapter presented an overview of computational models and formulations, a description of some error estimators in Boundary Element Methods (BEM) and in Finite Element Methods (FEM), and some perspectives of the use of these error estimators in Bayesian approaches for Model Validation.

Acknowledgements

The first author would like to acknowledge the support from the Structural Reliability Research Group at Vanderbilt University, led by Dr. Sankaran Mahadevan, where he was a Post-doctoral Research Associate in 2002 (*Structural Reliability Research Group - Faculty and Staff*, n.d.), and also to express this gratitude to Dr, Prodyot K. Basu, Civil Engineering, for the continuous Department support, advising, and assistance, during the first author's Post-Doctoral research period at Vanderbilt University, in 2009-2010.

References

Aboudi, J. (1991). Mechanics of composite materials : a unified micromechanical approach. *Studies in Applied Mechanics*, *29*.

Aboudi, J. (1996). Micromechanical analysis of composites by the method of cells - Update. *Applied Mechanics Reviews*, *49*(10). https://doi.org/10.1115/1.3101981

Ainsworth, M., & Oden, J. T. (1993). A unified approach to a posteriori error estimation using element residual methods. *Numerische Mathematik*, *65*(1). https://doi.org/10.1007/BF01385738

Ainsworth, M., & Oden, J. T. (1997). A posteriori error estimation in finite element analysis. In *Computer Methods in Applied Mechanics and Engineering* (Vol. 142, Issues 1–2). https://doi.org/10.1016/S0045-7825(96)01107-3

Aldroubi, A., & Papadakis, M. (1998). *Characterization and parameterization of multiwavelet bases*. https://doi.org/10.1090/conm/216/02967

Aldroubi, A., & Unser, M. (1993). Families of multiresolution and wavelet spaces with optimal properties. *Numerical Functional Analysis and Optimization*, *14*(5–6). https://doi.org/10.1080/01630569308816532

Aluru, N. R., & Li, G. (2001). Finite cloud method: A true meshless technique based on fixed reproducing kernel approximation. *International Journal for Numerical Methods in Engineering*, *50*(10). https://doi.org/10.1002/nme.124

Ammons, B. A., & Vable, M. (1998). An HR-method of mesh refinement for boundary element method. *International Journal for Numerical Methods in Engineering*, *43*(6). https://doi.org/10.1002/(SICI)1097-0207(19981130)43:6<979::AID-NME451>3.0.CO;2-J

Ang, A. H.-S., & Tang, W. H. (1984). *Probability Concepts in Engineering Planning and Design, Vol. 2: Decision, Risk, and Reliability*. John Wiley & Sons.

Armando Duarte, C., & Tinsley Oden, J. (1996). H-p Clouds - An h-p Meshless Method. *Numerical Methods for Partial Differential Equations*, *12*(6). https://doi.org/10.1002/(sici)1098-2426(199611)12:6<673::aid-num3>3.0.co;2-p

Arora, J. S. (2012). Introduction to Optimum Design Chapter 2. In *Introduction to Optimum Design*.

Babuška, I., & Melenk, J. M. (1997). The partition of unity method. *International Journal for Numerical Methods in Engineering*, *40*(4). https://doi.org/10.1002/(SICI)1097-0207(19970228)40:4<727::AID-NME86>3.0.CO;2-N

Babuška, I., Strouboulis, T., Upadhyay, C. S., & Gangaraj, S. K. (1995). A model study of element residual estimators for linear elliptic problems: The quality of the estimators in the interior of meshes of triangles and quadrilaterals. *Computers and Structures*, *57*(6). https://doi.org/10.1016/0045-7949(95)00075-R

Babuška, Ivo, Banerjee, U., & Osborn, J. E. (2003). Survey of meshless and generalized finite element methods: A unified approach. In *Acta Numerica* (Vol. 12). https://doi.org/10.1017/S0962492902000090

Basu, P. K. (2002). Multiphysics/Multiscale Modeling in Engineering Design. *Proceedings of Second Annual International Conference on Advances in Structural Engineering and Mechanics*.

Basu, P. K. (2007). Modeling and simulation in engineering design in the new millennium. *Proc. Int. Conf. on Civil Engineering in the New Millennium: - Opportunities and Challenges*, 108–141.

Basu, P. K., & Jorge, A. B. (2009). *Modeling of Physical Systems*.

Basu, P. K., Jorge, A. B., Badri, S., & Lin, J. (2003). Higher-Order Modeling of Continua by Finite-Element, Boundary-Element, Meshless, and Wavelet Methods. *Computers and Mathematics with Applications*. https://doi.org/10.1016/S0898-1221(03)90078-2

Basu, P. K., & Shah, S. (1998). Modeling singular problems of solid continua. *American Society of Mechanical Engineers, Petroleum Division (Publication) PD*.

Basu, P. K., & Shah, S. (2000). Accurate Modeling of Singular Problems of the Continua. *Int. Jl. Of Applied Science and Computations*, *7*, 1–19.

Belytschko, T., Lu, Y. Y., & Gu, L. (1994). Element-free Galerkin methods. *International Journal for Numerical Methods in Engineering*, *37*(2). https://doi.org/10.1002/nme.1620370205

Bensoussan, A., Lions, J.-L., Papanicolaou, G., & Caughey, T. K. (1979). Asymptotic Analysis of Periodic Structures. *Journal of Applied Mechanics*, *46*(2). https://doi.org/10.1115/1.3424588

Bhatnagar, P. L., Gross, E. P., & Krook, M. (1954). A model for collision processes in gases. I. Small amplitude processes in charged and neutral one-component systems. *Physical Review*, *94*(3). https://doi.org/10.1103/PhysRev.94.511

Burrus, C. S., Gopinath, R. A., & Guo, H. (1998). Introduction to Wavelets and Wavelet Transforms: A Primer. In *Recherche*.

Carey, V. P. (1999). Statistical Thermodynamics and Microscale Thermophysics. In *Statistical Thermodynamics and Microscale Thermophysics*. https://doi.org/10.1017/cbo9780511626395

Chao, R. M., & Lee, S. Y. (1999). An H-adaptive refinement BEM procedure using modified sample point error analysis in two-dimensional elastic problems. *Advances in Engineering Software*, *30*(4). https://doi.org/10.1016/S0965-9978(98)00085-4

Charafi, A., & Wrobel, L. C. (1997). A new h-adaptive refinement scheme for the boundary element method using local reanalysis. *Applied Mathematics and Computation*, *82*(2–3). https://doi.org/10.1016/S0096-3003(96)00028-8

Chessa, J., & Belytschko, T. (2004). Arbitrary discontinuities in space-time finite elements by level sets and X-FEM. *International Journal for Numerical Methods in Engineering*, *61*(15). https://doi.org/10.1002/nme.1155

Chopard, B., & Droz, M. (1998). Cellular Automata Modeling of Physical Systems. In *Cellular Automata Modeling of Physical Systems*. https://doi.org/10.1017/cbo9780511549755

Cohen, A., Daubechies, I., & Feauveau, J. -C. (1992). Biorthogonal bases of compactly supported wavelets. *Communications on Pure and Applied Mathematics*, *45*(5). https://doi.org/10.1002/cpa.3160450502

Cohen, A., & Masson, R. (1999). Wavelet methods for second-order elliptic problems, preconditioning, and adaptivity. *SIAM Journal of Scientific Computing*, *21*(3). https://doi.org/10.1137/S1064827597330613

Crisfield, M. A. (2001). Finite Element Multidisciplinary Analysis K.K. Gupta J.L. Meek American Institute of Aeronautics and Astronautics, 1801 Alexander Bell Drive, Reston, VA 20191, USA. 2000. 352pp. Illustrated. ISBN 1-56347-393-3. $64.95 (AIAA members), $89.95 (non-members). *The Aeronautical Journal*, *105*(1046). https://doi.org/10.1017/s0001924000025513

Dahmen, W. (1997). Wavelet and multiscale methods for operator equations. *Acta Numerica*, *6*(2). https://doi.org/10.1017/S0962492900002713

Daubechies, I. (1988). Orthonormal bases of compactly supported wavelets. *Communications on Pure and Applied Mathematics*, *41*(7). https://doi.org/10.1002/cpa.3160410705

Daubechies, I. (1992). Ten Lectures on Wavelets. In *Ten Lectures on Wavelets*. https://doi.org/10.1137/1.9781611970104

de Souza Eloy, F., Gomes, G. F., Ancelotti Jr, A. C., da Cunha Jr, S. S., Bombard, A. J. F., & Junqueira, D. M. (2018). Experimental dynamic analysis of composite sandwich beams with magnetorheological honeycomb core. *Engineering Structures,* 176, 231-242.

de Souza Eloy, F., Gomes, G. F., Ancelotti Jr, A. C., da Cunha Jr, S. S., Bombard, A. J. F., & Junqueira, D. M. (2019). A numerical-experimental dynamic analysis of composite sandwich beam with magnetorheological elastomer honeycomb core. *Composite Structures,* 209, 242-257.

Denda, M., & Dong, Y. F. (1999). An error estimation measure in the direct BEM formulation by the external Somigliana's identity. *Computer Methods in Applied Mechanics and Engineering*, *173*(3–4). https://doi.org/10.1016/S0045-7825(98)00296-5

Di Benedetto, R. M., Botelho, E. C., Gomes, G. F., Junqueira, D. M., & Junior, A. A. (2019). Impact energy absorption capability of thermoplastic commingled composites. *Composites Part B*: Engineering, 176, 107307.

Di Benedetto, R. M., Botelho, E. C., Janotti, A., Junior, A. A., & Gomes, G. F. (2021). Development of an artificial neural network for predicting energy absorption capability of thermoplastic commingled composites. *Composite Structures,* 257, 113131.

Di Benedetto, R. M., Gomes, G. F., Janotti, A., Junior, A. C. A., & Botelho, E. C. (2022). Statistical approach to optimize crashworthiness of thermoplastic commingled composites. *Materials Today Communications*, 103651.

Diniz, C.A., Méndez, Y., de Almeida, F.A., da Cunha Jr, S.S. and Gomes, G.F. (2021), "Optimum design of composite structures with ply drop-offs using response surface methodology", *Engineering Computations*, Vol. 38 No. 7, pp. 3036-3060. https://doi.org/10.1108/EC-07-2020-0354

Diniz, C.A., Pereira, J.L.J., da Cunha, S.S. et al. Drop-off Location Optimization in Hybrid CFRP/GFRP Composite Tubes Using Design of Experiments and SunFlower Optimization Algorithm. *Appl Compos Mater* (2022). https://doi.org/10.1007/s10443-022-10046-z

Ding, X., & Tsang, T. T. H. (2001). Large eddy simulation of turbulent flows by a least-squares finite element method. *International Journal for Numerical Methods in Fluids*, *37*(3). https://doi.org/10.1002/fld.172

Domingues, A. C. – Damage identification in light aerospace structures using modal strain energy method. (In Portuguese: Identificação de dano em estruturas aeroespaciais leves utilizando o método da energia de deformação modal). Master's Thesis, Integrity of Engineering Materials Program, University of Brasilia, 2019.

Domingues, A. C.; Anflor, C. T. M.; Carneiro, S. H. S. Damage Identification in Light Panels with Orthotropic Properties Using Modal Strain Energy In: Congreso Iberoamericano de Ingeniería Mecánica, 2019,Cartagena. *XIV Congreso Iberoamericano de Ingeniería Mecánica.* , 2019. pp276-280.https://www.uis.edu.co/webUIS/es/academia/facultades/fisicoMecanicas/escuelas/ingenieriaMecanica/cibim/MEMORIAS-CIBIM/A.pdf

Domingues, A. C.; Anflor, C. T. M.; Carneiro, S. H. S. Damage identification using modal strain energy in a structure with orthotropic properties In: International Congress of Mechanical Engineering, 2019, Uberlândia. *25th ABCM International Congress of Mechanical Engineering. 2019.* https://abcm.org.br/proceedings/view/COB2019/0089

Domingues, A. C. ; Santos, T. ; Anflor, C. T. M. ; Carneiro, S. H. S. . Damage Identification in a Cantilever Beam using Modal Strain Energy.. *In: 18th International Conference on Machine Design and Production, 2018, 2018*, Eskişehir. 18th International Conference on Machine Design and Production, 2018.

Donovan, G. C., Geronimo, J. S., & Hardin, D. P. (1996). Intertwining multiresolution analyses and the construction of piecewise-polynomial wavelets. *SIAM Journal on Mathematical Analysis*, *27*(6). https://doi.org/10.1137/S0036141094276160

Draper, D. (1995). Assessment and Propagation of Model Uncertainty. *Journal of the Royal Statistical Society: Series B (Methodological)*, *57*(1). https://doi.org/10.1111/j.2517-6161.1995.tb02015.x

Duarte, C. A. (1995). *A review of some meshless methods to solve partial differential equations, Technical report 95-06, TICAM*.

Edwards, G. (1984). A Bayesian procedure for drawing inferences from random data. *Reliability Engineering*, *9*(1). https://doi.org/10.1016/0143-8174(84)90002-7

Ellingwood, B., & Galambos, T. V. (1982). Probability-based criteria for structural design. *Structural Safety*, *1*(1). https://doi.org/10.1016/0167-4730(82)90012-1

Faria, L. E. R., Gomes, G. F., de Sousa, S. R. G., Bombard, A. J. F., & Ancelotti Jr, A. C. (2020). Dynamic experimental behavior of sandwich beams with honeycomb core filled with magnetic rheological gel: a statistical approach. Smart Materials and Structures, 29(11), 115044.

Frisch, U., Hasslacher, B., & Pomeau, Y. (1986). Lattice-gas automata for the Navier-Stokes equation. *Physical Review Letters*, *56*(14). https://doi.org/10.1103/PhysRevLett.56.1505

Ghanem, R. G., & Spanos, P. (1991). *Stochastic Finite Elements: A Spectral Approach*. Springer-Verlag. https://doi.org/10.1007/978-1-4612-3094-6

Ghosh, D. K., & Vanderplaats, G. N. (1997). Development of a flexible design optimization capability. *Proceedings of the Conference on Optimization in Industry*.

Gibson, I., Rosen, D. W., Stricker, B. Additive Manufacturing Technologies. Springer, 2010.

Guiggiani, M. (1996). Sensitivity analysis for boundary element error estimation and mesh refinement. *International Journal for Numerical Methods in Engineering*, *39*(17). https://doi.org/10.1002/(SICI)1097-0207(19960915)39:17<2907::AID-NME982>3.0.CO;2-0

Haldar, A., & Mahadevan, S. (1999). *Probability, Reliability, and Statistical Methods in Engineering Design*. Wiley.

Hu, Z., & Mahadevan, S. (2017). Uncertainty quantification and management in additive manufacturing: current status, needs, and opportunities. *The International Journal of Advanced Manufacturing Technology*, 93(5), 2855-2874.

Huebner, K. H., Dewhirst, D. L., Smith, D. E., & Byrom, T. G. (2008). *The finite element method for engineers*. John Wiley & Sons.

Isukapalli, S. S., & Georgopoulos, P. G. (1999). Computational Methods for the Efficient Sensitivity and Uncertainty Analysis of Models for Environmental and Biological Systems Towards a Framework for an Exposure and Dose Modeling and Analysis System. *Occupational Health*.

Jaswon, M. A., Symm, G. T., & Cruse, T. A. (1978). Integral Equation Methods in Potential Theory and Elastostatics. *Journal of Applied Mechanics*, *45*(4). https://doi.org/10.1115/1.3424468

Jeffreys, H. (1961). *Theory of Probability* (3rd ed.). Oxford University Press.

Jiang, B. (2000). The Least-Squares Finite Element Method-Theory and Applications in Computational Fluid Dynamics and Electromagnetics. *Journal of fluid mechanics*, *411*(1).

Jorge, A. B. (2002). *Self-regular BEM approaches and error estimation for linear elastic fracture mechanics in two dimensions* [Dissertation, ProQuest Dissertations Publishing]. https://catalog.library.vanderbilt.edu/discovery/fulldisplay?docid=cdi_proquest_journals_305487649&context=PC&vid=01VAN_INST:vanui&lang=en&search_scope=MyInst_and_CI&adaptor=Primo Central&tab=Everything&query=any,contains,Self-Regular BEM approaches and e

Jorge, A. B. (2004). Discretization of random fields in reliability structural analysis : error indicator methodology. *VI Simpósio Mineiro de Mecânica Computacional*. https://www.researchgate.net/publication/344286184_Discretization_of_random_fields_in_reliability_structural_analysis_error_indicator_methodology

Jorge, A. B., Cruse, T. A., & Fisher, T. S. (2003). Near-crack contour behaviour and extraction of log-singular stress terms of the self-regular traction boundary integral equation. *International Journal for Numerical Methods in Engineering*. https://doi.org/10.1002/nme.818

Jorge, A. B., Cruse, T. A., Fisher, T. S., & Ribeiro, G. O. (2003). A new variational self-regular traction-bem formulation for inter-element continuity of displacement derivatives. *Computational Mechanics*. https://doi.org/10.1007/s00466-003-0506-4

Jorge, A. B., Rebba, R., Mahadevan, S., & Huang, S. (2002). Model validation under uncertainty. *Part i: consistency issues in error estimation*.

Jorge, A. B., Ribeiro, G. O., Cruse, T. A., & Fisher, T. S. (2001). Self-regular boundary integral equation formulations for Laplace's equation in 2-D. *International Journal for Numerical Methods in Engineering*. https://doi.org/10.1002/nme.138

Jorge, A. B., Ribeiro, G. O., & Fisher, T. S. (2003). New approaches for error estimation and adaptivity for 2D potential boundary element methods. *International Journal for Numerical Methods in Engineering*. https://doi.org/10.1002/nme.559

Jorge, A. B., Ribeiro, G. O., & Fisher, T. S. (2005). Application of new error estimators based on gradient recovery and external domain approaches to 2D elastostatics problems. *Engineering Analysis with Boundary Elements*. https://doi.org/10.1016/j.enganabound.2005.03.004

Jorge, A. B., Ribeiro, G. O., & Fisher, T. S. (2001). Error estimation and adaptivity approaches in BEM. *BETEQ - Joint Meeting of International Conference on Boundary Element Techniques and International Association for Boundary Element Methods. Advances in Boundary Element Techniques II*, 117–126.

Jou, J., & Liu, J. L. (1999). A posteriori boundary element error estimation. *Journal of Computational and Applied Mathematics*, *106*(1). https://doi.org/10.1016/S0377-0427(99)00049-7

Kane, D., Gomes, G., Macanhan, V. and Ancelotti Jr, A. (2022), "The effect of ply drop-off on tensile strength of thermoplastic carbon fiber composite: a numerical and experimental study", Engineering Computations, Vol. 39 No. 6, pp. 2284-2305. https://doi.org/10.1108/EC-07-2021-0383

Karafiat, A. (1997). On hp- Error estimation in the BEM for a three-dimensional Helmholtz exterior problem. *Computer Methods in Applied Mechanics and Engineering*, *150*(1–4). https://doi.org/10.1016/S0045-7825(97)00091-1

Katunin, Andrzej (2010). Identification of multiple cracks in composite beams using discrete wavelet transform. *Scientific Problems of Machines Operation and Maintenance*, 45(2), 41-52. https://www.researchgate.net/profile/Andrzej-Katunin/publication/237085291

Katunin, A., dos Santos, J. V. A., & Lopes, H. “Damage identification by wavelet analysis of modal rotation differences”. In Structures (Vol. 30, pp. 1-10, 2021. ttps://www.sciencedirect.com/science/article/abs/pii/S2352012421000102

Kelly, D. W., Mills, R. J., Reizes, J. A., & Miller, A. D. (1987). A posteriori estimates of the solution error caused by discretization in the finite element, finite difference and boundary element methods. *International Journal for Numerical Methods in Engineering*, *24*(10). https://doi.org/10.1002/nme.1620241008

Kita, E., & Kamiya, N. (1994). Recent studies on adaptive boundary element methods. *Advances in Engineering Software*, *19*(1). https://doi.org/10.1016/0965-9978(94)90043-4

Kita, E., & Kamiya, N. (2001). Error estimation and adaptive mesh refinement in boundary element method, an overview. *Engineering Analysis with Boundary Elements*, *25*(7). https://doi.org/10.1016/S0955-7997(01)00018-2

Kontorova, T., & Frenkel, J. (1938). On the theory of plastic deformation and twinning. I. *Zhurnal Eksperimentalnoi I Teoreticheskoi Fiziki*, *8*(March).

Lancaster, P., & Salkauskas, K. (1981). Surfaces generated by moving least squares methods. *Mathematics of Computation*, *37*(155). https://doi.org/10.1090/s0025-5718-1981-0616367-1

Li, G., & Aluru, N. R. (2002). Boundary cloud method: A combined scattered point/boundary integral approach for boundary-only analysis. *Computer Methods in Applied Mechanics and Engineering*, *191*(21–22). https://doi.org/10.1016/S0045-7825(01)00415-7

Li, Y., Leboeuf, E. J., & Basu, P. K. (2005). Least-squares finite-element scheme for the lattice Boltzmann method on an unstructured mesh. *Physical Review E - Statistical, Nonlinear, and Soft Matter Physics*, *72*(4). https://doi.org/10.1103/PhysRevE.72.046711

Liang, M. T., Chen, J. T., & Yang, S. S. (1999). Error estimation for boundary element method. *Engineering Analysis with Boundary Elements*, *23*(3). https://doi.org/10.1016/s0955-7997(98)00086-1

Liapis, S. (1994). A review of error estimation and adaptivity in the boundary element method. *Engineering Analysis with Boundary Elements*, *14*(4). https://doi.org/10.1016/0955-7997(94)90061-2

Liapis, Stergios. (1996). An adaptive boundary element method for the solution of potential flow problems. *Engineering Analysis with Boundary Elements*, *18*(1). https://doi.org/10.1016/S0955-7997(96)00041-0

Liu, W. K., Karpov, E. G., & Park, H. S. (2006). Nano Mechanics and Materials: Theory, Multiscale Methods and Applications. In *Nano Mechanics and Materials: Theory, Multiscale Methods and Applications*. https://doi.org/10.1002/0470034106

Lopez, F., Witherell, P., & Lane, B. (2016). Identifying uncertainty in laser powder bed fusion additive manufacturing models. *Journal of Mechanical Design,* 138(11).

Mahadevan, S. (2002). Modeling and simulation for design under uncertainty. In K. P. Chong, S. Saigal, S. Thynell, & H. S. Morgan (Eds.), *Modeling and Simulation-Based Life Cycle Engineering* (pp. 276–290). Spon Press. https://doi.org/10.1201/9781482264715-29

Mendes, P. V. M., & Gomes, G. F. (2022). Analysis of the influence of damage on flutter speed in CFRP structures. Composite Structures, 280, 114931.

Menon, G., Paulino, G. H., & Mukherjee, S. (1999). Analysis of hypersingular residual error estimates in boundary element methods for potential problems. *Computer Methods in Applied Mechanics and Engineering*, *173*(3–4). https://doi.org/10.1016/S0045-7825(98)00297-7

Nayroles, B., Touzot, G., & Villon, P. (1992). Generalizing the finite element method: Diffuse approximation and diffuse elements. *Computational Mechanics*, *10*(5). https://doi.org/10.1007/BF00364252

Needleman, A. (1987). A continuum model for void nucleation by inclusion debonding. *Journal of Applied Mechanics, Transactions ASME*, *54*(3). https://doi.org/10.1115/1.3173064

Needleman, A. (1990a). An analysis of decohesion along an imperfect interface. *International Journal of Fracture*, *42*(1). https://doi.org/10.1007/BF00018611

Needleman, A. (1990b). An analysis of tensile decohesion along an interface. *Journal of the Mechanics and Physics of Solids*, *38*(3). https://doi.org/10.1016/0022-5096(90)90001-K

Noor, A. K., & Babuška, I. (1987). Quality assessment and control of finite element solutions. *Finite Elements in Analysis and Design*, *3*(1). https://doi.org/10.1016/0168-874X(87)90030-8

Oden, J. T., Demkowicz, L., Rachowicz, W., & Westermann, T. A. (1990). A posteriori error analysis in finite elements: The element residual method for symmetrizable problems with applications to compressible euler and Navier-stokes equations. *Computer Methods in Applied Mechanics and Engineering*, *82*(1–3). https://doi.org/10.1016/0045-7825(90)90164-H

Oden, J. Tinsley, Browne, J. C., Babuška, I., Liechti, K. M., & Demkowicz, L. F. (2003). A computational infrastructure for reliable computer simulations. *Lecture Notes in Computer Science (Including Subseries Lecture Notes in Artificial Intelligence and Lecture Notes in Bioinformatics)*, *2660*. https://doi.org/10.1007/3-540-44864-0_40

Oden, J. Tinsley, & Demkowicz, L. (1989). Advances in adaptive improvements: Survey of adaptive finite element methods in computational mechanics. In *State-of-the-Art Surveys on Computational Mechanics*.

Oden, J. Tinsley, & Vemaganti, K. S. (2000). Estimation of Local Modeling Error and Goal-Oriented Adaptive Modeling of Heterogeneous Materials: I. Error Estimates and Adaptive Algorithms. *Journal of Computational Physics*, *164*(1). https://doi.org/10.1006/jcph.2000.6585

París, F., & Cañas, J. (1997). *Boundary Element Method: Fundamentals and Applications*. Oxford University Press.

Paulino, G. H., Gray, L. J., & Zarikian, V. (1996). Hypersingular residuals - a new approach for error estimation in the boundary element method. *International Journal for Numerical Methods in Engineering*, *39*(12). https://doi.org/10.1002/(sici)1097-0207(19960630)39:12<2005::aid-nme940>3.0.co;2-d

Paulino, G. H., Shi, F., Mukherjee, S., & Ramesh, P. (1997). Nodal sensitivities as error estimates in computational mechanics. *Acta Mechanica*, *121*. https://doi.org/10.1007/BF01262532

Paulino, Glaucio H., & Gray, L. J. (1999). Galerkin Residuals for Adaptive Symmetric-Galerkin Boundary Element Methods. *Journal of Engineering Mechanics*, *125*(5). https://doi.org/10.1061/(asce)0733-9399(1999)125:5(575)

Pike, D. J., Box, G. E. P., & Draper, N. R. (1988). Empirical Model-Building and Response Surfaces. *Journal of the Royal Statistical Society. Series A (Statistics in Society)*, *151*(1). https://doi.org/10.2307/2982196

Porto, P. A. C., Jorge, A. B., & Ribeiro, G. O. (2005). Extension of the variational self-regular approach for the flux boundary element method formulation. In *CMES - Computer Modeling in Engineering and Sciences*. https://doi.org/10.3970/cmes.2005.010.065

Prabhakar, P., Sames, W. J., Dehoff, R., & Babu, S. S. (2015). Computational modeling of residual stress formation during the electron beam melting process for Inconel 718. *Additive Manufacturing*, 7, 83-91.

Ramos, H., Santiago, R., Alves, M., Theobald, P., Soe, S., & Brasil, R. (2019). Finite Element Modeling of Gyroid Structures Subjected to Impact Loadings. *MECSOL 2019 - Proceedings of the 7th International Symposium on Solid Mechanics,* ABCM, Sao Carlos, SP, Brazil.

Rao, S. S. (2019). *Engineering Optimization: Theory and Practice* (5th ed.). John Wiley & Sons. https://www.wiley.com/en-us/Engineering+Optimization%3A+Theory+and+Practice%2C+5th+Edition-p-9781119454793

Rebba, R. (2005). Model validation and design under uncertainty. *PhD Thesis*.

Rebba, R., & Mahadevan, S. (2006a). Model predictive capability assessment under uncertainty. *AIAA Journal*, *44*(10). https://doi.org/10.2514/1.19103

Rebba, R., & Mahadevan, S. (2006b). Statistical methods for model validation under uncertainty. *Collection of Technical Papers - AIAA/ASME/ASCE/AHS/ASC Structures, Structural Dynamics and Materials Conference*, *7*. https://doi.org/10.2514/6.2006-1997

Rebba, R., Mahadevan, S., & Huang, S. (2006). Validation and error estimation of computational models. *Reliability Engineering and System Safety*, *91*(10–11). https://doi.org/10.1016/j.ress.2005.11.035

Rebba, R., Mahadevan, S., & Zhang, R. (2003). Validation of uncertainty propagation models. *Collection of Technical Papers - AIAA/ASME/ASCE/AHS/ASC Structures, Structural Dynamics and Materials Conference*, *6*. https://doi.org/10.2514/6.2003-1913

Ribeiro, G. O., Ribeiro, T. S. A., Jorge, A. B., & Cruse, T. A. (2009). Evaluation of non-Singular BEM algorithms for potential problems. *Journal of the Brazilian Society of Mechanical Sciences and Engineering*. https://doi.org/10.1590/S1678-58782009000300012

Richards, S. A. (1997). Completed Richardson extrapolation in space and time. *Communications in Numerical Methods in Engineering*, *13*(7). https://doi.org/10.1002/(SICI)1099-0887(199707)13:7<573::AID-CNM84>3.0.CO;2-6

Sanchez-Palencia, E., & Zaoui, A. (1985). Homogenization Techniques for Composite Media. In *Homogenization Techniques for Composite Media*. Springer. https://link.springer.com/book/10.1007/3-540-17616-0

Santos, V. C., Jorge, A. B., & Cunha Jr, S. S. (2016). A Reliability Analysis Procedure for the Design of a Helicopter Composite Armor with Correlated Design Variables. *International Journal of Engineering Applied Sciences and Technology*, *1*(8), 7–18. http://www.ijeast.com/papers/7-18,Tesma108,IJEAST.pdf

Shepard, D. (1968). A two-dimensional interpolation function for irregularly-spaced data. *Proceedings of the 1968 23rd ACM National Conference, ACM 1968*. https://doi.org/10.1145/800186.810616

Shi, F., Ramesh, P., & Mukherjee, S. (1995). Adaptive mesh refinement of the boundary element method for potential problems by using mesh sensitivities as error indicators. *Computational Mechanics*, *16*(6). https://doi.org/10.1007/BF00370560

Shinozuka, M. (1983). Basic Analysis of Structural Safety. *Journal of Structural Engineering*, *109*(3). https://doi.org/10.1061/(asce)0733-9445(1983)109:3(721)

Smith, M., Guan, Z., & Cantwell, W. J. (2013). Finite element modelling of the compressive response of lattice structures manufactured using the selective laser melting technique. *International Journal of Mechanical Sciences*, 67, 28-41.

Sinou, Jean-Jacques. "A review of damage detection and health monitoring of mechanical systems from changes in the measurement of linear and non-linear vibrations." Mechanical vibrations: measurement, effects, and control, 643-702, 2009.

Smith, M., Mines, R.A.W., Cantwell, W.J., Static and impact behavior of a wing leading edge configuration with a micro lattice core. ICEM16, Cambridge, 2014.

Smith, C. J., Tammas-Williams, S., Hernandez-Nava, E., & Todd, I. (2017). Tailoring the thermal conductivity of the powder bed in Electron Beam Melting (EBM) *Additive Manufacturing. Scientific Reports*, 7(1), 1-8.

Soares, C. G. (1989). *Bayesian Prediction of Design Wave Heights*. https://doi.org/10.1007/978-3-642-83828-6_22

Structural Reliability Research Group - Faculty and Staff. (n.d.). Vanderbilt University. Retrieved June 29, 2022, from http://www.structural-reliability.vanderbilt.edu/faculty_staff.htm

Sukumar, N., Moran, B., & Belytschko, T. (1998). The natural element method in solid mechanics. *International Journal for Numerical Methods in Engineering*, *43*(5). https://doi.org/10.1002/(SICI)1097-0207(19981115)43:5<839::AID-NME423>3.0.CO;2-R

Sulsky, D., Zhou, S. J., & Schreyer, H. L. (1995). Application of a particle-in-cell method to solid mechanics. *Computer Physics Communications*, *87*(1–2). https://doi.org/10.1016/0010-4655(94)00170-7

Tatang, M. A., Pan, W., Prinn, R. G., & McRae, G. J. (1997). An efficient method for parametric uncertainty analysis of numerical geophysical models. *Journal of Geophysical Research Atmospheres*, *102*(18). https://doi.org/10.1029/97jd01654

Thoft-Christensen, P., & Baker, M. J. (1982). Structural Reliability Theory and Its Applications. In *Structural Reliability Theory and Its Applications*. https://doi.org/10.1007/978-3-642-68697-9

Tomlinson, G. A. (1929). CVI. A molecular theory of friction . *The London, Edinburgh, and Dublin Philosophical Magazine and Journal of Science*, *7*(46). https://doi.org/10.1080/14786440608564819

Tsai, D. H. (1979). The virial theorem and stress calculation in molecular dynamics. *The Journal of Chemical Physics*, *70*(3). https://doi.org/10.1063/1.437577

Varfolomeyev, I. V., Busch, M., & Petersilge, M. (1998). Characterization of the computational accuracy in surface crack problems. *International Journal for Numerical Methods in Engineering*, *41*(4). https://doi.org/10.1002/(SICI)1097-0207(19980228)41:4<721::AID-NME307>3.0.CO;2-G

Verfürth, R. (1994). A posteriori error estimation and adaptive mesh-refinement techniques. *Journal of Computational and Applied Mathematics*, *50*(1–3). https://doi.org/10.1016/0377-0427(94)90290-9

Volinsky, C. T., Madigan, D., Raftery, A. E., & Kronmal, R. A. (1997). Bayesian model averaging in proportional hazard models: Assessing the risk of a stroke. *Journal of the Royal Statistical Society. Series C: Applied Statistics*, *46*(4). https://doi.org/10.1111/1467-9876.00082

Wang, L., Basu, P. K., & Leiva, J. P. (2004). Automobile body reinforcement by finite element optimization. *Finite Elements in Analysis and Design*, *40*(8). https://doi.org/10.1016/S0168-874X(03)00118-5

Wang, L., Leiva, J. P., & Basu, P. K. (2003). Design optimization of automobile welds. *International Journal of Vehicle Design*, *31*(4). https://doi.org/10.1504/IJVD.2003.003352

Wendland, W., & Cruse, T. A. (1990). Boundary Element Analysis in Computational Fracture Mechanics. *Mathematics of Computation*, *55*(192). https://doi.org/10.2307/2008455

Weng, S.; Tian, W.; Zhu, H.; Xia,Y.; Gao, F.; Zhang, Y. 2017. Dynamic condensation approach to calculation of structural responses and response sensitivities. Mechanical Systems and Signal Processing Vol. 88 pp 302-317.

Wolf-Gladrow, D. A. (2000). 5 . Lattice Boltzmann Models 5 . 1 From lattice-gas cellular automata to lattice. In *Lattice-Gas Cellular Automata and Lattice Boltzmann Models, An Introduction*.

Xie Mukherjee, Y., & Mukherjee, S. (1997). The boundary node method for potential problems. *International Journal for Numerical Methods in Engineering*, *40*(5). https://doi.org/10.1002/(sici)1097-0207(19970315)40:5<797::aid-nme89>3.0.co

Zhan, J., & Yokoyama, M. (1997). An adaptive method for the determination of element degree for acquiring the desired accuracy in 2-D BEM. *Advances in Engineering Software*, *28*(4). https://doi.org/10.1016/s0965-9978(96)00054-3

Zhang, R., & Mahadevan, S. (2000). Model uncertainty and Bayesian updating in reliability-based inspection. *Structural Safety*, *22*(2). https://doi.org/10.1016/S0167-4730(00)00005-9

Zhang, R., & Mahadevan, S. (2003). Bayesian methodology for reliability model acceptance. *Reliability Engineering and System Safety*, *80*(1). https://doi.org/10.1016/S0951-8320(02)00269-7

Zhao, Z. (1998). A simple error indicator for adaptive boundary element method. *Computers and Structures*, *68*(5). https://doi.org/10.1016/S0045-7949(98)00081-9

Zhu, J. Z. (1997). A posteriori error estimation - The relationship between different procedures. *Computer Methods in Applied Mechanics and Engineering*, *150*(1–4). https://doi.org/10.1016/S0045-7825(97)00076-5

Zhu, J. Z., & Zienkiewicz, O. C. (1997). A posteriori error estimation and three-dimensional automatic mesh generation. *Finite Elements in Analysis and Design*, *25*(1-2 SPEC. ISS.). https://doi.org/10.1016/s0168-874x(96)00037-6

Zienkiewicz, O. C., & Zhu, J. Z. (1987). A simple error estimator and adaptive procedure for practical engineerng analysis. *International Journal for Numerical Methods in Engineering*, *24*(2). https://doi.org/10.1002/nme.1620240206

Zienkiewicz, O. C., & Zhu, J. Z. (1991). Adaptivity and mesh generation. *International Journal for Numerical Methods in Engineering*, *32*(4). https://doi.org/10.1002/nme.1620320409

Zienkiewicz, O. C., & Zhu, J. Z. (1992a). The superconvergent patch recovery and a posteriori error estimates. Part 1: The recovery technique. *International Journal for Numerical Methods in Engineering*, *33*(7). https://doi.org/10.1002/nme.1620330702

Zienkiewicz, O. C., & Zhu, J. Z. (1992b). The superconvergent patch recovery and a posteriori error estimates. Part 2: Error estimates and adaptivity. *International Journal for Numerical Methods in Engineering*, *33*(7). https://doi.org/10.1002/nme.1620330703

Zienkiewicz, Olgierd C., & Taylor, R. L. (1994). The finite element method. Volume 1: Basic formulation and linear problems. In *The finite element method* (Vol. 3).

Zimmerman, J. A., Webb, E. B., Hoyt, J. J., Jones, R. E., Klein, P. A., & Bammann, D. J. (2004). Calculation of stress in atomistic simulation. *Modelling and Simulation in Materials Science and Engineering*, *12*(4). https://doi.org/10.1088/0965-0393/12/4/S03